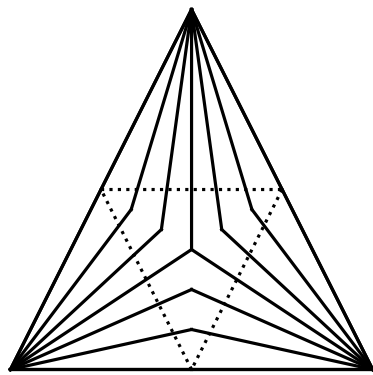


Imperial College of Science, Technology and Medicine
Department of Physics

Interacting quantum many body systems I have known and loved

Thomas Hodson



Submitted in part fulfilment of the requirements for the degree of
Doctor of Philosophy in Physics of Imperial College of Science, Technology and Medicine
June 2022

Abstract

Etiam velit ut sit amet, consetetur adipiscitur elit. Ut purus elit, vestibulum ut, placerat ac, adipiscitur vitae, felis. Curabitur dictum gravida mauris. Nam arcu libero, nonummy eget, consetetur id, vulputate a, magna. Donec vehicula augue eu neque. Pellentesque habitant morbi tristique senectus et netus et malesuada fames ac turpis egestas. Mauris ut leo. Cras viverra metus rhoncus sem. Nulla et lectus vestibulum urna fringilla ultrices. Phasellus eu tellus sit amet tortor gravida placerat. Integer sapien est, iaculis in, pretium quis, viverra ac, nunc. Praesent eget sem vel leo ultrices bibendum. Aenean faucibus. Morbi dolor nulla, malesuada eu, pulvinar at, mollis ac, nulla. Curabitur auctor semper nulla. Donec varius orci eget risus. Duis nibh mi, congue eu, accumsan eleifend, sagittis quis, diam. Duis eget orci sit amet orci dignissim rutrum.

Versions of this document

A PDF version of document is available online with either [normal](#) or [double](#) line spacing. An [HTML version](#) is also available with some figures animated.

Statement of Originality

I declare that the following work is entirely my own except where stated otherwise. Contributions from collaborators and others have been acknowledged by standard referencing practices. I have permissions to reproduce any third party copyrighted material which are included at the end of this thesis.

Copyright Declaration

The copyright of this thesis rests with the author. Unless otherwise indicated, its contents are licensed under a Creative Commons Attribution-Non Commercial 4.0 International Licence (CC BY-NC). Under this licence, you may copy and redistribute the material in any medium or format. You may also create and distribute modified versions of the work. This is on the condition that: you credit the author and do not use it, or any derivative works, for a commercial purpose. When reusing or sharing this work, ensure you make the licence terms clear to others by naming the licence and linking to the licence text. Where a work has been adapted, you should indicate that the work has been changed and describe those changes. Please seek permission from the copyright holder for uses of this work that are not included in this licence or permitted under UK Copyright Law.

Contents

Abstract	1
1 Introduction	8
1.1 Interacting Quantum Many Body Systems	9
1.2 Mott Insulators	10
1.3 Quantum Spin Liquids	13
References	17
2 Background	24
2.1 The Falicov Kimball Model	25
2.1.1 The Model	25
2.1.2 Phase Diagrams	26
2.1.3 Long Ranged Ising model	28
2.2 The Kitaev Honeycomb Model	31
2.2.1 The Spin Hamiltonian	31
2.2.2 The Spin Model	32
2.2.3 The Majorana Model	34
2.2.4 The Fermion Problem	35
2.2.5 An Emergent Gauge Field	36
2.2.6 Anyons, Topology and the Chern number	39
2.2.7 Ground State Phases	41
2.3 Disorder and Localisation	43
2.3.1 Topological Disorder	44
2.3.2 Diagnosing Localisation in practice	45
References	48
3 The Long-Range Falicov-Kimball Model	56
3.1 The Model	57

3.2	Methods	59
3.2.1	Thermodynamics of the LRFK Model	59
3.2.2	Markov Chain Monte Carlo and Emergent Disorder	60
3.2.3	Scaling	61
3.3	Results	63
3.3.1	Phase Diagram	63
3.3.2	Localisation Properties	65
3.4	Discussion and Conclusion	68
	References	71
4	The Amorphous Kitaev Honeycomb Model	74
4.1	The Model	75
4.1.1	The Euler Equation	79
4.2	Methods	80
4.2.1	Voronisation	80
4.2.2	Colouring the Bonds	80
4.2.3	Mapping between flux sectors and bond sectors	82
4.3	Results	84
4.3.1	The Ground State Flux Sector	84
4.3.2	Ground State Phase Diagram	84
4.3.3	Anderson Transition to a Thermal Metal	87
4.4	Conclusion	89
	References	93
5	Conclusion	101
5.1	Material Realisations	103
5.1.1	Amorphous Materials	103
5.1.2	Metal Organic Frameworks	103
5.2	Discussion	103
	References	104
Appendices		105
A.1	Particle-Hole Symmetry	106
A.2	Evaluation of the Fermion Free Energy	107
A.3	Markov Chain Monte Carlo	108
A.3.1	Direct Random Sampling	108

A.3.2	MCMC Sampling	108
A.3.3	Implementation of MCMC	109
A.3.4	Global and Detailed balance equations	109
A.3.5	The Metropolis-Hastings Algorithm	110
A.3.6	Two Step Trick	112
A.4	Lattice Generation	116
A.4.1	Graph Representation	116
A.4.2	Encoding edge-colouring problems as SAT instances	117
A.5	Lattice Colouring	119
A.6	The Projector	120
	References	122

List of Figures

1.1	A murmuration of Starlings	9
1.2	Interacting Quantum Many Body Systems Venn Diagram	11
1.3	Falicov-Kimball Model Diagram	13
1.4	Phase Diagram	14
2.1	Cubic Lattice dispersion with disorder	26
2.2	Falicov-Kimball Temperatue-Interaction Phase Diagrams	27
2.3	Domain walls in the long range Ising Model	28
2.4	Long Range Ising Model Behaviour	30
2.5	The Kitaev Honeycomb Model	31
2.6	A Visual Intro to the Kitaev Model	32
2.7	We can construct arbitrary loops from plaquette fluxes.	33
2.8	Gauge Symmetries	37
2.9	Plaquettes in the Kitaev Model	38
2.10	Topological Fluxes	39
2.11	Braiding in Two Dimensions	40
2.12	Kitaev Honeycomb Model Phase Diagram	41
2.13	Localisation length vs diameter	45
3.1	Falicov-Kimball Model Diagram	58
3.2	Comparison of different proposal distributions	59
3.3	Binder Cumulants	62
3.4	Long Range Falicov Kimball Model Phase Diagram	63
3.5	Energy resolved DOS(ω) in the difference phases.	64
3.6	Scaling of IPR(ω) against system size N	66
3.7	The transition from CDW to the Mott phase	67
3.8	The transition from CDW to the Anderson Phase	68
3.9	FK model compared to binary disorder model: DOS	69
3.10	FK model compared to binary disorder model: IPR Scaling	70

4.1	The Kitaev Honeycomb Model	76
4.2	State Decomposition	77
4.3	Majorana Bound States	78
4.4	Lattice Construction	80
4.5	Colourings of an Amorphous Lattice	81
4.6	Finding Bond Sectors from Flux Sectors	82
4.7	The Ground State Phase Diagram	85
4.8	Local Chern Markers	87
4.9	Edges States and Density of States	88
4.10	Finite Size Scaing of the Fermion Gap	89
4.11	Transition to a Thermal Metal	90
4.12	Distinctive Oscillations in the Density of States	91
A.1	Autocorrelation in MCMC	113
A.2	Comparison of different proposal distributions	114
A.3	Bloch's Theorem and the Torus	116
A.4	Computation Time Spent on Different Procedures.	117
A.5	How the different Hilbert Spaces relate to one another	120

Chapter 1

Introduction



Figure 1.1: A murmuration of starlings. Dorset, UK. Credit [Tanya Hart](#), “Studland Starlings”, 2017, [CC BY-SA 3.0](#)

1.1 Interacting Quantum Many Body Systems

When you take many objects and let them interact together, it is often easier to describe the behaviour of the group as a whole rather than the behaviour of the individual objects. Consider a flock of starlings like that of fig. 1.1. Watching the flock you’ll see that it has a distinct outline, that waves of density will sometimes propagate through the closely packed birds and that the flock seems to respond to predators as a distinct object. The natural description of this phenomenon is in terms of the flock, not the individual birds.

The behaviours of the flock are an *emergent phenomenon*. The starlings are only interacting with their immediate six or seven neighbours [1, 2], what a physicist would call a *local interaction*. There is much philosophical debate about how exactly to define emergence [3, 4]. For our purposes, it is enough to say that emergence is the fact that the aggregate behaviour of many interacting objects may necessitate a radically different description from that of the individual objects.

To give an example closer to the topic at hand, our understanding of thermodynamics began with bulk properties like heat, energy, pressure and temperature [5]. It was only later that we gained an understanding of how these properties emerge from microscopic interactions between very large numbers of particles [6].

At its heart, condensed matter is the study of the behaviours that can emerge from large

numbers of interacting quantum objects at low energy. When these three properties are present together (a large number of objects, those objects being quantum and the presence interactions between the objects), we call it an interacting quantum many body system. From these three ingredients, nature builds all manner of weird and wonderful materials.

Historically, we first made headway by ignoring interactions and quantum properties and looking at purely many-body systems. The ideal gas law and the Drude classical electron gas [7] are good examples. Including interactions leads to the Ising model [8], the Landau theory [9] and the classical theory of phase transitions [10]. In contrast, condensed matter theory got its start in quantum many-body theory where the only electron-electron interaction considered is the Pauli exclusion principle. Bloch's theorem [11], the core result of band theory, predicted the properties of non-interacting electrons in crystal lattices. It predicted, in particular, that band insulators arise when the electrons bands are filled, leaving the fermi level in a bandgap [7]. In the same vein, advances were made in understanding the quantum origins of magnetism, including ferromagnetism and antiferromagnetism [12].

The development of Landau-Fermi Liquid theory explained why band theory works so well even where an analysis of the relevant energies suggests that it should not [13]. Landau Fermi Liquid theory demonstrates that, in many cases where electron-electron interactions are significant, the system can still be described in terms of generalised non-interacting quasiparticles. This happens when the properties of the quasiparticles in the interacting system can be smoothly connected to the free fermions of the non-interacting system.

However, there are systems where even Landau Fermi Liquid theory fails. An effective theoretical description of these systems must include electron-electron correlations. They are thus called strongly correlated materials [14]. The canonical examples are superconductivity [15], the fractional quantum hall effect [16] and the Mott insulators [17, 18]. We'll start by looking at the latter but shall see that there are many links between the three topics.

1.2 Mott Insulators

Mott insulators (MIs) are remarkable because their electrical insulator properties come not from having filled bands but from electron-electron interactions other than Pauli exclusion. Electrical conductivity, the bulk movement of electrons, requires both that there are electronic states very close in energy to the ground state and that those states are delocalised so that they can contribute to macroscopic transport. Band insulators are systems whose Fermi level falls within a gap in the density of states and thus fail the first criteria. Band insulators derive their character from the characteristics of the underlying lattice. A third kind of insulator, the Anderson insulators, have only localised electronic states near the fermi level and therefore fail the second criteria. In a later section, I will discuss Anderson insulators and the disorder that drives them.

Both band and Anderson insulators occur without electron-electron interactions. MIs, by contrast, require a many body picture to understand and thus elude band theory and single-particle methods.

The theory of MIs developed out of the observation that band theory erroneously predicts that many transition metal oxides are conductive [19]. It was suggested that electron-electron inter-

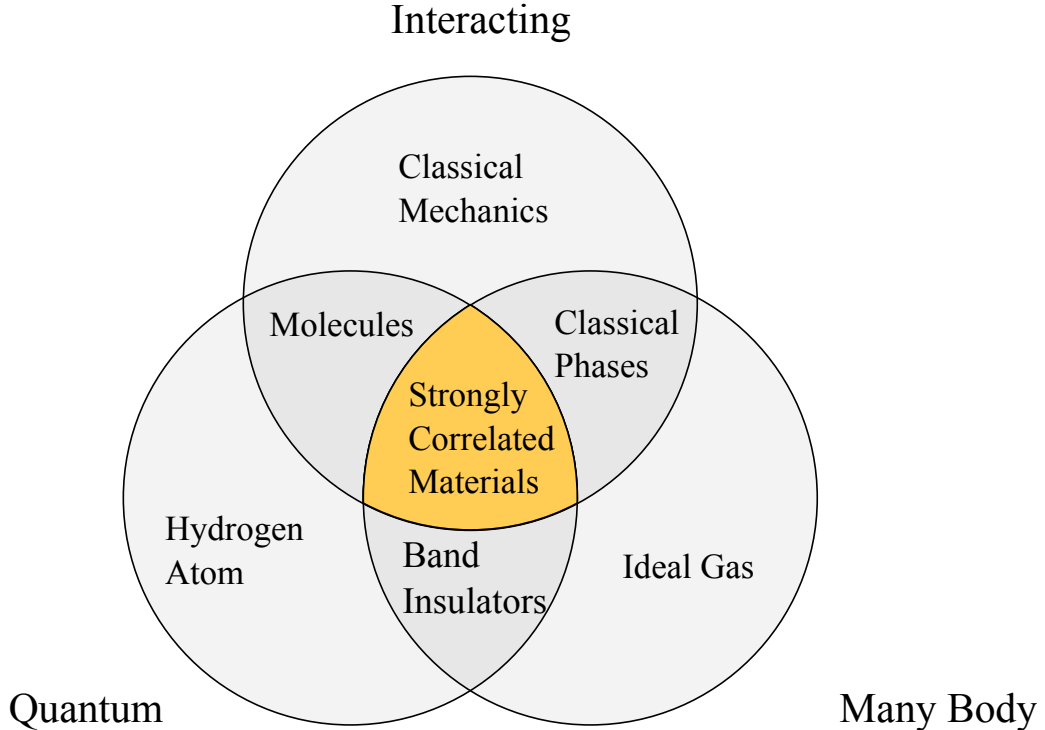


Figure 1.2: Three key adjectives. *Many Body*: systems considered in the limit of large numbers of particles. *Quantum*: objects whose behaviour requires quantum mechanics to describe accurately. *Interacting*: the constituent particles of the system affect one another via forces, either directly or indirectly. When taken together, these three properties can give rise to strongly correlated materials.

actions were the cause of this effect [20]. Interest grew with the discovery of high temperature superconductivity in the cuprates in 1986 [21] which is believed to arise as the result of a doped MI state [22].

The canonical toy model of the MI is the Hubbard model [23–25] of spin-1/2 fermions hopping on the lattice with hopping parameter t and electron-electron repulsion U

$$H_{\text{H}} = -t \sum_{\langle i,j \rangle \alpha} c_{i\alpha}^\dagger c_{j\alpha} + U \sum_i n_{i\uparrow} n_{i\downarrow} - \mu \sum_{i,\alpha} n_{i\alpha}, \quad (1.1)$$

where $c_{i\alpha}^\dagger$ creates a spin α electron at site i and the number operator $n_{i\alpha}$ measures the number of electrons with spin α at site i . The sum runs over lattice neighbours $\langle i, j \rangle$ including both $\langle i, j \rangle$ and $\langle j, i \rangle$ so that the model is Hermitian.

In the non-interacting limit $U \ll t$, the model reduces to free fermions and the many-body ground state is a separable product of Bloch waves filled up to the Fermi level. On the other hand, the ground state in the interacting limit $U \gg t$ is a direct product of the local Hilbert spaces $|0\rangle, |\uparrow\rangle, |\downarrow\rangle, |\uparrow\downarrow\rangle$. At half filling, one electron per site, each site becomes a *local moment* in the reduced Hilbert space $|\uparrow\rangle, |\downarrow\rangle$ and thus acts like a spin-1/2 [26].

The Mott insulating phase occurs at half filling $\mu = \frac{U}{2}$. Here the model can be rewritten in a symmetric form

$$H_H = -t \sum_{\langle i,j \rangle \alpha} c_{i\alpha}^\dagger c_{j\alpha} + U \sum_i (n_{i\uparrow} - \frac{1}{2})(n_{i\downarrow} - \frac{1}{2}). \quad (1.2)$$

The basic reason that the half filled state is insulating seems trivial. Any excitation must include states of double occupancy that cost energy U . Hence, the system has a finite bandgap and is an interaction-driven MI. Depending on the lattice, the local moments may then order antiferromagnetically. Originally it was proposed that this antiferromagnetic (AFM) order was actually the reason for the insulating behaviour. This would make sense since AFM order doubles the unit cell and can turn a system into a band insulator with an even number of electrons per unit cell [27]. However, MIs have been found without magnetic order [28, 29]. Instead, the local moments may form a highly entangled state known as a quantum spin liquid, which will be discussed shortly.

Various theoretical treatments of the Hubbard model have been made, including those based on Fermi liquid theory, mean field treatments, the local density approximation (LDA) [30], dynamical mean-field theory [31], density matrix renormalisation group methods [32–34] and Markov chain Monte Carlo [35–37]. None of these approaches are perfect. Strong correlations are poorly described by Fermi liquid theory and LDA approaches while mean field approximations do poorly in low dimensional systems. This theoretical difficulty has made the Hubbard model a target for cold atom simulations [38].

From here, the discussion will branch in two directions. First, I will discuss a limit of the Hubbard model called the Falicov-Kimball model. Second, I will look at quantum spin liquids and the Kitaev honeycomb model.

The Falicov-Kimball Model

The Falicov-Kimball (FK) model was originally introduced to describe the metal-insulator transition in f-electron system [25, 39]. The FK model is the limit of the Hubbard model as the mass of one of the spins states of the electron is taken to infinity. This gives a model with two fermion species, one itinerant and one entirely immobile. The number operators for the immobile fermions are therefore conserved quantities and can be treated like classical degrees of freedom. For our purposes, it will be useful to replace the immobile fermions with a classical Ising background field $S_i = \pm 1$.

$$H_{FK} = -t \sum_{\langle i,j \rangle} c_i^\dagger c_j + U \sum_i S_i (c_i^\dagger c_i - \frac{1}{2}). \quad (1.3)$$

The physics of states near the metal-insulator transition is still poorly understood [40, 41]. As a result, the FK model provides a rich test bed to explore interaction-driven metal-insulator transition physics. Despite its simplicity, the model has a rich phase diagram in $D \geq 2$ dimensions. It shows a Mott insulator transition even at high temperature, similar to the corresponding Hubbard Model [42]. In one dimension, the ground state phenomenology as a function of filling can be rich [43], but the system is disordered for all $T > 0$ [44]. The model has also been a

 Spins $S_i = \pm 1$ Interaction $U S_i (\hat{n}_i - 1/2)$

 Fermions $\hat{n}_i = \{0, 1\}$ — Hopping $-t \hat{c}_i^\dagger \hat{c}_{i+1}$

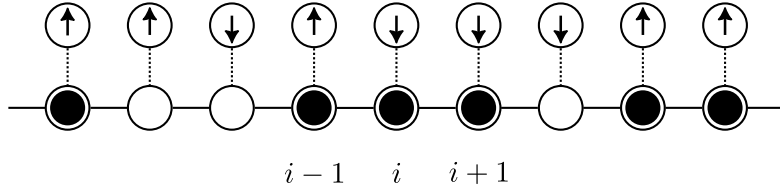


Figure 1.3: The Falicov-Kimball model can be viewed as a model of classical spins S_i coupled to spinless fermions \hat{c}_i where the fermions are mobile with hopping t and the fermions are coupled to the spins by an Ising type interaction with strength U .

test-bed for many-body methods. Interest took off when an exact dynamical mean-field theory solution in the infinite dimensional case was found [45–48].

In chapter 3, I will introduce a generalized Falicov-Kimball model in one dimension I call the Long-Range Falicov-Kimball model. With the addition of long-range interactions in the background field, the model shows a similarly rich phase diagram like its higher dimensional cousins. Our goal is to understand the Mott transition in more detail, the phase transition into a charge density wave state and how the localisation properties of the fermionic sector behave in one dimension. We were particularly interested to see if correlations in the disorder potential are enough to bring about localisation effects, such as mobility edges, that are normally only seen in higher dimensions. I use an exact Markov chain Monte Carlo method to map the phase diagram and compute the energy-resolved localisation properties of the fermions. We observe what appears to be a hint of coexisting localised and delocalised states. However, after careful comparison to an Anderson model of uncorrelated binary disorder about a background charge density wave field, we confirm that the fermionic sector does fully localise at larger system sizes as expected for one dimensional systems.

1.3 Quantum Spin Liquids

Turning to the other key topic of this thesis, we have already discussed the AFM ordering of local moments in the Mott insulating state. Landau-Ginzburg-Wilson theory characterises phases of matter as inextricably linked to the emergence of long range order via a spontaneously broken symmetry. Within this paradigm, we would not expect any interesting phases of matter not associated with AFM or other long-range order. However, Anderson first proposed in 1973 [49] that, if long range order is suppressed by some mechanism, it might lead to a liquid-like state even at zero temperature: a Quantum Spin Liquid (QSL).

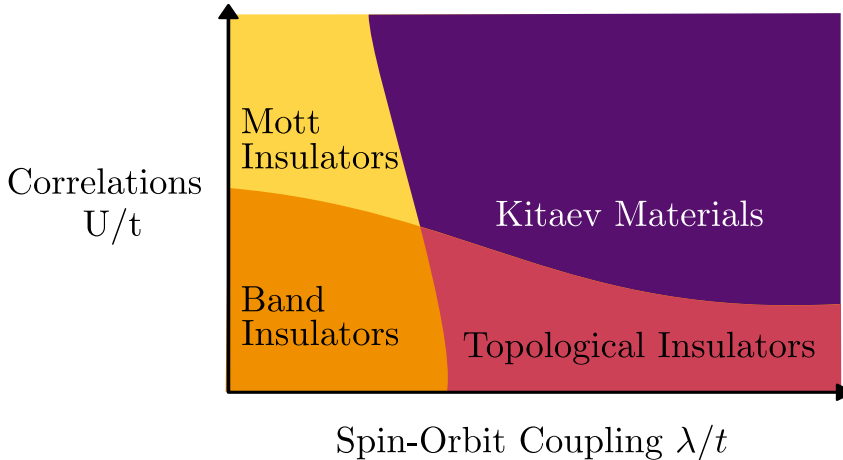


Figure 1.4: How Kitaev materials fit into the picture of strongly correlated systems. Interactions are required to open a Mott gap and localise the electrons into local moments, while spin-orbit correlations are required to produce the strongly anisotropic spin-spin couplings of the Kitaev model. Reproduced from [56].

This QSL state would exist at zero or very low temperatures. Therefore, we would expect quantum effects to be very strong, which will have far reaching consequences. It was the discovery of a different phase, however, that really kickstarted interest in the topic. The fractional quantum Hall state, discovered in the 1980s [50] is an explicit example of an interacting electron system that falls outside of the Landau-Ginzburg-Wilson paradigm¹. It shares many phenomenological properties with the QSL state. They both exhibit fractionalised excitations, braiding statistics and non-trivial topological properties [55]. The many-body ground state of such systems acts as a complex and highly entangled vacuum. This vacuum can support quasiparticle excitations with properties unbound from that of the Dirac fermions of the standard model.

How do we actually make a QSL? Frustration is one mechanism that we can use to suppress magnetic order in spin models [56]. Frustration can be geometric. Triangular lattices, for instance, cannot support AFM order. It can also come about as a result of spin-orbit coupling or other physics. There are also other routes to QSLs besides frustrated spin systems that we will not discuss here [57–59].

Spin-orbit coupling is a relativistic effect that, very roughly, corresponds to the fact that in the frame of reference of a moving electron the electric field of nearby nuclei looks like a magnetic field to which the electron spin couples. This couples the spatial and spin parts of the electron wavefunction. The lattice structure can therefore influence the form of the spin-spin interactions, leading to spatial anisotropy in the effective interactions. This spatial anisotropy can frustrate an MI state [60, 61] leading to more exotic ground states than the AFM order we have seen so far. As with the Hubbard model, interaction effects are only strong or weak in comparison to the bandwidth or hopping integral t . Hence, we will see strong frustration in

¹In fact the FQH state *can* be described within a Ginzburg-Landau like paradigm but it requires a non-local order parameter [51, 52]. Phases like this are said to possess *topological order* defined by the fact that they cannot be smoothly deformed into a product state [53, 54].

materials with strong spin-orbit coupling λ relative to their bandwidth t .

In certain transition metal based compounds, such as those based on Iridium and Ruthenium, the lattice structure, strong spin-orbit coupling and narrow bandwidths lead to effective spin- $\frac{1}{2}$ Mott insulating states with strongly anisotropic spin-spin couplings. These transition metal compounds, known as Kitaev materials, draw their name from the celebrated Kitaev Honeycomb model which is expected to model their low temperature behaviour [56, 62–65].

At this point, we can sketch out a phase diagram like that of fig. 1.4. When both electron-electron interactions U and spin-orbit couplings λ are small relative to the bandwidth t , we recover standard band theory of band insulators and metals. In the upper left, we have the simple Mott insulating state as described by the Hubbard model. In the lower right, strong spin-orbit coupling gives rise to topological insulators characterised by symmetry protected edge modes and non-zero Chern number. Kitaev materials occur in the region where strong electron-electron interaction and spin-orbit coupling interact. See [66] for a more expansive version of this diagram.

The Kitaev Honeycomb model [67] was one of the first exactly solvable spin models with a QSL ground state. It is defined on the two dimensional honeycomb lattice and provides an exactly solvable model that can be reduced to a free fermion problem via a mapping to Majorana fermions. This yields an extensive number of static \mathbb{Z}_2 fluxes tied to an emergent gauge field. The model is remarkable not only for its QSL ground state, but also for its fractionalised excitations with non-trivial braiding statistics. It has a rich phase diagram hosting gapless, Abelian and non-Abelian phases [68] and a finite temperature phase transition to a thermal metal state [69]. It has been proposed that its non-Abelian excitations could be used to support robust topological quantum computing [70–72].

The Kitaev model and FK model have quite a bit of conceptual overlap. They are both effectively models of spinless fermions coupled to a classical Ising background field. This is what makes them exactly solvable. At finite temperatures, fluctuations in their background fields provide an effective disorder potential for the fermionic sector, so both models can be studied at finite temperature with Markov chain Monte Carlo methods [69, 73].

As Kitaev points out in his original paper, the model remains solvable on any tri-coordinated $z = 3$ graph which can be 3-edge-coloured. Indeed many generalisations of the model exist [74–78]. Notably, the Yao-Kivelson model [79] introduces triangular plaquettes to the honeycomb lattice leading to spontaneous chiral symmetry breaking. These extensions all retain translation symmetry. This is likely because edge-colouring, finding the ground state and understanding the QSL properties are much harder without it [80, 81]. Undeterred, this gap lead us to wonder what might happen if we remove translation symmetry from the Kitaev model. This would be a model of a tri-coordinated, highly bond anisotropic but otherwise amorphous material.

Amorphous materials do not have long-range lattice regularities but may have short-range regularities in the lattice structure, such as fixed coordination number z as in some covalent compounds. The best examples are amorphous Silicon and Germanium with $z = 4$ which are used to make thin-film solar cells [82, 83]. Recently, it has been shown that topological insulating phases can exist in amorphous systems. Amorphous topological insulators are characterised by similar protected edge states to their translation invariant cousins and generalised topological bulk invariants [84–90]. However, research on amorphous electronic systems has mostly focused on non-interacting systems with a few exceptions, for example, to account for the observation

of superconductivity [91–95] in amorphous materials or very recently to understand the effect of strong electron repulsion in TIs [96].

Amorphous *magnetic* systems have been investigated since the 1960s, mostly through the adaptation of theoretical tools developed for disordered systems [97–100] and with numerical methods [101, 102]. Research on classical Heisenberg and Ising models accounts for the observed behaviour of ferromagnetism, disordered antiferromagnetism and widely observed spin glass behaviour [103]. However, the role of spin-anisotropic interactions and quantum effects in amorphous magnets has not been addressed.

In [chapter 4](#), I will address the question of whether frustrated magnetic interactions on amorphous lattices can give rise to genuine quantum phases, i.e. to long-range entangled quantum spin liquids (QSL) [104–107]. We will find that the answer is yes. I will introduce the Amorphous Kitaev (AK) model, a generalisation of the Kitaev honeycomb model to random lattices with fixed coordination number three. I will show that this model is a solvable, amorphous, chiral spin liquid. As with the Yao-Kivelson model [79], the AK model retains its exact solubility but the presence of plaquettes with an odd number of sides leads to a spontaneous breaking of time reversal symmetry. I will confirm prior observations that the form of the ground state is relatively simple [77, 108] and unearth a rich phase diagram displaying Abelian as well as a non-Abelian chiral spin liquid phases. Furthermore, I will show that the system undergoes a finite-temperature phase transition to a thermal metal state and discuss possible experimental realisations.

The next chapter, [Chapter 2](#), will introduce some necessary background to the Falicov-Kimball model, the Kitaev Honeycomb model, and disorder and localisation.

References

- [1] A. J. King and D. J. Sumpter, “Murmurations”, *Current Biology* **22**, R112–R114 (2012) (cit. on p. 9).
- [2] M. Ballerini et al., “Interaction ruling animal collective behavior depends on topological rather than metric distance: Evidence from a field study”, *Proceedings of the National Academy of Sciences* **105**, 1232–1237 (2008) 10.1073/pnas.0711437105 (cit. on p. 9).
- [3] P. W. Anderson, “More Is Different”, *Science* **177**, 393–396 (1972) 10.1126/science.177.4047.393 (cit. on p. 9).
- [4] S. Kivelson and S. A. Kivelson, “Defining emergence in physics”, *npj Quant Mater* **1**, 1–2 (2016) 10.1038/npjquantmats.2016.24 (cit. on p. 9).
- [5] W. M. Saslow, “A History of Thermodynamics: The Missing Manual”, *Entropy* (Basel) **22**, 77 (2020) 10.3390/e22010077, pmid: 33285852 (cit. on p. 9).
- [6] D. Flamm, *History and outlook of statistical physics*, Mar. 4, 1998, 10.48550/arXiv.physics/9803005, arXiv:physics/9803005 (cit. on p. 9).
- [7] N. W. Ashcroft and N. D. Mermin, *Solid State Physics* (Holt, Rinehart and Winston, 1976), 868 pp., Google Books: 1C9HAQAAIAAJ (cit. on p. 10).
- [8] E. Ising, “Beitrag zur Theorie des Ferromagnetismus”, *Z. Physik* **31**, 253–258 (1925) 10.1007/BF02980577 (cit. on p. 10).
- [9] L. D. Landau and E. M. Lifshitz, *Fluid mechanics: Landau and lifshitz: Course of theoretical physics, volume 6*, Vol. 6 (Elsevier, 2013) (cit. on p. 10).
- [10] G. Jaeger, “The Ehrenfest Classification of Phase Transitions: Introduction and Evolution”, *Arch Hist Exact Sc.* **53**, 51–81 (1998) 10.1007/s004070050021 (cit. on p. 10).
- [11] F. Bloch, “Über die Quantenmechanik der Elektronen in Kristallgittern”, *Z. Physik* **52**, 555–600 (1929) 10.1007/BF01339455 (cit. on p. 10).
- [12] S. Blundell, *Magnetism in Condensed Matter* (OUP Oxford, Oct. 4, 2001), 256 pp., Google Books: OGhGmgEACAAJ (cit. on p. 10).
- [13] X.-G. Wen, *Quantum Field Theory of Many-Body Systems: From the Origin of Sound to an Origin of Light and Electrons*, Oxford Graduate Texts (Oxford University Press, Oxford, 2007), 520 pp., 10.1093/acprof:oso/9780199227259.001.0001 (cit. on p. 10).
- [14] E. Morosan, D. Natelson, A. H. Nevidomskyy, and Q. Si, “Strongly Correlated Materials”, *Adv. Mater.* **24**, 4896–4923 (2012) 10.1002/adma.201202018, arXiv:1309.4473 (cit. on p. 10).
- [15] J. Bardeen, L. N. Cooper, and J. R. Schrieffer, “Microscopic Theory of Superconductivity”, *Phys. Rev.* **106**, 162–164 (1957) 10.1103/PhysRev.106.162 (cit. on p. 10).
- [16] D. E. Feldman and B. I. Halperin, “Fractional charge and fractional statistics in the quantum Hall effects”, *Rep. Prog. Phys.* **84**, 076501 (2021) 10.1088/1361-6633/ac03aa (cit. on p. 10).
- [17] N. F. Mott, “The Basis of the Electron Theory of Metals, with Special Reference to the Transition Metals”, *Proc. Phys. Soc. A* **62**, 416–422 (1949) 10.1088/0370-1298/62/7/303 (cit. on p. 10).

- [18] M. P. A. Fisher, “Mott insulators, Spin liquids and Quantum Disordered Superconductivity”, in *Aspects topologiques de la physique en basse dimension. Topological aspects of low dimensional systems*, Vol. 69, edited by A. Comtet, T. Jolicœur, S. Ouvry, and F. David, Les Houches - Ecole d’Ete de Physique Theorique (Springer Berlin Heidelberg, Berlin, Heidelberg, 1999), pp. 575–641, [10.1007/3-540-46637-1_8](https://doi.org/10.1007/3-540-46637-1_8) (cit. on p. 10).
- [19] J. H. de Boer and E. J. W. Verwey, “Semi-conductors with partially and with completely filled 3d-lattice bands”, *Proc. Phys. Soc.* **49**, 59–71 (1937) [10.1088/0959-5309/49/4S/307](https://doi.org/10.1088/0959-5309/49/4S/307) (cit. on p. 10).
- [20] N. F. Mott and R. Peierls, “Discussion of the paper by de Boer and Verwey”, *Proc. Phys. Soc.* **49**, 72–73 (1937) [10.1088/0959-5309/49/4S/308](https://doi.org/10.1088/0959-5309/49/4S/308) (cit. on p. 11).
- [21] J. G. Bednorz and K. A. Müller, “Possible highT_c superconductivity in the Ba-La-Cu-O system”, *Z. Physik B - Condensed Matter* **64**, 189–193 (1986) [10.1007/BF01303701](https://doi.org/10.1007/BF01303701) (cit. on p. 11).
- [22] P. A. Lee, N. Nagaosa, and X.-G. Wen, “Doping a Mott insulator: Physics of high-temperature superconductivity”, *Rev. Mod. Phys.* **78**, 17–85 (2006) [10.1103/RevModPhys.78.17](https://doi.org/10.1103/RevModPhys.78.17) (cit. on p. 11).
- [23] M. C. Gutzwiller, “Effect of Correlation on the Ferromagnetism of Transition Metals”, *Phys. Rev. Lett.* **10**, 159–162 (1963) [10.1103/PhysRevLett.10.159](https://doi.org/10.1103/PhysRevLett.10.159) (cit. on p. 11).
- [24] J. Kanamori, “Electron Correlation and Ferromagnetism of Transition Metals”, *Progress of Theoretical Physics* **30**, 275–289 (1963) [10.1143/PTP.30.275](https://doi.org/10.1143/PTP.30.275) (cit. on p. 11).
- [25] Hubbard, J., “Electron correlations in narrow energy bands”, *Proceedings of the Royal Society of London. Series A. Mathematical and Physical Sciences* **276**, 238–257 (1963) [10.1098/rspa.1963.0204](https://doi.org/10.1098/rspa.1963.0204) (cit. on pp. 11–12).
- [26] J. Hubbard and B. H. Flowers, “Electron correlations in narrow energy bands III. An improved solution”, *Proceedings of the Royal Society of London. Series A. Mathematical and Physical Sciences* **281**, 401–419 (1964) [10.1098/rspa.1964.0190](https://doi.org/10.1098/rspa.1964.0190) (cit. on p. 11).
- [27] N. Mott, *Metal-Insulator Transitions* (CRC Press, London, Aug. 20, 1990), 296 pp., [10.1201/b12795](https://doi.org/10.1201/b12795) (cit. on p. 12).
- [28] K. T. Law and P. A. Lee, “1T-TaS₂ as a quantum spin liquid”, *Proceedings of the National Academy of Sciences* **114**, 6996–7000 (2017) [10.1073/pnas.1706769114](https://doi.org/10.1073/pnas.1706769114) (cit. on p. 12).
- [29] A. Ribak et al., “Gapless excitations in the ground state of \$1T\text{\textbackslash}text{\{\\ensuremath{-}\}}\text{\{}\\mathrm{TaS}\\text{\}}\text{\{-}\{2\}\\$}”, *Phys. Rev. B* **96**, 195131 (2017) [10.1103/PhysRevB.96.195131](https://doi.org/10.1103/PhysRevB.96.195131) (cit. on p. 12).
- [30] J. C. Slater, “Magnetic Effects and the Hartree-Fock Equation”, *Phys. Rev.* **82**, 538–541 (1951) [10.1103/PhysRev.82.538](https://doi.org/10.1103/PhysRev.82.538) (cit. on p. 12).
- [31] M. Greiner et al., “Quantum phase transition from a superfluid to a Mott insulator in a gas of ultracold atoms”, *Nature* **415**, 39 (2002) [10.1038/415039a](https://doi.org/10.1038/415039a) (cit. on p. 12).
- [32] K. A. Hallberg, “New trends in density matrix renormalization”, *Advances in Physics* **55**, 477–526 (2006) [10.1080/00018730600766432](https://doi.org/10.1080/00018730600766432) (cit. on p. 12).
- [33] U. Schollwöck, “The density-matrix renormalization group”, *Rev. Mod. Phys.* **77**, 259–315 (2005) [10.1103/RevModPhys.77.259](https://doi.org/10.1103/RevModPhys.77.259) (cit. on p. 12).

- [34] S. R. White, “Density matrix formulation for quantum renormalization groups”, *Phys. Rev. Lett.* **69**, 2863–2866 (1992) 10.1103/PhysRevLett.69.2863 (cit. on p. 12).
- [35] R. Blankenbecler, D. J. Scalapino, and R. L. Sugar, “Monte Carlo calculations of coupled boson-fermion systems. I”, *Phys. Rev. D* **24**, 2278–2286 (1981) 10.1103/PhysRevD.24.2278 (cit. on p. 12).
- [36] J. E. Hirsch, “Discrete Hubbard-Stratonovich transformation for fermion lattice models”, *Phys. Rev. B* **28**, 4059–4061 (1983) 10.1103/PhysRevB.28.4059 (cit. on p. 12).
- [37] S. R. White et al., “Numerical study of the two-dimensional Hubbard model”, *Phys. Rev. B* **40**, 506–516 (1989) 10.1103/PhysRevB.40.506 (cit. on p. 12).
- [38] A. Mazurenko et al., “A cold-atom Fermi–Hubbard antiferromagnet”, *Nature* **545**, 462–466 (2017) 10.1038/nature22362 (cit. on p. 12).
- [39] L. M. Falicov and J. C. Kimball, “Simple Model for Semiconductor-Metal Transitions: Sm $\{\mathrm{B}\}_6$ and Transition-Metal Oxides”, *Phys. Rev. Lett.* **22**, 997–999 (1969) 10.1103/PhysRevLett.22.997 (cit. on p. 12).
- [40] D. Belitz and T. R. Kirkpatrick, “The Anderson-Mott transition”, *Rev. Mod. Phys.* **66**, 261–380 (1994) 10.1103/RevModPhys.66.261 (cit. on p. 12).
- [41] D. M. Basko, I. L. Aleiner, and B. L. Altshuler, “Metal–insulator transition in a weakly interacting many-electron system with localized single-particle states”, *Annals of Physics* **321**, 1126–1205 (2006) 10.1016/j.aop.2005.11.014 (cit. on p. 12).
- [42] U. Brandt and C. Mielsch, “Thermodynamics and correlation functions of the Falicov–Kimball model in large dimensions”, *Z. Physik B - Condensed Matter* **75**, 365–370 (1989) 10.1007/BF01321824 (cit. on p. 12).
- [43] C. Gruber, J. Iwanski, J. Jedrzejewski, and P. Lemberger, “Ground states of the spinless Falicov–Kimball model”, *Phys. Rev. B* **41**, 2198–2209 (1990) 10.1103/PhysRevB.41.2198 (cit. on p. 12).
- [44] T. Kennedy and E. H. Lieb, “An itinerant electron model with crystalline or magnetic long range order”, *Physica A: Statistical Mechanics and its Applications* **138**, 320–358 (1986) 10.1016/0378-4371(86)90188-3 (cit. on p. 12).
- [45] A. E. Antipov, E. Gull, and S. Kirchner, “Critical Exponents of Strongly Correlated Fermion Systems from Diagrammatic Multiscale Methods”, *Phys. Rev. Lett.* **112**, 226401 (2014) 10.1103/PhysRevLett.112.226401 (cit. on p. 13).
- [46] T. Ribic, G. Rohringer, and K. Held, “Nonlocal correlations and spectral properties of the Falicov–Kimball model”, *Phys. Rev. B* **93**, 195105 (2016) 10.1103/PhysRevB.93.195105, arXiv:1602.07161 (cit. on p. 13).
- [47] J. K. Freericks and V. Zlatić, “Exact dynamical mean-field theory of the Falicov–Kimball model”, *Rev. Mod. Phys.* **75**, 1333–1382 (2003) 10.1103/RevModPhys.75.1333 (cit. on p. 13).
- [48] A. J. Herrmann, N. Tsuji, M. Eckstein, and P. Werner, “Nonequilibrium Dynamical Cluster Approximation study of the Falicov–Kimball Model”, *Phys. Rev. B* **94**, 245114 (2016) 10.1103/PhysRevB.94.245114, arXiv:1609.04708 (cit. on p. 13).
- [49] P. W. Anderson, “Resonating valence bonds: A new kind of insulator?”, *Materials Research Bulletin* **8**, 153–160 (1973) 10.1016/0025-5408(73)90167-0 (cit. on p. 13).

- [50] R. B. Laughlin, “Anomalous Quantum Hall Effect: An Incompressible Quantum Fluid with Fractionally Charged Excitations”, *Phys. Rev. Lett.* **50**, 1395–1398 (1983) 10.1103/PhysRevLett.50.1395 (cit. on p. 14).
- [51] S. M. Girvin and A. H. MacDonald, “Off-diagonal long-range order, oblique confinement, and the fractional quantum Hall effect”, *Phys. Rev. Lett.* **58**, 1252–1255 (1987) 10.1103/PhysRevLett.58.1252 (cit. on p. 14).
- [52] N. Read, “Order Parameter and Ginzburg-Landau Theory for the Fractional Quantum Hall Effect”, *Phys. Rev. Lett.* **62**, 86–89 (1989) 10.1103/PhysRevLett.62.86 (cit. on p. 14).
- [53] X. Chen, Z.-C. Gu, and X.-G. Wen, “Local unitary transformation, long-range quantum entanglement, wave function renormalization, and topological order”, *Phys. Rev. B* **82**, 155138 (2010) 10.1103/PhysRevB.82.155138 (cit. on p. 14).
- [54] X.-G. Wen, “Quantum orders and symmetric spin liquids”, *Phys. Rev. B* **65**, 165113 (2002) 10.1103/PhysRevB.65.165113 (cit. on p. 14).
- [55] C. Broholm et al., “Quantum spin liquids”, *Science* **367**, eaay0668 (2020) 10.1126/science.aay0668 (cit. on p. 14).
- [56] S. Trebst and C. Hickey, “Kitaev materials”, *Physics Reports, Kitaev Materials* **950**, 1–37 (2022) 10.1016/j.physrep.2021.11.003 (cit. on pp. 14–15).
- [57] L. Balents, M. P. A. Fisher, and C. Nayak, “Nodal Liquid Theory of the Pseudo-Gap Phase of High-Tc Superconductors”, *Int. J. Mod. Phys. B* **12**, 1033–1068 (1998) 10.1142/S0217979298000570 (cit. on p. 14).
- [58] L. Balents, M. P. A. Fisher, and C. Nayak, “Dual order parameter for the nodal liquid”, *Phys. Rev. B* **60**, 1654–1667 (1999) 10.1103/PhysRevB.60.1654 (cit. on p. 14).
- [59] H.-H. Lin, L. Balents, and M. P. A. Fisher, “Exact SO(8) symmetry in the weakly-interacting two-leg ladder”, *Phys. Rev. B* **58**, 1794–1825 (1998) 10.1103/PhysRevB.58.1794 (cit. on p. 14).
- [60] G. Jackeli and G. Khaliullin, “Mott Insulators in the Strong Spin-Orbit Coupling Limit: From Heisenberg to a Quantum Compass and Kitaev Models”, *Phys. Rev. Lett.* **102**, 017205 (2009) 10.1103/PhysRevLett.102.017205 (cit. on p. 14).
- [61] G. Khaliullin, “Orbital Order and Fluctuations in Mott Insulators”, *Progress of Theoretical Physics Supplement* **160**, 155–202 (2005) 10.1143/PTPS.160.155 (cit. on p. 14).
- [62] G. Jackeli and G. Khaliullin, “Mott insulators in the strong spin-orbit coupling limit: from Heisenberg to a quantum compass and Kitaev models”, *Physical Review Letters* **102**, 017205 (2009) 10.1103/PhysRevLett.102.017205 (cit. on p. 15).
- [63] M. Hermanns, I. Kimchi, and J. Knolle, “Physics of the kitaev model: Fractionalization, dynamic correlations, and material connections”, *Annual Review of Condensed Matter Physics* **9**, 17–33 (2018) 10.1146/annurev-conmatphys-033117-053934 (cit. on p. 15).
- [64] S. M. Winter et al., “Models and materials for generalized Kitaev magnetism”, *Journal of Physics: Condensed Matter* **29**, 493002 (2017) (cit. on p. 15).
- [65] H. Takagi et al., “Concept and realization of Kitaev quantum spin liquids”, *Nature Reviews Physics* **1**, 264–280 (2019) (cit. on p. 15).
- [66] W. Witczak-Krempa, G. Chen, Y. B. Kim, and L. Balents, “Correlated Quantum Phenomena in the Strong Spin-Orbit Regime”, *Annual Review of Condensed Matter Physics* **5**, 57–82 (2014) 10.1146/annurev-conmatphys-020911-125138 (cit. on p. 15).

- [67] A. Kitaev, “Anyons in an exactly solved model and beyond”, *Annals of Physics*, January Special Issue **321**, 2–111 (2006) 10.1016/j.aop.2005.10.005 (cit. on p. 15).
- [68] J. Knolle, D. L. Kovrizhin, J. T. Chalker, and R. Moessner, “Dynamics of fractionalization in quantum spin liquids”, *Phys. Rev. B* **92**, 115127 (2015) 10.1103/PhysRevB.92.115127 (cit. on p. 15).
- [69] C. N. Self, J. Knolle, S. Iblisdir, and J. K. Pachos, “Thermally induced metallic phase in a gapped quantum spin liquid - a Monte Carlo study of the Kitaev model with parity projection”, *Phys. Rev. B* **99**, 045142 (2019) 10.1103/PhysRevB.99.045142, arXiv:1807.07926 [cond-mat, physics:quant-ph] (cit. on p. 15).
- [70] A. Y. Kitaev, “Fault-tolerant quantum computation by anyons”, *Annals of Physics* **303**, 2–30 (2003) 10.1016/S0003-4916(02)00018-0 (cit. on p. 15).
- [71] M. Freedman, A. Kitaev, M. Larsen, and Z. Wang, “Topological quantum computation”, *Bull. Amer. Math. Soc.* **40**, 31–38 (2003) 10.1090/S0273-0979-02-00964-3 (cit. on p. 15).
- [72] C. Nayak et al., “Non-Abelian anyons and topological quantum computation”, *Rev. Mod. Phys.* **80**, 1083–1159 (2008) 10.1103/RevModPhys.80.1083 (cit. on p. 15).
- [73] A. E. Antipov, Y. Javanmard, P. Ribeiro, and S. Kirchner, “Interaction-Tuned Anderson versus Mott Localization”, *Phys. Rev. Lett.* **117**, 146601 (2016) 10.1103/PhysRevLett.117.146601 (cit. on p. 15).
- [74] G. Baskaran, S. Mandal, and R. Shankar, “Exact results for spin dynamics and fractionalization in the kitaev model”, *Phys. Rev. Lett.* **98**, 247201 (2007) 10.1103/PhysRevLett.98.247201 (cit. on p. 15).
- [75] G. Baskaran, D. Sen, and R. Shankar, “Spin- S Kitaev model: Classical ground states, order from disorder, and exact correlation functions”, *Phys. Rev. B* **78**, 115116 (2008) 10.1103/PhysRevB.78.115116 (cit. on p. 15).
- [76] Z. Nussinov and G. Ortiz, “Bond algebras and exact solvability of Hamiltonians: spin $S=\frac{1}{2}$ multilayer systems”, *Physical Review B* **79**, 214440 (2009) 10.1103/PhysRevB.79.214440 (cit. on p. 15).
- [77] K. O’Brien, M. Hermanns, and S. Trebst, “Classification of gapless Z_2 spin liquids in three-dimensional Kitaev models”, *Phys. Rev. B* **93**, 085101 (2016) 10.1103/PhysRevB.93.085101 (cit. on pp. 15–16).
- [78] M. Hermanns, K. O’Brien, and S. Trebst, “Weyl spin liquids”, *Physical Review Letters* **114**, 157202 (2015) (cit. on p. 15).
- [79] H. Yao and S. A. Kivelson, “An exact chiral spin liquid with non-Abelian anyons”, *Phys. Rev. Lett.* **99**, 247203 (2007) 10.1103/PhysRevLett.99.247203, arXiv:0708.0040 (cit. on pp. 15–16).
- [80] T. Eschmann et al., “Thermodynamics of a gauge-frustrated Kitaev spin liquid”, *Physical Review Research* **1**, 032011(R) (2019) (cit. on p. 15).
- [81] V. Peri et al., “Non-Abelian chiral spin liquid on a simple non-Archimedean lattice”, *Phys. Rev. B* **101**, 041114 (2020) 10.1103/PhysRevB.101.041114 (cit. on p. 15).
- [82] D. Weaire and M. F. Thorpe, “Electronic properties of an amorphous solid. I. A simple tight-binding theory”, *Phys. Rev. B* **4**, 2508–2520 (1971) 10.1103/PhysRevB.4.2508 (cit. on p. 15).

- [83] G. Betteridge, “A possible model of amorphous silicon and germanium”, *Journal of Physics C: Solid State Physics* **6**, L427 (1973) (cit. on p. 15).
- [84] N. P. Mitchell et al., “Amorphous topological insulators constructed from random point sets”, *Nature Phys* **14**, 380–385 (2018) [10.1038/s41567-017-0024-5](https://doi.org/10.1038/s41567-017-0024-5) (cit. on p. 15).
- [85] A. Agarwala, “Topological insulators in amorphous systems”, in *Excursions in ill-condensed quantum matter* (Springer, 2019), pp. 61–79 (cit. on p. 15).
- [86] Q. Marsal, D. Varjas, and A. G. Grushin, “Topological Weaire-Thorpe models of amorphous matter”, *Proc. Natl. Acad. Sci. U.S.A.* **117**, 30260–30265 (2020) [10.1073/pnas.2007384117](https://doi.org/10.1073/pnas.2007384117) (cit. on p. 15).
- [87] M. Costa et al., “Toward realistic amorphous topological insulators”, *Nano letters* **19**, 8941–8946 (2019) (cit. on p. 15).
- [88] A. Agarwala, V. Juričić, and B. Roy, “Higher-order topological insulators in amorphous solids”, *Physical Review Research* **2**, 012067 (2020) (cit. on p. 15).
- [89] H. Spring, A. Akhmerov, and D. Varjas, “Amorphous topological phases protected by continuous rotation symmetry”, *SciPost Physics* **11**, 022 (2021) (cit. on p. 15).
- [90] P. Corbae et al., “Evidence for topological surface states in amorphous Bi - {2} Se - {3}”, 2019, [arXiv:1910.13412](https://arxiv.org/abs/1910.13412) (cit. on p. 15).
- [91] W. Buckel and R. Hilsch, “Einfluß der kondensation bei tiefen temperaturen auf den elektrischen widerstand und die supraleitung für verschiedene metalle”, *Zeitschrift für Physik* **138**, 109–120 (1954) (cit. on p. 16).
- [92] W. McMillan and J. Mochel, “Electron tunneling experiments on amorphous ge 1- x au x”, *Physical Review Letters* **46**, 556 (1981) (cit. on p. 16).
- [93] L. V. Meisel and P. J. Cote, “Eliashberg function in amorphous metals”, *Phys. Rev. B* **23**, 5834–5838 (1981) [10.1103/PhysRevB.23.5834](https://doi.org/10.1103/PhysRevB.23.5834) (cit. on p. 16).
- [94] G. Bergmann, “Amorphous metals and their superconductivity”, *Physics Reports* **27**, 159–185 (1976) (cit. on p. 16).
- [95] S. Manna, S. K. Das, and B. Roy, *Noncrystalline topological superconductors*, July 5, 2022, [arXiv:2207.02203 \[cond-mat\]](https://arxiv.org/abs/2207.02203), <http://arxiv.org/abs/2207.02203> (visited on 08/22/2022) (cit. on p. 16).
- [96] S. Kim, A. Agarwala, and D. Chowdhury, “Fractionalization and topology in amorphous electronic solids”, 2022, [arXiv:2205.11523](https://arxiv.org/abs/2205.11523) (cit. on p. 16).
- [97] A. Aharony, “Critical behavior of amorphous magnets”, *Physical Review B* **12**, 1038 (1975) (cit. on p. 16).
- [98] G. A. Petrakovskii, “Amorphous magnetic materials”, *Soviet Physics Uspekhi* **24**, 511–525 (1981) [10.1070/pu1981v024n06abeh004850](https://doi.org/10.1070/pu1981v024n06abeh004850) (cit. on p. 16).
- [99] T. Kaneyoshi, *Introduction to amorphous magnets* (World Scientific Publishing Company, 1992) (cit. on p. 16).
- [100] T. Kaneyoshi, ed., *Amorphous magnetism*, CRC Revivals (CRC Press, Boca Raton, 2018) (cit. on p. 16).
- [101] M. Fähnle, “Monte Carlo study of phase transitions in bond-and site-disordered Ising and classical Heisenberg ferromagnets”, *Journal of magnetism and magnetic materials* **45**, 279–287 (1984) (cit. on p. 16).

- [102] J. Plascak, L. E. Zamora, and G. P. Alcazar, “Ising model for disordered ferromagnetic Fe- Al alloys”, *Physical Review B* **61**, 3188 (2000) (cit. on p. 16).
- [103] J. Coey, “Amorphous magnetic order”, *Journal of Applied Physics* **49**, 1646–1652 (1978) (cit. on p. 16).
- [104] P. W. Anderson, “Resonating valence bonds: a new kind of insulator?”, *Mater. Res. Bull.* **8**, 153–160 (1973) (cit. on p. 16).
- [105] J. Knolle and R. Moessner, “A field guide to spin liquids”, *Annual Review of Condensed Matter Physics* **10**, 451–472 (2019) [10.1146/annurev-conmatphys-031218-013401](https://doi.org/10.1146/annurev-conmatphys-031218-013401) (cit. on p. 16).
- [106] L. Savary and L. Balents, “Quantum spin liquids: a review”, *Reports on Progress in Physics* **80**, 016502 (2017) (cit. on p. 16).
- [107] C. Lacroix, P. Mendels, and F. Mila, eds., *Introduction to frustrated magnetism*, Vol. 164, Springer-Series in Solid State Sciences (Springer-Verlag, Berlin Heidelberg, 2011) (cit. on p. 16).
- [108] T. Eschmann et al., “Thermodynamic classification of three-dimensional Kitaev spin liquids”, *Phys. Rev. B* **102**, 075125 (2020) [10.1103/PhysRevB.102.075125](https://doi.org/10.1103/PhysRevB.102.075125) (cit. on p. 16).

Chapter 2

Background

2.1 The Falicov Kimball Model

2.1.1 The Model

The Falicov-Kimball (FK) model is one of the simplest models of the correlated electron problem. It captures the essence of the interaction between itinerant and localized electrons. It was originally introduced to explain the metal-insulator transition in f-electron systems but in its long history it has been interpreted variously as a model of electrons and ions, binary alloys or of crystal formation [1–4]. In terms of immobile fermions d_i and light fermions c_i and with chemical potential fixed at half-filling, the model reads

$$H_{\text{FK}} = U \sum_i (d_i^\dagger d_i - \frac{1}{2}) (c_i^\dagger c_i - \frac{1}{2}) - t \sum_{\langle i,j \rangle} c_i^\dagger c_j. \quad (2.1)$$

Here we will only discuss the hypercubic lattices, i.e the chain, the square lattice, the cubic lattice and so on. The connection to the Hubbard model is that we have relabelled the up and down spin electron states and removed the hopping term for one spin state, the equivalent of taking the limit of infinite mass ratio [5].

Like other exactly solvable models [6], the FK model possesses extensively many conserved degrees of freedom $[d_i^\dagger d_i, H] = 0$. Similarly, the Kitaev Model model contains an extensive number of conserved fluxes. So in both models, the Hilbert space breaks up into a set of sectors in which these operators take a definite value. Crucially, this reduces the interaction terms in the model from being quartic in fermion operators to quadratic. This is what makes the two models exactly solvable, in contrast to the Hubbard model. For the FK model the interaction term $(d_i^\dagger d_i - \frac{1}{2}) (c_i^\dagger c_i - \frac{1}{2})$ becomes quadratic when $d_i^\dagger d_i$ is replaced with one of its eigenvalues $\{0, 1\}$. The same thing happens in the Kitaev model, though after first applying a clever transformation which we will discuss later.

Due to Pauli exclusion, maximum filling occurs when each lattice site is fully occupied, $\langle n_c + n_d \rangle = 2$. Here we will focus on the half filled case $\langle n_c + n_d \rangle = 1$. The ground state phenomenology as the model is doped away from the half-filled state can be rich [7, 8] but the half-filled point has symmetries that make it particularly interesting. From this point on we will only consider the half-filled point.

At half-filling and on bipartite lattices, the FK the model is particle-hole (PH) symmetric. That is, the Hamiltonian anticommutes with the particle hole operator $\mathcal{P} H \mathcal{P}^{-1} = -H$. As a consequence, the energy spectrum is symmetric about $E = 0$, which is the Fermi energy. The particle hole operator corresponds to the substitution $c_i^\dagger \rightarrow \epsilon_i c_i, d_i^\dagger \rightarrow d_i$ where $\epsilon_i = +1$ for the A sublattice and -1 for the B sublattice [9]. The absence of a hopping term for the heavy electrons means they do not need the factor of ϵ_i but they would need it in the corresponding Hubbard model. See appendix A.1 for a full derivation of the PH symmetry.

We will later add a long range interaction between the localised electrons at which point we will replace the immobile fermions with a classical Ising field $S_i = 1 - 2d_i^\dagger d_i = \pm 1$ which I will refer to as the spins.

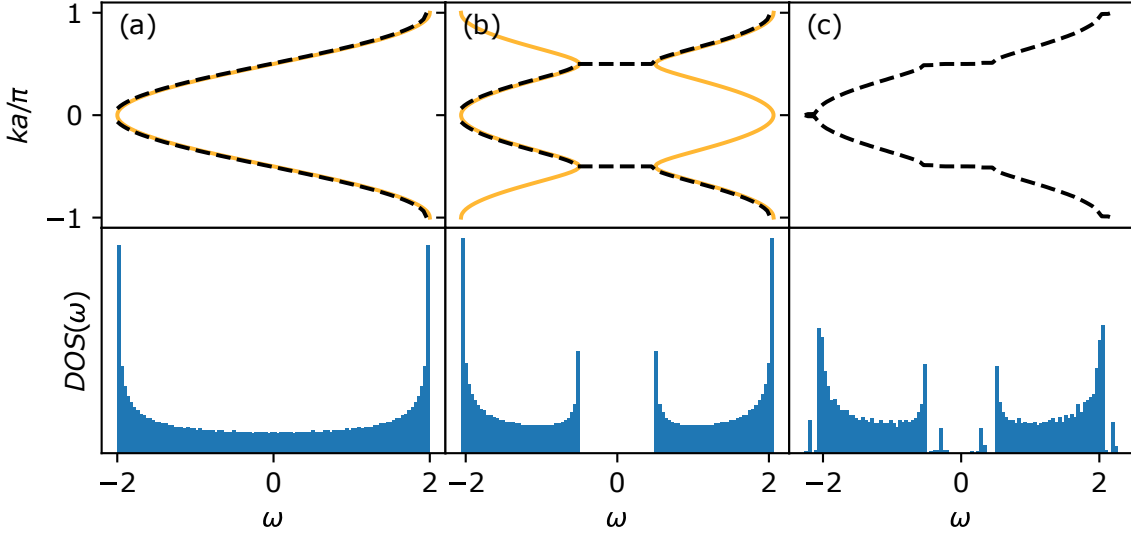


Figure 2.1: The dispersion (upper row) and density of states (lower row) obtained from a cubic lattice model $H = \sum_i V_i c_i^\dagger c_i - t \sum_{\langle i,j \rangle} c_i^\dagger c_j$ in one dimension. (a) With no external potential. (b) With a static charge density wave background $V_i = (-1)^i$ (c) A static charge density wave background with 2% binary disorder. The top rows shows the analytic dispersion in orange compared with the integral of the DOS in dotted black.

$$H_{\text{FK}} = U \sum_i S_i (c_i^\dagger c_i - \frac{1}{2}) - t \sum_{\langle i,j \rangle} c_i^\dagger c_j. \quad (2.2)$$

The FK model can be solved exactly with dynamic mean field theory in the infinite dimensional limit [10–13] but has radically different behaviour in lower dimensional systems.

2.1.2 Phase Diagrams

In dimensions greater than one, the FK model exhibits a phase transition at some U dependent critical temperature $T_c(U)$ to a low temperature ordered phase [15]. In terms of the heavy electrons this corresponds to them occupying only one of the two sublattices A and B, known as a charge density wave (CDW) phase. In terms of spins this is an AFM phase.

In the disordered region above $T_c(U)$ there are two insulating phases. For weak interactions $U \ll t$, thermal fluctuations in the spins act as an effective disorder potential for the fermions, causing them to localise and giving rise to an Anderson insulating (AI) phase [16] which we will discuss more in section 2.3. For strong interactions $U \gg t$, the spins are not ordered but nevertheless their interaction with the electrons opens a gap, leading to a Mott insulator analogous to that of the Hubbard model [17]. The presence of an interaction driven phase like the Mott insulator in an exactly solvable model is part of what makes the FK model such an interesting system.

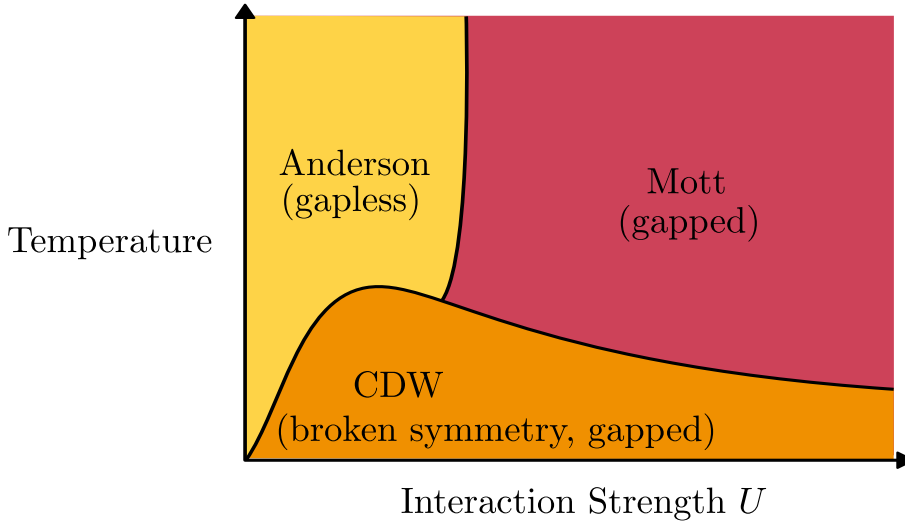


Figure 2.2: Schematic Phase diagram of the Falicov-Kimball model in dimensions greater than two. At low temperature the classical fermions (spins) settle into an ordered charge density wave state (antiferromagnetic state). The schematic diagram for the Hubbard model is the same. Reproduced from [10, 14]

By contrast, in the one dimensional FK model there is no finite-temperature phase transition (FTPT) to an ordered CDW phase [18]. Indeed dimensionality is crucial for the physics of both localisation and FTPTs. In one dimension, disorder generally dominates: even the weakest disorder exponentially localises *all* single particle eigenstates. In the one dimensional FK model this means the whole spectrum is localised at all finite temperatures [19–21]. Though at low temperatures the localisation length may be so large that the states appear extended in finite sized systems [14]. Only longer-range correlations of the disorder potential can potentially induce localisation-delocalisation transitions in one dimension [22–24]

The absence of finite temperature ordered phases in one dimensional systems is a general feature. It can be understood as a consequence of the fact that domain walls are energetically cheap in one dimension. Thermodynamically, short-range interactions just cannot overcome the entropy of thermal defects in one dimension. However, the addition of longer range interactions can overcome this [25, 26].

However, the absence of an FTPT in the short ranged FK chain is far from obvious because the Ruderman-Kittel-Kasuya-Yosida (RKKY) interaction mediated by the fermions [27–30] decays as r^{-1} in one dimension [31]. This could in principle induce the necessary long-range interactions for the classical Ising background to order at low temperatures [25, 32]. However, Kennedy and Lieb established rigorously that at half-filling a CDW phase only exists at $T = 0$ for the one dimensional FK model [26].

The one dimensional FK model has been studied numerically, perturbatively in interaction strength U and in the continuum limit [33]. The main results are that for attractive $U > U_c$ the system forms electron spin bound state ‘atoms’ which repel on another [34] and that the ground state phase diagram has a fractal structure as a function of electron filling, a devil’s staircase [35, 36].

---- Long Range Interaction $J_{ij}S_iS_j$ — Short Range Interaction S_iS_{i+1}

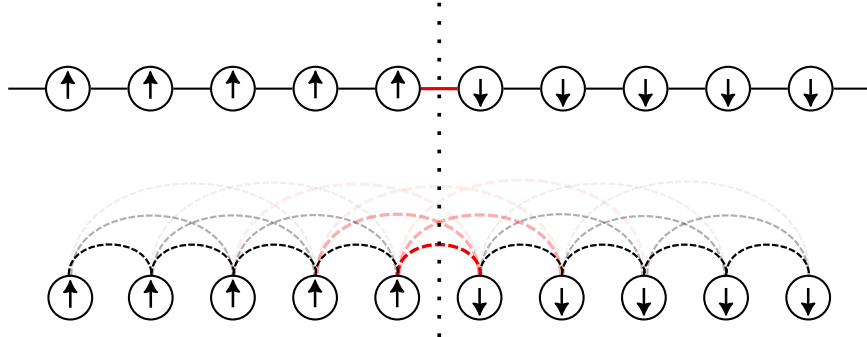


Figure 2.3: Domain walls in the one dimensional Ising model cost finite energy because they affect only one interaction while in the long range Ising model it depends on how the interactions decay with distance.

Based on this primacy of dimensionality, we will go digging into the one dimensional case. In chapter 3 we will construct a generalised one-dimensional FK model with long-range interactions which induces the otherwise forbidden CDW phase at non-zero temperature. To do this we will draw on theory of the Long Range Ising Model which is the subject of the next section.

2.1.3 Long Ranged Ising model

The suppression of phase transitions is a common phenomena in one dimensional systems and the Ising model serves as the canonical illustration of this. In terms of classical spins $S_i = \pm 1$ the standard Ising model reads

$$H_I = \sum_{\langle ij \rangle} S_i S_j \quad (2.3)$$

Like the FK model, the Ising model shows an FTPT to an ordered state only in two dimensions and above. This can be understood via Peierls' argument [25, 26] to be a consequence of the low energy penalty for domain walls in one dimensional systems.

Following Peierls' argument, consider the difference in free energy $\Delta F = \Delta E - T\Delta S$ between an ordered state and a state with single domain wall as in fig. 2.3. If this value is negative it implies that the ordered state is unstable with respect to domain wall defects, and they will thus proliferate, destroying the ordered phase. If we consider the scaling of the two terms with system size L we see that short range interactions produce a constant energy penalty ΔE for a domain wall. In contrast, the number of such single domain wall states scales linearly with system size so the entropy is $\propto \ln L$. Thus the entropic contribution dominates (eventually) in the thermodynamic limit and no finite temperature order is possible. In two dimensions

and above, the energy penalty of a large domain wall scales like L^{d-1} which is why they can support ordered phases. This argument does not quite apply to the FK model because of the aforementioned RKKY interaction. Instead this argument will give us insight into how to recover an ordered phase in the one dimensional FK model.

In contrast the long range Ising (LRI) model H_{LRI} can have an FTPT in one dimension.

$$H_{\text{LRI}} = \sum_{ij} J(|i - j|) S_i S_j = J \sum_{i \neq j} |i - j|^{-\alpha} S_i S_j \quad (2.4)$$

Renormalisation group analyses show that the LRI model has an ordered phase in 1D for $1 < \alpha < 2$ [37]. Peierls' argument can be extended [32] to long range interactions to provide intuition for why this is the case. Again considering the energy difference between the ordered state $|\dots \uparrow\uparrow\uparrow\uparrow \dots\rangle$ and a domain wall state $|\dots \uparrow\uparrow\downarrow\downarrow \dots\rangle$. In the case of the LRI model, careful counting shows that this energy penalty is

$$\Delta E \propto \sum_{n=1}^{\infty} n J(n) \quad (2.5)$$

because each interaction between spins separated across the domain by a bond length n can be drawn between n equivalent pairs of sites. The behaviour then depends crucially on how eq. (2.5) scales with system size. Ruelle proved rigorously for a very general class of 1D systems that if ΔE or its many-body generalisation converges to a constant in the thermodynamic limit then the free energy is analytic [38]. This rules out a finite order phase transition, though not one of the Kosterlitz-Thouless type. Dyson also proves this though with a slightly different condition on $J(n)$ [37].

With a power law form for $J(n)$, there are a few cases to consider:

For $\alpha = 0$ i.e infinite range interactions, the Ising model is exactly solvable and mean field theory is exact [39]. This limit is the same as the infinite dimensional limit.

For $\alpha \leq 1$ we have very slowly decaying interactions. ΔE does not converge as a function of system size so the Hamiltonian is non-extensive, a topic not without some considerable controversy [40–42] that we will not consider further here.

For $1 < \alpha < 2$, we get a phase transition to an ordered state at a finite temperature, this is what we want!

For $\alpha = 2$, the energy of domain walls diverges logarithmically, and this turns out to be a Kostelitz-Thouless transition [32].

Finally, for $2 < \alpha$ we have very quickly decaying interactions and domain walls again have a finite energy penalty, hence Peirels' argument holds and there is no phase transition.

One final complexity is that for $\frac{3}{2} < \alpha < 2$ renormalisation group methods show that the critical point has non-universal critical exponents that depend on α [43]. To avoid this potential confounding factors we will park ourselves at $\alpha = 1.25$ when we apply these ideas to the FK model.

Non-Extensive	Finite Temperature Ordered Phase	Short-Ranged
$\alpha = 1$	$3/2$	2

Figure 2.4: The thermodynamic behaviour of the long range Ising model $H_{\text{LRI}} = J \sum_{i \neq j} |i - j|^{-\alpha} S_i S_j$ as the exponent of the interaction α is varied. In my simulations I stick to a value of $\alpha = \frac{5}{4}$ the complexity of non-universal critical exponents.

Were we to extend this to arbitrary dimension d we would find that thermodynamics properties generally both d and α , long range interactions can modify the ‘effective dimension’ of thermodynamic systems [44].

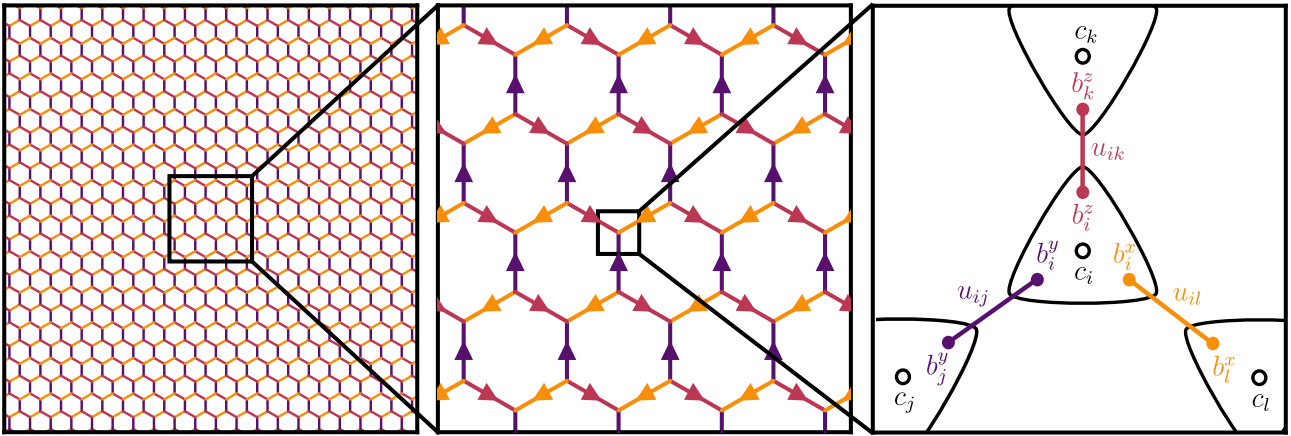


Figure 2.5: (a) The Kitaev honeycomb model is defined on a honeycomb lattice. The special feature of the honeycomb lattice that makes the model solvable is that each vertex is joined by exactly three bonds, i.e. the lattice is trivalent. One of three labels is assigned to each bond (x, y, z) here represented by colour. (b). After transforming to the Majorana representation we get an emergent gauge degree of freedom $u_{jk} = \pm 1$ that lives on each bond, the bond variables. These are antisymmetric, $u_{jk} = -u_{kj}$, so we represent them graphically with arrows on each bond that point in the direction that $u_{jk} = +1$ (c). The Majorana transformation can be visualised as breaking each spin into four Majoranas b_i^x, b_i^y, b_i^z, c_i . The x, y and z Majoranas then pair along the bonds forming conserved \mathbb{Z}_2 bond operators $u_{jk} = \langle ib_i^\alpha b_j^\alpha \rangle$. The remaining c_i operators form an effective quadratic Hamiltonian $H = \frac{i}{4} \sum_{\langle i,j \rangle_\alpha} 2J^\alpha u_{ij} \hat{c}_i \hat{c}_j$.

2.2 The Kitaev Honeycomb Model

2.2.1 The Spin Hamiltonian

This section introduces the Kitaev honeycomb (KH) model. The KH model is an exactly solvable model of interacting spin-1/2 spins on the vertices of a honeycomb lattice. Each bond in the lattice is assigned a label $\alpha \in \{x, y, z\}$ and that bond couple two spins along the α axis. See fig. 2.5 for a diagram of the setup.

This gives us the Hamiltonian

$$H = - \sum_{\langle j,k \rangle_\alpha} J^\alpha \sigma_j^\alpha \sigma_k^\alpha, \quad (2.6)$$

where σ_j^α is the α component of a Pauli matrix acting on site j and $\langle j, k \rangle_\alpha$ is a pair of nearest-neighbour indices connected by an α -bond with exchange coupling J^α . Kitaev introduced this model in his seminal 2006 paper [45].

The KH can arise as the result of strong spin-orbit couplings in, for example, the transition metal based compounds [46–50]. The model is highly frustrated: each spin would like to align along a different direction with each of its three neighbours but this cannot be achieved even classically [51, 52]. This frustration leads the model to have a quantum spin liquid (QSL) ground state, a complex many body state with a high degree of entanglement but no long range magnetic order even at zero temperature. While the possibility of a QSL ground state was suggested much earlier [53], the KH model was the first exactly solvable models of the QSL state. The KH model has a rich ground state phase diagram with gapless and gapped phases, the

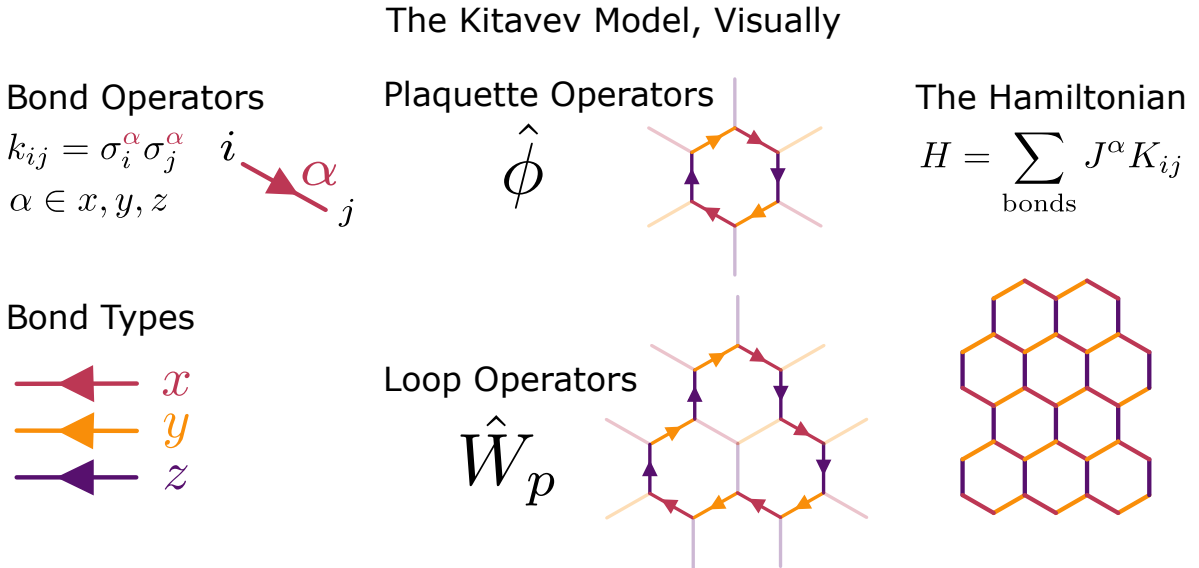


Figure 2.6: A visual introduction to the Kitaev Model.

latter supporting fractionalised quasiparticles with both Abelian and non-Abelian quasiparticle excitations. Anyons have been the subject of much attention because, among other reasons, they can be braided through spacetime to achieve noise tolerant quantum computations [54]. At finite temperature the KH model undergoes a phase transition to a thermal metal state [55]. The KH model can be solved exactly via a mapping to Majorana fermions. This mapping yields an extensive number of static \mathbb{Z}_2 fluxes tied to an emergent gauge field with the remaining fermions governed by a free fermion hamiltonian.

This section will go over the standard model in detail, first discussing [the spin model](#), then detailing the transformation to a [Majorana hamiltonian](#) that allows a full solution while enlarging the Hamiltonian. We will discuss the properties of the [emergent gauge fields](#) and the projector. The [next section](#) will discuss anyons, topology and the Chern number, using the Kitaev model as an explicit example of these topics. Finally we will discuss the ground state found via Lieb's theorem as well as work on generalisations of the ground state to other lattices. Finally we will look at the [phase diagram](#).

2.2.2 The Spin Model

As discussed in the introduction, spin hamiltonians like that of the Kitaev model arise in electronic systems as the result the balance of multiple effects [49]. For instance, in certain transition metal systems with d^5 valence electrons, crystal field and spin-orbit couplings conspire to shift and split the d orbitals into moments with spin $j = 1/2$ and $j = 3/2$. Of these, the bandwidth t of the $j = 1/2$ band is small, meaning that even relatively meagre electron correlations (such those induced by the U term in the Hubbard model) can lead to the opening of a Mott gap. From there we have a $j = 1/2$ Mott insulator whose effective spin-spin interactions are again shaped by the lattice geometry and spin-orbit coupling leading some materials to have strong bond-directional Ising-type interactions [56, 57]. In the Kitaev Model the bond directionality refers to the fact that the coupling axis α in terms like $\sigma_j^\alpha \sigma_k^\alpha$ is strongly bond dependent.

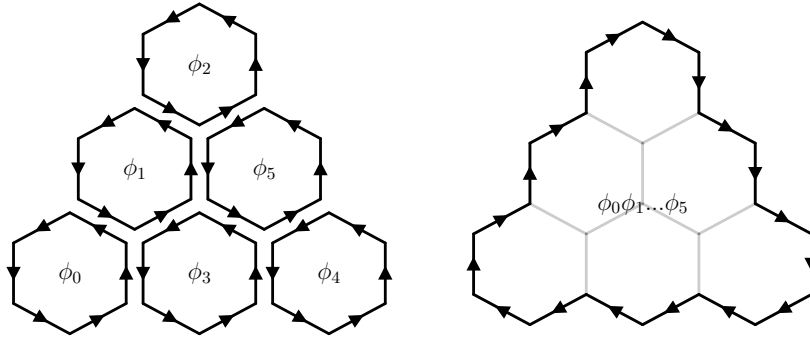


Figure 2.7: In the Kitaev Honeycomb model, Wilson loop operators $\hat{W}_p = \prod_{\langle i,j \rangle_\alpha \in p} \sigma_i^\alpha \sigma_j^\alpha$ can be composed via multiplication to produce arbitrary contractible loops. As a consequence we need only to keep track of the value of the flux through each plaquette ϕ_i . This relationship between the u_{ij} around a region and fluxes with one is evocative of Stokes' theorem for classical electromagnetism. In fact it turns out to be the exponential of it as we shall make explicit later.

In the spin hamiltonian eq. (2.6) we can already tease out a set of conserved fluxes that will be key to the model's solution. These fluxes are the expectations of Wilson loop operators

$$\hat{W}_p = \prod_{\langle i,j \rangle_\alpha \in p} \sigma_i^\alpha \sigma_j^\alpha, \quad (2.7)$$

the products of bonds winding around a closed path p on the lattice. These operators commute with the Hamiltonian and so have no time dynamics. The winding direction does not matter so long as it is fixed. By convention we will always use clockwise. Each closed path on the lattice is associated with a flux. The number of conserved quantities grows linearly with system size and is thus extensive, this is a common property for exactly solvable systems and can be compared to the heavy electrons present in the Falicov-Kimball model. The square of two loop operators is one so any contractible loop can be expressed as a product of loops around plaquettes of the lattice, as in fig. 2.7. For the honeycomb lattice the plaquettes are the hexagons. The expectations of \hat{W}_p through each plaquette, the fluxes, are therefore enough to describe the whole flux sector. We will focus on these fluxes, denoting them by ϕ_i . Once we have made the mapping to the Majorana Hamiltonian I will explain how these fluxes can be connected to an emergent B field which makes their interpretation as fluxes clear.

It is worth noting in passing that the effective Hamiltonian for many Kitaev materials incorporates a contribution from an isotropic Heisenberg term $\sum_{i,j} \vec{\sigma}_i \cdot \vec{\sigma}_j$, this is referred to as the Heisenberg-Kitaev Model [58]. Materials for which the Kitaev term dominates are generally known as Kitaev Materials. See [49] for a full discussion of Kitaev Materials.

As with the Falicov-Kimball model, the KH model has a extensive number of conserved quantities, the fluxes. As with the FK model it will make sense to work in the simultaneous eigenbasis of the fluxes and the Hamiltonian so that we can treat the fluxes like a classical degree of freedom. This is part of what makes the model tractable. We will find that the ground state of the

model corresponds to some particular choice of fluxes. We will refer to local excitations away from the flux ground state as *vortices*. In order to fully solve the model however, we must first move to a Majorana picture.

2.2.3 The Majorana Model

Majorana fermions are something like ‘half of a complex fermion’ and are their own antiparticle. From a set of N fermionic creation f_i^\dagger and annihilation f_i operators we can construct $2N$ Majorana operators c_m . We can do this construction in multiple ways subject to only mild constraints required to keep the overall commutation relations correct [45]. Majorana operators square to one but otherwise have standard fermionic commutation relations.

N spins can be mapped to N fermions with the well known Jordan-Wigner transformation and indeed this approach can be used to solve the Kitaev model [59]. Here I will introduce the method Kitaev used in the original paper as this forms the basis for the results that will be presented in this thesis. Rather than mapping to N fermions, Kitaev maps to $4N$ Majoranas, effectively $2N$ fermions. In contrast to the Jordan-Wigner approach which makes fermions out of strings of spin operators in order to correctly produce fermionic commutation relations, the Kitaev transformation maps each spin locally to four Majoranas. The downside is that this enlarges the Hilbert space from 2^N to 4^N . We will have to employ a projector \hat{P} to come back down to the physical Hilbert space later. As everything is local, I will drop the site indices ijk in expressions that refer to only a single site.

The mapping is defined in terms of four Majoranas per site b_i^x , b_i^y , b_i^z , c_i such that

$$\tilde{\sigma}^x = ib^x c, \quad \tilde{\sigma}^y = ib^y c, \quad \tilde{\sigma}^z = ib^z c \quad (2.8)$$

The tildes on the spin operators $\tilde{\sigma}_i^\alpha$ emphasize that they live in this new extended Hilbert space and are only equivalent to the original spin operators after applying a projector \hat{P} . The form of the projection operator can be understood in a few ways. From a group-theoretic perspective, before projection, the operators $\{\tilde{\sigma}^x, \tilde{\sigma}^y, \tilde{\sigma}^z\}$ form a representation of the gamma group $G_{3,0}$. The gamma groups $G_{p,q}$ have p generators that square to the identity and q that square (roughly) to -1 . The generators otherwise obey standard anticommutation relations. The well known gamma matrices $\{\gamma^0, \gamma^1, \gamma^2, \gamma^3\}$ represent $G_{1,3}$ the quaternions $G_{0,3}$ and the Pauli matrices $G_{3,0}$.

The Pauli matrices, however, have the additional property that the *chiral element* $\sigma^x \sigma^y \sigma^z = i$ is not fully determined by the group properties of $G_{3,0}$ but it is equal to i in the Pauli matrices. Therefore to fully reproduce the algebra of the Pauli matrices we must project into the subspace where $\tilde{\sigma}^x \tilde{\sigma}^y \tilde{\sigma}^z = +i$. The chiral element of the gamma matrices for instance $\gamma_5 = i\gamma^0\gamma^1\gamma^2\gamma^3$ is of central importance in quantum field theory. See [60] for more discussion of this group theoretic view.

So the projector must project onto the subspace where $\tilde{\sigma}^x \tilde{\sigma}^y \tilde{\sigma}^z = i$. If we work this through we find that in general $\tilde{\sigma}^x \tilde{\sigma}^y \tilde{\sigma}^z = iD$ where $D = b^x b^y b^z c$ must be the identity for every site. In other words, we can only work with *physical states* $|\phi\rangle$ that satisfy $D_i |\phi\rangle = |\phi\rangle$ for all sites i . From this we construct an on-site projector $P_i = \frac{1+D_i}{2}$ and the overall projector is simply $P = \prod_i P_i$.

Another way to see what this is doing physically is to explicitly construct the two intermediate fermionic operators f and g that give rise to these four Majoranas. Denoting a fermion state by $|n_f, n_g\rangle$ the Hilbert space is the set $\{|00\rangle, |01\rangle, |10\rangle, |11\rangle\}$. We can map these to Majoranas with, for example, this definition

$$\begin{aligned} b^x &= (f + f^\dagger), \quad b^y = -i(f - f^\dagger), \\ b^z &= (g + g^\dagger), \quad c = -i(g - g^\dagger), \end{aligned} \tag{2.9}$$

Working through the algebra we see that the operator $D = b^x b^y b^z c$ is equal to the fermion parity $D = -(2n_f - 1)(2n_g - 1) = \pm 1$ where n_f, n_g are the number operators. So setting $D = 1$ everywhere is equivalent to restricting to the $\{|01\rangle, |10\rangle\}$ though we could equally well have used the other one.

Expanding the product $\prod_i P_i$ out, we find that the projector corresponds to a symmetrisation over $\{u_{ij}\}$ states within a flux sector and overall fermion parity $\prod_i D_i$. The significance of this is that an arbitrary many body state can be made to have non-zero overlap with the physical subspace via the addition or removal of just a single fermion. This implies that in the thermodynamic limit the projection step is not generally necessary to extract physical results, see [61] or [appendix A.5](#) for more details.

We can now rewrite the spin hamiltonian in Majorana form with the caveat that they are only strictly equivalent after projection. The Ising interactions $\sigma_j^\alpha \sigma_k^\alpha$ decouple into the form $-i(ib_i^\alpha b_j^\alpha)c_i c_j$. We factor out the *bond operators* $\hat{u}_{ij} = ib_i^\alpha b_j^\alpha$ which are Hermitian and, remarkably, commute with the Hamiltonian and each other.

$$\begin{aligned} \tilde{H} &= - \sum_{\langle i,j \rangle_\alpha} J^\alpha \tilde{\sigma}_i^\alpha \tilde{\sigma}_j^\alpha \\ &= i \sum_{\langle i,j \rangle_\alpha} J^\alpha \hat{u}_{ij} \hat{c}_i \hat{c}_j \end{aligned} \tag{2.10}$$

The bond operators \hat{u}_{ij} square to one so have eigenvalues ± 1 . As they're conserved we will work in their eigenbasis and take off the hats in the Hamiltonian.

$$H = i \sum_{\langle i,j \rangle_\alpha} J^\alpha u_{ij} \hat{c}_i \hat{c}_j \tag{2.11}$$

2.2.4 The Fermion Problem

We now have a quadratic Hamiltonian, eq. (2.11), coupled to a classical field u_{ij} . What follows is relatively standard theory for quadratic Hamiltonians [62].

Because of the antisymmetry $J^\alpha u_{ij}$, the eigenvalues of eq. (2.11) come in pairs $\pm \epsilon_m$. We organise the eigenmodes of H into pairs, such that b_m and b'_m have energies ϵ_m and $-\epsilon_m$. The transformation Q

$$(c_1, c_2 \dots c_{2N})Q = (b_1, b'_1, b_2, b'_2 \dots b_N, b'_N) \quad (2.12)$$

puts the Hamiltonian into normal mode form

$$H = \frac{i}{2} \sum_m \epsilon_m b_m b'_m. \quad (2.13)$$

The determinant of Q appears when evaluating the projector explicitly, otherwise, the b_m are merely an intermediate step. From them, we form fermionic operators

$$f_i = \frac{1}{2}(b_m + i b'_m) \quad (2.14)$$

with their associated number operators $n_i = f_i^\dagger f_i$. These let us write the Hamiltonian neatly as

$$H = \sum_m \epsilon_m (n_m - \frac{1}{2}). \quad (2.15)$$

The energy of the ground state $|n_m = 0\rangle$ of the many body system at fixed $\{u_{ij}\}$ is

$$E_0 = -\frac{1}{2} \sum_m \epsilon_m \quad (2.16)$$

and we can construct any state from a particular choice of $n_m = 0, 1$. If we only care about the ground state energy E_0 , it is possible to skip forming the fermionic operators. The eigenvalues obtained directly from diagonalising $J^\alpha u_{ij}$ come in $\pm \epsilon_m$ pairs. We can take half the absolute value of the set to recover $\sum_m \epsilon_m$ directly.

2.2.5 An Emergent Gauge Field

We have transformed the spin Hamiltonian into a Majorana hamiltonian $H = i \sum_{\langle i,j \rangle_\alpha} J^\alpha u_{ij} \hat{c}_i \hat{c}_j$ describing the dynamics of a classical field u_{ij} and Majoranas c_i . It is natural to ask how the classical field u_{ij} relates to the fluxes of the original spin model. We can evaluate the fluxes ϕ_i in terms of the bond operators

$$\phi_i = \prod_{\langle j,k \rangle \in \mathcal{P}_i} i u_{jk}. \quad (2.17)$$

In addition, the bond operators form a highly degenerate description of the system. The operators $D_i = b_i^x b_i^y b_i^z c_i$ commute with H forming a set of local symmetries. The action of D_i on a state is to flip the values of the three u_{ij} bonds that connect to site i . This changes the bond configuration $\{u_{ij}\}$ but leaves the flux configuration $\{\phi_i\}$ unchanged. Physically, we

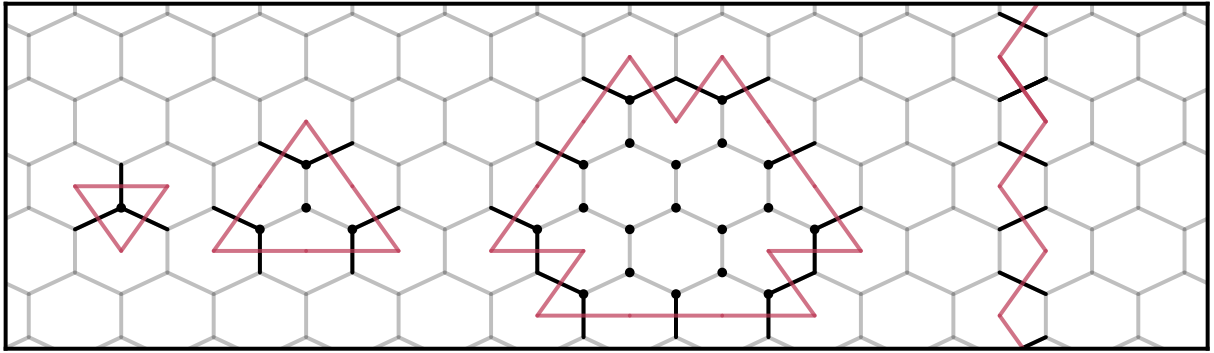


Figure 2.8: A honeycomb lattice with edges in light grey, along with its dual, the triangle lattice in light blue. The vertices of the dual lattice are the faces of the original lattice and, hence, are the locations of the vortices. (Left) The action of the gauge operator D_j at a vertex is to flip the value of the three u_{jk} variables (black lines) surrounding site j . The corresponding edges of the dual lattice (red lines) form a closed triangle. (Middle) Composing multiple adjacent D_j operators produces a large closed dual loop or multiple disconnected dual loops. Dual loops are not directed like Wilson loops. (Right) A non-contractible loop which cannot be produced by composing D_j operators. All three operators can be thought of as the action of a vortex-vortex pair that is created, one of them is transported around the loop, and then the two annihilate again. Note that every plaquette has an even number of u_{ij} s flipped on its edge. Therefore, all retain the same flux ϕ_i .

interpret u_{ij} as a gauge field with a high degree of degeneracy and $\{D_i\}$ as the set of gauge symmetries. The Majorana bond operators u_{ij} are an emergent, classical, \mathbb{Z}_2 gauge field! The flux configuration $\{\phi_i\}$ is what encodes physical information about the system without all the gauge degeneracy.

The ground state of the Kitaev Honeycomb model is the all one flux configuration $\{\phi_i = +1 \forall i\}$. This can be proven via Lieb's theorem [63] which gives the lowest energy magnetic flux configuration for a system of electrons hopping in a magnetic field. Kitaev remarks in his original paper that he was not initially aware of the relevance of Lieb's 1994 result. This is not surprising because at first glance the two models seem quite different but the connection is quite instructive for understanding the Kitaev Model and its generalisations.

Lieb discusses a model of mobile electrons

$$H = \sum_{ij} t_{ij} c_i^\dagger c_j \quad (2.18)$$

where the hopping terms $t_{ij} = |t_{ij}| \exp(i\theta_{ij})$ incorporate Aharonov-Bohm (AB) phases [64] θ_{ij} . The AB phases model the effect of a slowly varying magnetic field on the electrons through the integral of the magnetic vector potential $\theta_{ij} = \int_i^j \vec{A} \cdot d\vec{l}$, a Peierls substitution [65]. If we map the Majorana form of the Kitaev model to Lieb's model we see that our $t_{ij} = iJ^\alpha u_{ij}$. The $i u_{ij} = \pm i$ correspond to AB phases $\theta_{ij} = \pi/2$ or $3\pi/2$ along each bond.

Stokes' theorem tells us that the magnetic flux Q_m through a surface S is related to the line

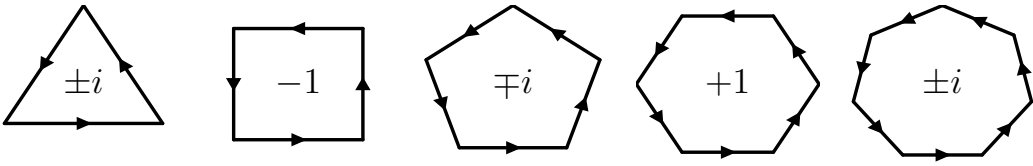


Figure 2.9: Lieb’s theorem gives the ground state flux configuration for even sided plaquettes in systems with at least one translationally invariant direction [63]. These labels correspond to the Kitaev fluxes ϕ_i rather than the magnetic fluxes Q_i of Lieb’s original paper ($\phi_i = \exp\{iQ_i\}$). Other work has extended Lieb’s theorem numerically to arbitrary plaquettes, [66–69]. The additional twofold degeneracy of the $\pm i$, $\mp i$ terms is a consequence of the odd sided plaquettes breaking chiral symmetry. Chiral symmetry is spontaneously broken in the ground state [67].

integral of \vec{A} along the boundary of the surface ∂S which in the discrete case reduces to the sum of the AB phases along the path. We can thus rewrite eq. (2.17) as

$$\begin{aligned} \phi_i &= \prod_{\mathcal{P}_i} i u_{jk} \\ &= \prod_{\mathcal{P}_i} \exp\{i\theta_{jk}\} \\ &= \exp\left(i \sum_{\mathcal{P}_i} \theta_{jk}\right) \\ &= \exp\left(i \oint_{\mathcal{P}_i} \vec{A} \cdot d\vec{l}\right) \\ &= \exp(iQ_i) \end{aligned} \tag{2.19}$$

Thus we can interpret the fluxes ϕ_i as the exponential of magnetic fluxes Q_m of some fictitious gauge field \vec{A} and the bond operators as $iu_{ij} = \exp i \int_i^j \vec{A} \cdot d\vec{l}$. In this analogy to classical electromagnetism, the sets $\{u_{ij}\}$ that correspond to the same $\{\phi_i\}$ are all gauge equivalent as we have already seen via other means. The fact that fluxes can be written as products of bond operators and composed is a consequence of eq. (2.19). If the lattice contains odd plaquettes, as in the Yao-Kivelson model [70], the complex fluxes that appear are a sign that chiral symmetry has been broken.

In full, Lieb’s theorem states that the ground state has magnetic flux $Q_i = \sum_{\mathcal{P}_i} \theta_{ij} = \pi \pmod{2\pi}$ for plaquettes with $0 \pmod{4}$ sides and $0 \pmod{2\pi}$ for plaquettes with $2 \pmod{4}$ sides. In terms of our fluxes, this means $\phi = -1$ for squares, $\phi = 1$ for hexagons and so on.

While Lieb’s theorem is restricted to bipartite lattices with translational symmetry, other works has shown numerically that it tends to hold for more general lattices too [66–69]. From this we find that the generalisation to odd sided plaquettes is similar but with an additional chiral symmetry, so $\phi = \pm i$ for plaquettes with $1 \pmod{4}$ sides and $\mp i$ for those with $3 \pmod{4}$ sides. Overall we can write $\phi = -(\pm i)^{n_{\text{sides}}}$. Later I will present numerical evidence that this rule continues to hold for general amorphous lattices.

Understanding u_{ij} as a gauge field provides another way to understand the action of the pro-

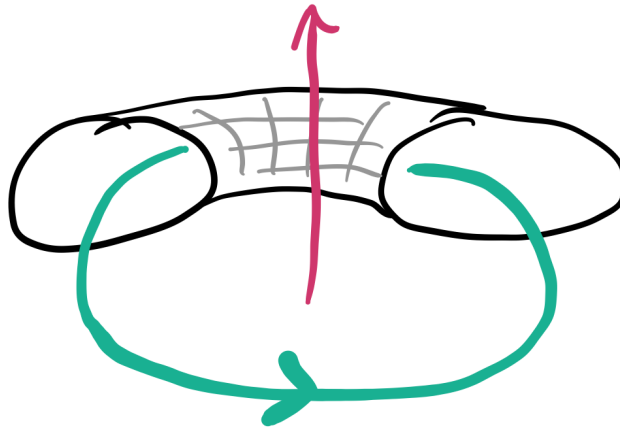


Figure 2.10: Wilson loops that wind the major or minor diameters of the torus measure flux winding through the hole of the doughnut/torus (red) or through the filling (green). If they made doughnuts which had both had a jam filling and a hole, this analogy would be a lot easier to make [71].

jector. The local projector $P_i = \frac{1+D_i}{2}$ applied to a state constructs a superposition of the original state and the gauge equivalent state linked to it by flipping the three u_{ij} around site i . The overall projector $P = \prod_i P_i$ can thus be understood as a symmetrisation over all gauge equivalent states, removing the gauge degeneracy introduced by the mapping from spins to Majoranas.

A final but important point to mention is that the local fluxes ϕ_i are not quite all there is. We've seen that products of ϕ_i can be used to construct the flux associated with arbitrary contractible loops. On the plane contractible loops are all there is. However, on the torus we can construct two global fluxes Φ_x and Φ_y which correspond to paths tracing the major and minor axes. The four sectors spanned by the ± 1 values of these fluxes are gapped away from one another but only by virtual tunnelling processes so the gap decays exponentially with system size [45]. Physically Φ_x and Φ_y could be thought of as measuring the flux that threads through the hole of the doughnut. In general, surfaces with genus g have g ‘handles’ and $2g$ of these global fluxes. At first glance it may seem this would not have much relevance to physical realisations of the Kitaev model that will likely have a planar geometry with open boundary conditions. However these fluxes are closely linked to topology and the existence of anyonic quasiparticle excitations in the model, which we will discuss next.

2.2.6 Anyons, Topology and the Chern number

To discuss different ground state phases of the KH model we must first review the topic of anyons and topology. The standard argument for the existence of Fermions and Bosons goes like this: the quantum state of a system must pick up a factor of ± 1 if two identical particles are swapped. Only ± 1 are allowed since swapping twice must correspond to the identity. This argument works in three dimensions for states without topological degeneracy, which seems to be true of the real world, but condensed matter systems are subject to no such constraints.

In gapped condensed matter systems, all equal time correlators decay exponentially with dis-

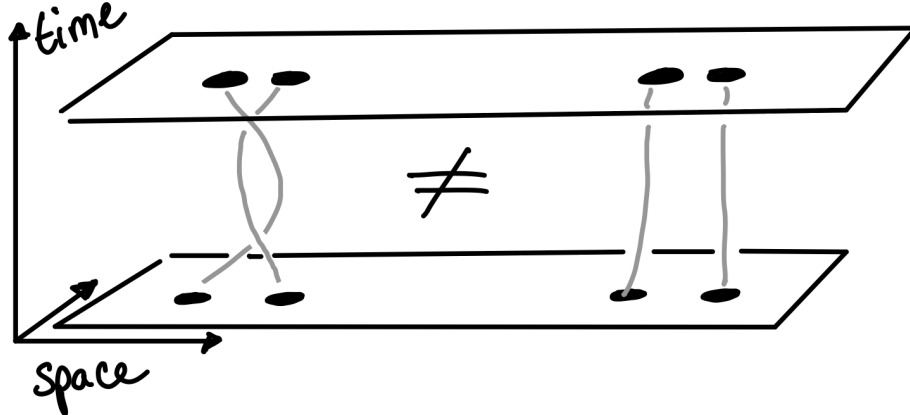


Figure 2.11: Worldlines of particles in two dimensions can become tangled or *braided* with one another.

tance [72]. Put another way, gapped systems support quasiparticles with a definite location in space and finite extent. As such it is meaningful to consider what would happen to the overall quantum state if we were to adiabatically carry out a series of swaps as described above. This is known as braiding. Recently, braiding in topological systems has attracted interest because of proposals to use ground state degeneracy to implement both passively fault tolerant and actively stabilised quantum computations [73–75].

First we realise that in two dimensions, swapping identical particles twice is not topologically equivalent to the identity, see fig. 2.11. Instead it corresponds to encircling one particle around the other. This means we can in general pick up any complex phase $e^{i\theta}$, hence the name **any**-ons upon exchange. These are known as Abelian anyons because complex multiplication commutes and hence the group of braiding operations forms an Abelian group.

The KH model has a topologically degenerate ground state with sectors labelled by the values of the topological fluxes (Φ_x, Φ_y). Consider the operation in which a quasiparticle pair is created from the ground state, transported around one of the non-contractible loops and then annihilated together, call them \mathcal{T}_x and \mathcal{T}_y . These operations move the system around within the ground state manifold and they need not commute. This leads to non-Abelian anyons. As Kitaev points out, these operations are not specific to the torus: the operation $\mathcal{T}_x \mathcal{T}_y \mathcal{T}_x^{-1} \mathcal{T}_y^{-1}$ corresponds to an operation in which none of the particles crosses the torus, rather one simply winds around the other, hence these effects are relevant even for the planar case.

In condensed matter systems, the existence of anyonic excitations automatically implies the system has topological ground state degeneracy on the torus [76] and indeed anyons and topology are intimately linked [77–79]. The Chern number ν , a concept originally used to describe complex vector bundles in algebraic topology [80], has found use in physics as a powerful diagnostic tool for topological systems. Kitaev showed that there is a full classification of anyonic statistics in terms of ν (mod 16) but relevant to us is that vortices in the KH model are Abelian when the Chern number is even and non-Abelian when the Chern number is odd. Non-Abelian statistics of the vortices in the KH model arise due to unpaired Majorana modes that are bound to them.

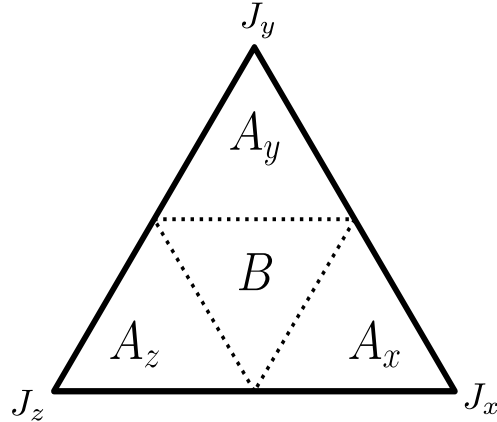


Figure 2.12: Setting the energy scale of the Kitaev Model with the constraint that $J_x + J_y + J_z = 1$ yields a triangular phase diagram where each of the corners represents $J_\alpha = 1$. For each corner α the region $|J_\alpha| > |J_\beta| + |J_\gamma|$ supports a gapped non-Abelian phase equivalent to that of the Toric code [73, 81]. The point around equal coupling $J_x = J_y = J_z$, the B phase, is gapless. The B phase is known a Majorana metal and on the honeycomb lattice it has a Dirac cone dispersion similar to that of graphene.

2.2.7 Ground State Phases

Setting the overall energy scale with the constraint $J_x + J_y + J_z = 1$ yields a triangular phase diagram. In each of the corners one of the spin-coupling directions dominates, $|J_\alpha| > |J_\beta| + |J_\gamma|$, yielding three equivalent A_α phases while the central triangle around $J_x = J_y = J_z$ is called the B phase. Both phases support two kinds of quasiparticles, fermions and \mathbb{Z}_2 -vortices. In the A phases, the vortices have bosonic statistics with respect to themselves but act like fermions with respect to the fermions, hence they are Abelian anyons. This phase has the same anyonic structure as the Toric code [73]. The B phase can be described as a semi-metal of the Majorana fermions [49]. Since the B phase is gapless, the quasiparticles aren't localised and so don't have braiding statistics.

An external magnetic can be used to break chiral symmetry. The lowest order term that breaks chiral symmetry but retains the solvability of the model is the three spin term

$$\sum_{(i,j,k)} \sigma_i^\alpha \sigma_j^\beta \sigma_k^\gamma \quad (2.20)$$

where the sum (i, j, k) runs over consecutive indices around plaquettes. The addition of this to the spin model leads to two bond terms in the corresponding Majorana model. The effect of breaking chiral symmetry is to open a gap in the B phase. The vortices of the gapped B phase are non-Abelian anyons. This phase has the same anyonic exchange statistics as $p_x + ip_y$ superconductor [82], the Moore-Read state for the $\nu = 5/2$ fractional quantum Hall state [83] and many other systems [84–88]. Collectively these systems have attracted interest as possible physical realisations for braiding based quantum computers.

At finite temperatures, recent work has shown that the KH model undergoes a transition to a thermal metal phase.

To surmise, the Kitaev Honeycomb model is remarkable because it combines three key properties. First, the form of the Hamiltonian plausibly be realised by a real material. Candidate materials, such as α -RuCl₃, are known to have sufficiently strong spin-orbit coupling and the correct lattice structure to behave according to the Kitaev Honeycomb model with small corrections [49, 89]. Second, its ground state is the canonical example of the long sought after quantum spin liquid state, its dynamical spin-spin correlation functions are zero beyond nearest neighbour separation [90]. Its excitations are anyons, particles that can only exist in two dimensions that break the normal fermion/boson dichotomy.

Third, and perhaps most importantly, this model is a rare many body interacting quantum system that can be treated analytically. It is exactly solvable. We can explicitly write down its many body ground states in terms of single particle states [45]. The solubility of the Kitaev Honeycomb Model, like the Falicov-Kimball model of chapter 1, comes about because the model has extensively many conserved degrees of freedom. These conserved quantities can be factored out as classical degrees of freedom, leaving behind a non-interacting quantum model that is easy to solve.

2.3 Disorder and Localisation

Disorder is a fact of life for the condensed matter physicist. No sample will ever be completely free of contamination or of structural defects. The classical Drude theory of electron conductivity envisages electrons as scattering off impurities. In this model one would expect the electrical conductivity to be proportional to the mean free path [91], decreasing smoothly as the number of defects increases. However, Anderson in 1958 [16] showed that in a simple model, there is some critical level of disorder at which **all** single particle eigenstates localise.

What would later be known as Anderson localisation is characterised by exponentially localised eigenfunctions $\psi(x) \sim e^{-x/\lambda}$ which cannot contribute to transport processes. The localisation length λ is the typical scale of localised states and can be extracted with transmission matrix methods [92]. Anderson localisation provided a different kind of insulator to that of the band insulator.

The Anderson model is about the simplest model of disorder one could imagine

$$H = -t \sum_{\langle jk \rangle} c_j^\dagger c_k + \sum_j V_j c_j^\dagger c_j. \quad (2.21)$$

It is one of non-interacting fermions subject to a disorder potential V_j drawn uniformly from the interval $[-W, W]$. The discovery of localisation in quantum systems was surprising at the time given the seeming ubiquity of extended Bloch states. Within the Anderson model, all the states localise at the same disorder strength W . Later Mott showed that in other contexts extended Bloch states and localised states can coexist at the same disorder strength but at different energies. The transition in energy between localised and extended states is known as a mobility edge [93].

Localisation phenomena are strongly dimension dependent. In three dimensions the scaling theory of localisation [21, 94] shows that Anderson localisation is a critical phenomenon with critical exponents both for how the conductivity vanishes with energy when approaching the mobility edge and for how the localisation length increases below it. By contrast, in one dimension disorder generally dominates. Even the weakest disorder exponentially localises *all* single particle eigenstates in the one dimensional Anderson model. Only long-range spatial correlations of the disorder potential can induce delocalisation [22–24, 95–97].

Later localisation was found in disordered interacting many-body systems:

$$H = -t \sum_{\langle jk \rangle} c_j^\dagger c_k + \sum_j V_j c_j^\dagger c_j + U \sum_{jk} n_j n_k \quad (2.22)$$

Here, in contrast to the Anderson model, localisation phenomena are robust to weak perturbations of the Hamiltonian. This is called many-body localisation (MBL) [98, 99].

Both MBL and Anderson localisation depend crucially on the presence of *quenched* disorder. Quenched disorder takes the form a static background field drawn from an arbitrary probability distribution to which the model is coupled. Disorder may also be introduced into the initial state of the system rather than the Hamiltonian. This has led to ongoing interest in the possibility of disorder-free localisation where the disorder is instead *annealed*. In this scenario the disorder

necessary to generate localisation is generated entirely from the thermal fluctuations of the model.

The concept of disorder-free localisation was first proposed in the context of Helium mixtures [100] and then extended to heavy-light mixtures in which multiple species with large mass ratios interact. The idea is that the heavier particles act as an effective disorder potential for the lighter ones, inducing localisation. Two such models [101, 102] instead find that the models thermalise exponentially slowly in system size, which Ref. [101] dubs Quasi-MBL.

True disorder-free localisation does occur in exactly solvable models with extensively many conserved quantities [6]. As conserved quantities have no time dynamics this can be thought of as taking the separation of timescales to the infinite limit. The localisation phenomena present in the Falicov-Kimball model are instead the result of annealed disorder. A strong separation of timescales means that the heavy species is approximated as immobile with respect to the lighter itinerant species. At finite temperature the heavy species acts as a disorder potential for the lighter one. However, in contrast to quenched disorder, the probability distribution of annealed disorder is entirely determined by the thermodynamics of the Hamiltonian. In the two dimensional FK model this leads to multiple phases where localisation effects are relevant. At low temperatures the heavy species orders to a symmetry broken CDW phase, leading to a traditional band gap insulator. At higher temperatures however thermal disorder causes the light species to localise. At weak coupling, the localisation length can be very large, so finite sized systems may still conduct, an effect known as weak localisation [14].

In Chapter 3 we will consider a generalised FK model in one dimension and study how the disorder generated near a one dimensional thermodynamic phase transition interacts with localisation physics.

2.3.1 Topological Disorder

So far we have considered disorder as a static or dynamic field coupled to a model defined on a translation invariant lattice. Another kind of disordered system that worthy of study are amorphous systems. Amorphous systems have disordered bond connectivity, so called *topological disorder*. As discussed in the introduction these include amorphous semiconductors such as amorphous Germanium and Silicon [103–106]. While materials do not have long range lattice structure they can enforce local constraints such as the approximate coordination number $z = 4$ of silicon.

Topological disorder can be qualitatively different from other disordered systems. Disordered graphs are constrained by fixed coordination number and the Euler equation. A standard method for generating such graphs with coordination number $d + 1$ is Voronoi tessellation [107, 108]. The Harris [109] and the Imry-Mar [110] criteria are key results on the effect of disorder on thermodynamic phase transitions. The Harris criterion signals when disorder will affect the universality of a thermodynamic critical point while the Imry-Ma criterion simply forbids the formation of long range ordered states in $d \leq 2$ dimensions in the presence of disorder. Both these criteria are modified for the case of topological disorder. This is because the Euler equation and vertex degree constraints lead to strong anti-correlations which mean that topological disorder is effectively weaker than standard disorder in two dimensions [111, 112]. This does

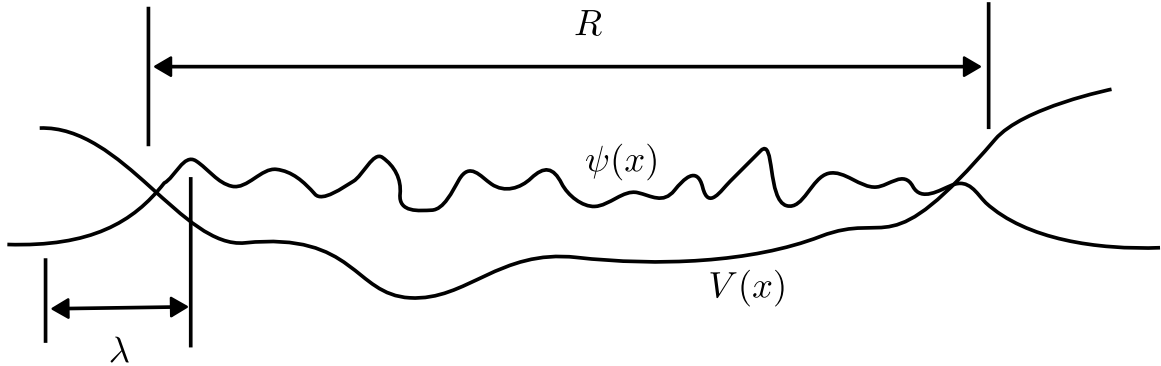


Figure 2.13: A localised state ψ in a potential well that has formed from random fluctuations in the disorder potential $V(x)$. The localisation length λ governs how quickly the state decays away from the well while the diameter R of the state is controlled by the size of the well. Reproduced from [21].

not apply to three dimensional Voronoi lattices where the Euler equation contains an extra volume term and so is effectively a weaker constraint.

Lastly it is worth exploring how quantum spin liquids and disorder interact. The KH model has been studied subject to both flux [113] and bond [114] disorder. In some instances it seems that disorder can even promote the formation of a QSL ground state [115]. It has also been shown that the KH model exhibits disorder free localisation after a quantum quench [116].

In chapter 4 we will put the Kitaev model onto two dimensional Voronoi lattices and show that much of the rich character of the model is preserved despite the lack of long range order.

2.3.2 Diagnosing Localisation in practice

Looking at practical tools for diagnosing localisation, there are a few standard methods [21].

The most direct method would be to fit a function of the form $\psi(x) = f(x)e^{-|x-x_0|/\lambda}$ to each single particle wavefunction to extract the localisation length λ . This method is little used in practice since it requires storing and processing full wavefunctions which quickly becomes expensive for large systems.

For low dimensional systems with quenched disorder, transfer matrix methods can be used to directly extract the localisation length. These work by turning the time independent Schrödinger equation $\hat{H}|\psi\rangle = E|\psi\rangle$ into a matrix equation linking the amplitude of ψ on each $d - 1$ dimensional slice of the system to the next and looking at average properties of this transmission matrix. This method is less useful for systems like the FK model where the disorder as a whole must be sampled from the thermodynamic ensemble. It is also problematic for the Kitaev

Model on an amorphous lattice as the slicing procedure is complex to define in the absence of a regular lattice.

A more versatile method is based on the inverse participation ratio (IPR). The IPR is defined for a normalised wave function $\psi_i = \psi(x_i)$, $\sum_i |\psi_i|^2 = 1$ as its fourth moment [21]:

$$P^{-1} = \sum_i |\psi_i|^4 \quad (2.23)$$

The name derive from the fact that this operator acts as a measure of the volume where the wavefunction is significantly different from zero. They can alternatively be thought of as providing a measure of the average diameter R from $R = P^{1/d}$. See fig. 2.13 for the distinction between R and λ .

For localised states, the *inverse* participation ratio P^{-1} is independent of system size while for plane wave states in d dimensions $P^{-1} = L^{-d}$. States may also be intermediate between localised and extended, described by their fractal dimensionality $d > d^* > 0$:

$$P(L)^{-1} \sim L^{-d^*} \quad (2.24)$$

Such intermediate states tend to appear as critical phenomena near mobility edges [117]. For finite size systems, these relations only hold once the system size L is much greater than the localisation length. When the localisation length is comparable to the system size the states still contribute to transport, this is the aforementioned weak localisation effect [118, 119].

In both chapters to follow I will use an energy resolved IPR

$$\begin{aligned} DOS(\omega) &= \sum_n \delta(\omega - \epsilon_n) \\ IPR(\omega) &= DOS(\omega)^{-1} \sum_{n,i} \delta(\omega - \epsilon_n) |\psi_{n,i}|^4 \end{aligned} \quad (2.25)$$

Where $\psi_{n,i}$ is the wavefunction corresponding to the energy ϵ_n at the i th site. In practice I bin the energies and IPRs into a fine energy grid and use the mean within each bin.

Chapter Summary

In this chapter we have covered the Falicov-Kimball model, the Kitaev Honeycomb model and the theory of disorder and localisation. We saw that the FK model is one of immobile species (spins) interacting with an itinerant quantum species (electrons). While the KH model is specified in terms of spins on a honeycomb lattice interacting via a highly anisotropic Ising coupling, it can be transformed into one of Majorana fermions interacting with a classical gauge field that supports immobile flux excitations. In each case it is the immobile species that makes each model exactly solvable. Both models have rich ground state and thermodynamic phase diagrams. The last part of this chapter dealt with disorder and how it almost inevitably leads to localisation. Both the FK and KH models are effectively disordered at finite temperatures by their immobile species. In the next chapter we will look at a version of the FK model in one

dimension augmented with long range interactions in order to retain its ordered phase. The model is translation invariant but we will see that it exhibits disorder free localisation. After that we will look at the KH model defined on an amorphous lattice with vertex degree $z = 3$.

References

- [1] Hubbard, J., “Electron correlations in narrow energy bands”, *Proceedings of the Royal Society of London. Series A. Mathematical and Physical Sciences* **276**, 238–257 (1963) 10.1098/rspa.1963.0204 (cit. on p. 25).
- [2] L. M. Falicov and J. C. Kimball, “Simple Model for Semiconductor-Metal Transitions: Sm $\{\backslash\mathrm{B}\}_{-6}$ and Transition-Metal Oxides”, *Phys. Rev. Lett.* **22**, 997–999 (1969) 10.1103/PhysRevLett.22.997 (cit. on p. 25).
- [3] C. Gruber and N. Macris, “The Falicov-Kimball model: A review of exact results and extensions”, *Helvetica Physica Acta* **69** (1996) (cit. on p. 25).
- [4] C. Gruber and D. Ueltschi, “The Falicov-Kimball model”, in *Encyclopedia of mathematical physics. 1, 1*, (Elsevier, Amsterdam, 2006) (cit. on p. 25).
- [5] P. de Vries, K. Michielsen, and H. De Raedt, “The simplified Hubbard model in one and two dimensions”, *Z. Physik B - Condensed Matter* **92**, 353–362 (1993) 10.1007/BF01308754 (cit. on p. 25).
- [6] A. Smith, J. Knolle, D. L. Kovrizhin, and R. Moessner, “Disorder-Free Localization”, *Phys. Rev. Lett.* **118**, 266601 (2017) 10.1103/PhysRevLett.118.266601 (cit. on pp. 25, 44).
- [7] J. Jedrzejewski and R. Lemanski, “Falicov–Kimball Models of Collective Phenomena in Solids (A Concise Guide)”, *Acta Physica Polonica B* **32**, 3243 (2001), <http://adsabs.harvard.edu/abs/2001AcPPB..32.3243J> (visited on 09/18/2020) (cit. on p. 25).
- [8] C. Gruber, J. Iwanski, J. Jedrzejewski, and P. Lemberger, “Ground states of the spinless Falicov-Kimball model”, *Phys. Rev. B* **41**, 2198–2209 (1990) 10.1103/PhysRevB.41.2198 (cit. on p. 25).
- [9] C. Gruber and D. Ueltschi, “The Falicov-Kimball model”, Feb. 16, 2005, arXiv:math-ph/0502041, <http://arxiv.org/abs/math-ph/0502041> (visited on 07/01/2019) (cit. on p. 25).
- [10] A. E. Antipov, E. Gull, and S. Kirchner, “Critical Exponents of Strongly Correlated Fermion Systems from Diagrammatic Multiscale Methods”, *Phys. Rev. Lett.* **112**, 226401 (2014) 10.1103/PhysRevLett.112.226401 (cit. on pp. 26–27).
- [11] T. Ribic, G. Rohringer, and K. Held, “Nonlocal correlations and spectral properties of the Falicov-Kimball model”, *Phys. Rev. B* **93**, 195105 (2016) 10.1103/PhysRevB.93.195105, arXiv:1602.07161 (cit. on p. 26).
- [12] J. K. Freericks and V. Zlatić, “Exact dynamical mean-field theory of the Falicov-Kimball model”, *Rev. Mod. Phys.* **75**, 1333–1382 (2003) 10.1103/RevModPhys.75.1333 (cit. on p. 26).
- [13] A. J. Herrmann, N. Tsuji, M. Eckstein, and P. Werner, “Nonequilibrium Dynamical Cluster Approximation study of the Falicov-Kimball Model”, *Phys. Rev. B* **94**, 245114 (2016) 10.1103/PhysRevB.94.245114, arXiv:1609.04708 (cit. on p. 26).
- [14] A. E. Antipov, Y. Javanmard, P. Ribeiro, and S. Kirchner, “Interaction-Tuned Anderson versus Mott Localization”, *Phys. Rev. Lett.* **117**, 146601 (2016) 10.1103/PhysRevLett.117.146601 (cit. on pp. 27, 44).

- [15] M. M. Maśka and K. Czajka, “Thermodynamics of the two-dimensional Falicov-Kimball model: A classical Monte Carlo study”, *Phys. Rev. B* **74**, 035109 (2006) 10.1103 / PhysRevB.74.035109, arXiv:cond-mat/0504533 (cit. on p. 26).
- [16] P. W. Anderson, “Absence of Diffusion in Certain Random Lattices”, *Phys. Rev.* **109**, 1492–1505 (1958) 10.1103/PhysRev.109.1492 (cit. on pp. 26, 43).
- [17] U. Brandt and C. Mielsch, “Thermodynamics and correlation functions of the Falicov-Kimball model in large dimensions”, *Z. Physik B - Condensed Matter* **75**, 365–370 (1989) 10.1007/BF01321824 (cit. on p. 26).
- [18] E. H. Lieb and F. Y. Wu, “Absence of Mott Transition in an Exact Solution of the Short-Range, One-Band Model in One Dimension”, *Phys. Rev. Lett.* **20**, 1445–1448 (1968) 10.1103/PhysRevLett.20.1445 (cit. on p. 27).
- [19] I. Y. Gol’dshtain, S. A. Molchanov, and L. A. Pastur, “A pure point spectrum of the stochastic one-dimensional schrödinger operator”, *Funct Anal Its Appl* **11**, 1–8 (1977) 10.1007/BF01135526 (cit. on p. 27).
- [20] E. Abrahams, P. W. Anderson, D. C. Licciardello, and T. V. Ramakrishnan, “Scaling Theory of Localization: Absence of Quantum Diffusion in Two Dimensions”, *Phys. Rev. Lett.* **42**, 673–676 (1979) 10.1103/PhysRevLett.42.673 (cit. on p. 27).
- [21] B. Kramer and A. MacKinnon, “Localization: theory and experiment”, *Rep. Prog. Phys.* **56**, 1469–1564 (1993) 10.1088/0034-4885/56/12/001 (cit. on pp. 27, 43, 45–46).
- [22] S. Aubry and G. André, “Analyticity breaking and Anderson localization in incommensurate lattices”, Proceedings, VIII International Colloquium on Group-Theoretical Methods in Physics **3**, 18 (1980) (cit. on pp. 27, 43).
- [23] S. Das Sarma, S. He, and X. C. Xie, “Localization, mobility edges, and metal-insulator transition in a class of one-dimensional slowly varying deterministic potentials”, *Phys. Rev. B* **41**, 5544–5565 (1990) 10.1103/PhysRevB.41.5544 (cit. on pp. 27, 43).
- [24] D. H. Dunlap, H.-L. Wu, and P. W. Phillips, “Absence of localization in a random-dimer model”, *Phys. Rev. Lett.* **65**, 88–91 (1990) 10.1103/PhysRevLett.65.88 (cit. on pp. 27, 43).
- [25] R. Peierls, “On Ising’s model of ferromagnetism”, *Mathematical Proceedings of the Cambridge Philosophical Society* **32**, 477–481 (1936) 10.1017/S0305004100019174 (cit. on pp. 27–28).
- [26] T. Kennedy and E. H. Lieb, “An itinerant electron model with crystalline or magnetic long range order”, *Physica A: Statistical Mechanics and its Applications* **138**, 320–358 (1986) 10.1016/0378-4371(86)90188-3 (cit. on pp. 27–28).
- [27] T. Kasuya, “A Theory of Metallic Ferro- and Antiferromagnetism on Zener’s Model”, *Prog Theor Phys* **16**, 45–57 (1956) 10.1143/PTP.16.45 (cit. on p. 27).
- [28] M. A. Ruderman and C. Kittel, “Indirect Exchange Coupling of Nuclear Magnetic Moments by Conduction Electrons”, *Phys. Rev.* **96**, 99–102 (1954) 10.1103/PhysRev.96.99 (cit. on p. 27).
- [29] J. H. Van Vleck, “Note on the Interactions between the Spins of Magnetic Ions or Nuclei in Metals”, *Rev. Mod. Phys.* **34**, 681–686 (1962) 10.1103/RevModPhys.34.681 (cit. on p. 27).
- [30] K. Yosida, “Magnetic Properties of Cu-Mn Alloys”, *Phys. Rev.* **106**, 893–898 (1957) 10.1103/PhysRev.106.893 (cit. on p. 27).

- [31] T. M. Rusin and W. Zawadzki, “On calculation of RKKY range function in one dimension”, *Journal of Magnetism and Magnetic Materials* **441**, 387–391 (2017) 10.1016/j.jmmm.2017.06.007, arXiv:1701.06198 (cit. on p. 27).
- [32] D. J. Thouless, “Long-Range Order in One-Dimensional Ising Systems”, *Phys. Rev.* **187**, 732–733 (1969) 10.1103/PhysRev.187.732 (cit. on pp. 27, 29).
- [33] R. J. Bursill, “One dimensional continuum Falicov-Kimball model in the strongly correlated limit”, *Physica A: Statistical Mechanics and its Applications* **206**, 521–543 (1994) 10.1016/0378-4371(94)90322-0 (cit. on p. 27).
- [34] C. Gruber, J. L. Lebowitz, and N. Macris, “Ground-State Energy and Low-Temperature Behavior of the One-Dimensional Falicov-Kimball Model”, *EPL* **21**, 389–394 (1993) 10.1209/0295-5075/21/4/002 (cit. on p. 27).
- [35] J. K. Freericks and L. M. Falicov, “Two-state one-dimensional spinless Fermi gas”, *Phys. Rev. B* **41**, 2163–2172 (1990) 10.1103/PhysRevB.41.2163 (cit. on p. 27).
- [36] C. Micheletti, A. B. Harris, and J. M. Yeomans, “A complete devil’s staircase in the Falicov-Kimball model”, *J. Phys. A: Math. Gen.* **30**, L711–L717 (1997) 10.1088/0305-4470/30/21/002, arXiv:cond-mat/9612137 (cit. on p. 27).
- [37] F. J. Dyson, “Existence of a phase-transition in a one-dimensional Ising ferromagnet”, *Commun. Math. Phys.* **12**, 91–107 (1969) 10.1007/BF01645907 (cit. on p. 29).
- [38] D. Ruelle, “Statistical mechanics of a one-dimensional lattice gas”, *Comm. Math. Phys.* **9**, 267–278 (1968), <https://mathscinet.ams.org/mathscinet-getitem?mr=0234697> (visited on 01/28/2019) (cit. on p. 29).
- [39] H. J. Lipkin, N. Meshkov, and A. J. Glick, “Validity of many-body approximation methods for a solvable model. (I). Exact solutions and perturbation theory”, *Nuclear Physics* **62**, 188–198 (1965) 10.1016/0029-5582(65)90862-X (cit. on p. 29).
- [40] D. H. E. Gross, “Non-extensive Hamiltonian systems follow Boltzmann’s principle not Tsallis statistics. – Phase Transitions, Second Law of Thermodynamics”, *Physica A: Statistical Mechanics and its Applications* **305**, 99–105 (2002) 10.1016/S0378-4371(01)00646-X, arXiv:cond-mat/0106496 (cit. on p. 29).
- [41] J. F. Lutsko and J. P. Boon, “Questioning the validity of non-extensive thermodynamics for classical Hamiltonian systems”, *EPL* **95**, 20006 (2011) 10.1209/0295-5075/95/20006 (cit. on p. 29).
- [42] Q. A. Wang, “Comment on ‘Nonextensive hamiltonian systems follow Boltzmann’s principle not Tsallis statistics-phase transition, second law of thermodynamics’ by Gross”, 2003, <https://hal.archives-ouvertes.fr/hal-00009462> (visited on 08/26/2022) (cit. on p. 29).
- [43] M. E. Fisher, S.-k. Ma, and B. G. Nickel, “Critical Exponents for Long-Range Interactions”, *Phys. Rev. Lett.* **29**, 917–920 (1972) 10.1103/PhysRevLett.29.917 (cit. on p. 29).
- [44] M. C. Angelini, G. Parisi, and F. Ricci-Tersenghi, “Relations between short-range and long-range Ising models”, *Phys. Rev. E* **89**, 062120 (2014) 10.1103/PhysRevE.89.062120 (cit. on p. 30).
- [45] A. Kitaev, “Anyons in an exactly solved model and beyond”, *Annals of Physics*, January Special Issue **321**, 2–111 (2006) 10.1016/j.aop.2005.10.005 (cit. on pp. 31, 34, 39, 42).

- [46] G. Jackeli and G. Khaliullin, “Mott insulators in the strong spin-orbit coupling limit: from Heisenberg to a quantum compass and Kitaev models”, *Physical Review Letters* **102**, 017205 (2009) [10.1103/PhysRevLett.102.017205](https://doi.org/10.1103/PhysRevLett.102.017205) (cit. on p. 31).
- [47] M. Hermanns, I. Kimchi, and J. Knolle, “Physics of the kitaev model: Fractionalization, dynamic correlations, and material connections”, *Annual Review of Condensed Matter Physics* **9**, 17–33 (2018) [10.1146/annurev-conmatphys-033117-053934](https://doi.org/10.1146/annurev-conmatphys-033117-053934) (cit. on p. 31).
- [48] S. M. Winter et al., “Models and materials for generalized Kitaev magnetism”, *Journal of Physics: Condensed Matter* **29**, 493002 (2017) (cit. on p. 31).
- [49] S. Trebst and C. Hickey, “Kitaev materials”, *Physics Reports, Kitaev Materials* **950**, 1–37 (2022) [10.1016/j.physrep.2021.11.003](https://doi.org/10.1016/j.physrep.2021.11.003) (cit. on pp. 31–33, 41–42).
- [50] H. Takagi et al., “Concept and realization of Kitaev quantum spin liquids”, *Nature Reviews Physics* **1**, 264–280 (2019) (cit. on p. 31).
- [51] S. Chandra, K. Ramola, and D. Dhar, “Classical Heisenberg spins on a hexagonal lattice with Kitaev couplings”, *Phys. Rev. E* **82**, 031113 (2010) [10.1103/PhysRevE.82.031113](https://doi.org/10.1103/PhysRevE.82.031113) (cit. on p. 31).
- [52] E. Sela, H.-C. Jiang, M. H. Gerlach, and S. Trebst, “Order-by-disorder and spin-orbital liquids in a distorted Heisenberg-Kitaev model”, *Phys. Rev. B* **90**, 035113 (2014) [10.1103/PhysRevB.90.035113](https://doi.org/10.1103/PhysRevB.90.035113) (cit. on p. 31).
- [53] P. W. Anderson, “Resonating valence bonds: A new kind of insulator?”, *Materials Research Bulletin* **8**, 153–160 (1973) [10.1016/0025-5408\(73\)90167-0](https://doi.org/10.1016/0025-5408(73)90167-0) (cit. on p. 31).
- [54] M. Freedman, A. Kitaev, M. Larsen, and Z. Wang, “Topological quantum computation”, *Bull. Amer. Math. Soc.* **40**, 31–38 (2003) [10.1090/S0273-0979-02-00964-3](https://doi.org/10.1090/S0273-0979-02-00964-3) (cit. on p. 32).
- [55] C. N. Self, J. Knolle, S. Iblisdir, and J. K. Pachos, “Thermally induced metallic phase in a gapped quantum spin liquid - a Monte Carlo study of the Kitaev model with parity projection”, *Phys. Rev. B* **99**, 045142 (2019) [10.1103/PhysRevB.99.045142](https://doi.org/10.1103/PhysRevB.99.045142), arXiv:1807.07926 [cond-mat, physics:quant-ph] (cit. on p. 32).
- [56] G. Jackeli and G. Khaliullin, “Mott Insulators in the Strong Spin-Orbit Coupling Limit: From Heisenberg to a Quantum Compass and Kitaev Models”, *Phys. Rev. Lett.* **102**, 017205 (2009) [10.1103/PhysRevLett.102.017205](https://doi.org/10.1103/PhysRevLett.102.017205) (cit. on p. 32).
- [57] G. Khaliullin, “Orbital Order and Fluctuations in Mott Insulators”, *Progress of Theoretical Physics Supplement* **160**, 155–202 (2005) [10.1143/PTPS.160.155](https://doi.org/10.1143/PTPS.160.155) (cit. on p. 32).
- [58] J. Chaloupka, G. Jackeli, and G. Khaliullin, “Kitaev-Heisenberg Model on a Honeycomb Lattice: Possible Exotic Phases in Iridium Oxides $\{A\}_2\{\mathrm{IrO}\}_3$ ”, *Phys. Rev. Lett.* **105**, 027204 (2010) [10.1103/PhysRevLett.105.027204](https://doi.org/10.1103/PhysRevLett.105.027204) (cit. on p. 33).
- [59] H.-D. Chen and Z. Nussinov, “Exact results of the Kitaev model on a hexagonal lattice: spin states, string and brane correlators, and anyonic excitations”, *J. Phys. A: Math. Theor.* **41**, 075001 (2008) [10.1088/1751-8113/41/7/075001](https://doi.org/10.1088/1751-8113/41/7/075001) (cit. on p. 34).
- [60] M. Petitjean, “Chirality of Dirac Spinors Revisited”, *Symmetry* **12**, 616 (2020) [10.3390/sym12040616](https://doi.org/10.3390/sym12040616) (cit. on p. 34).
- [61] F. L. Pedrocchi, S. Chesi, and D. Loss, “Physical solutions of the Kitaev honeycomb model”, *Phys. Rev. B* **84**, 165414 (2011) [10.1103/PhysRevB.84.165414](https://doi.org/10.1103/PhysRevB.84.165414) (cit. on p. 35).
- [62] J.-P. Blaizot and G. Ripka, *Quantum theory of finite systems* (The MIT Press, 1986) (cit. on p. 35).

- [63] E. H. Lieb, “Flux Phase of the Half-Filled Band”, *Physical Review Letters* **73**, 2158–2161 (1994) [10.1103/PhysRevLett.73.2158](https://doi.org/10.1103/PhysRevLett.73.2158) (cit. on pp. 37–38).
- [64] Y. Aharonov and D. Bohm, “Significance of Electromagnetic Potentials in the Quantum Theory”, *Phys. Rev.* **115**, 485–491 (1959) [10.1103/PhysRev.115.485](https://doi.org/10.1103/PhysRev.115.485) (cit. on p. 37).
- [65] R. Peierls, “Zur Theorie des Diamagnetismus von Leitungselektronen”, *Z. Physik* **80**, 763–791 (1933) [10.1007/BF01342591](https://doi.org/10.1007/BF01342591) (cit. on p. 37).
- [66] T. Eschmann et al., “Thermodynamic classification of three-dimensional Kitaev spin liquids”, *Phys. Rev. B* **102**, 075125 (2020) [10.1103/PhysRevB.102.075125](https://doi.org/10.1103/PhysRevB.102.075125) (cit. on p. 38).
- [67] H. Yao, S.-C. Zhang, and S. A. Kivelson, “Algebraic spin liquid in an exactly solvable spin model”, *Phys. Rev. Lett.* **102**, 217202 (2009) [10.1103/PhysRevLett.102.217202](https://doi.org/10.1103/PhysRevLett.102.217202) (cit. on p. 38).
- [68] T. Eschmann et al., “Thermodynamics of a gauge-frustrated Kitaev spin liquid”, *Physical Review Research* **1**, 032011(R) (2019) (cit. on p. 38).
- [69] V. Peri et al., “Non-Abelian chiral spin liquid on a simple non-Archimedean lattice”, *Phys. Rev. B* **101**, 041114 (2020) [10.1103/PhysRevB.101.041114](https://doi.org/10.1103/PhysRevB.101.041114) (cit. on p. 38).
- [70] H. Yao and S. A. Kivelson, “An exact chiral spin liquid with non-Abelian anyons”, *Phys. Rev. Lett.* **99**, 247203 (2007) [10.1103/PhysRevLett.99.247203](https://doi.org/10.1103/PhysRevLett.99.247203), arXiv:0708.0040 (cit. on p. 38).
- [71] M. Parker, director, *Why does this balloon have -1 holes?*, <https://www.youtube.com/watch?v=ymF1bp-qrjU> (visited on 08/02/2022) (cit. on p. 39).
- [72] M. B. Hastings, “Lieb-Schultz-Mattis in higher dimensions”, *Phys. Rev. B* **69**, 104431 (2004) [10.1103/PhysRevB.69.104431](https://doi.org/10.1103/PhysRevB.69.104431) (cit. on p. 40).
- [73] A. Y. Kitaev, “Fault-tolerant quantum computation by anyons”, *Annals of Physics* **303**, 2–30 (2003) [10.1016/S0003-4916\(02\)00018-0](https://doi.org/10.1016/S0003-4916(02)00018-0) (cit. on pp. 40–41).
- [74] D. Poulin, “Stabilizer Formalism for Operator Quantum Error Correction”, *Phys. Rev. Lett.* **95**, 230504 (2005) [10.1103/PhysRevLett.95.230504](https://doi.org/10.1103/PhysRevLett.95.230504) (cit. on p. 40).
- [75] M. B. Hastings and J. Haah, “Dynamically Generated Logical Qubits”, *Quantum* **5**, 564 (2021) [10.22331/q-2021-10-19-564](https://doi.org/10.22331/q-2021-10-19-564), arXiv:2107.02194 [quant-ph] (cit. on p. 40).
- [76] T. Einarsson, “Fractional statistics on a torus”, *Phys. Rev. Lett.* **64**, 1995–1998 (1990) [10.1103/PhysRevLett.64.1995](https://doi.org/10.1103/PhysRevLett.64.1995) (cit. on p. 40).
- [77] M. Oshikawa et al., “Topological degeneracy of non-Abelian states for dummies”, *Annals of Physics* **322**, 1477–1498 (2007) [10.1016/j.aop.2006.08.001](https://doi.org/10.1016/j.aop.2006.08.001) (cit. on p. 40).
- [78] S. B. Chung, H. Yao, T. L. Hughes, and E.-A. Kim, “Topological quantum phase transition in an exactly solvable model of a chiral spin liquid at finite temperature”, *Phys. Rev. B* **81**, 060403 (2010) [10.1103/PhysRevB.81.060403](https://doi.org/10.1103/PhysRevB.81.060403) (cit. on p. 40).
- [79] H. Yao, S.-C. Zhang, and S. A. Kivelson, “Algebraic Spin Liquid in an Exactly Solvable Spin Model”, *Phys. Rev. Lett.* **102**, 217202 (2009) [10.1103/PhysRevLett.102.217202](https://doi.org/10.1103/PhysRevLett.102.217202) (cit. on p. 40).
- [80] S.-s. Chern, “Characteristic Classes of Hermitian Manifolds”, *Annals of Mathematics* **47**, 85–121 (1946) [10.2307/1969037](https://doi.org/10.2307/1969037), JSTOR: 1969037 (cit. on p. 40).

- [81] A. Y. Kitaev, “Quantum communication, computing, and measurement”, in Proceedings of the 3rd international conference of quantum communication and measurement, new york: Plenum (1997) (cit. on p. 41).
- [82] N. Read and D. Green, “Paired states of fermions in two dimensions with breaking of parity and time-reversal symmetries and the fractional quantum Hall effect”, *Phys. Rev. B* **61**, 10267–10297 (2000) 10.1103/PhysRevB.61.10267 (cit. on p. 41).
- [83] G. Moore and N. Read, “Nonabelions in the fractional quantum hall effect”, *Nuclear Physics B* **360**, 362–396 (1991) 10.1016/0550-3213(91)90407-O (cit. on p. 41).
- [84] J. Alicea et al., “Non-Abelian statistics and topological quantum information processing in 1D wire networks”, *Nature Phys* **7**, 412–417 (2011) 10.1038/nphys1915 (cit. on p. 41).
- [85] L. Fu and C. L. Kane, “Superconducting Proximity Effect and Majorana Fermions at the Surface of a Topological Insulator”, *Phys. Rev. Lett.* **100**, 096407 (2008) 10.1103/PhysRevLett.100.096407 (cit. on p. 41).
- [86] R. M. Lutchyn, J. D. Sau, and S. Das Sarma, “Majorana Fermions and a Topological Phase Transition in Semiconductor-Superconductor Heterostructures”, *Phys. Rev. Lett.* **105**, 077001 (2010) 10.1103/PhysRevLett.105.077001 (cit. on p. 41).
- [87] Y. Oreg, G. Refael, and F. von Oppen, “Helical Liquids and Majorana Bound States in Quantum Wires”, *Phys. Rev. Lett.* **105**, 177002 (2010) 10.1103/PhysRevLett.105.177002 (cit. on p. 41).
- [88] J. D. Sau, R. M. Lutchyn, S. Tewari, and S. Das Sarma, “Generic New Platform for Topological Quantum Computation Using Semiconductor Heterostructures”, *Phys. Rev. Lett.* **104**, 040502 (2010) 10.1103/PhysRevLett.104.040502 (cit. on p. 41).
- [89] A. Banerjee et al., “Proximate Kitaev Quantum Spin Liquid Behaviour in $\{\backslash\alpha\}$ -RuCl $_3$ ”, *Nature Mater* **15**, 733–740 (2016) 10.1038/nmat4604, arXiv:1504.08037 [cond-mat] (cit. on p. 42).
- [90] G. Baskaran, S. Mandal, and R. Shankar, “Exact Results for Spin Dynamics and Fractionalization in the Kitaev Model”, *Phys. Rev. Lett.* **98**, 247201 (2007) 10.1103/PhysRevLett.98.247201 (cit. on p. 42).
- [91] A. Lagendijk, B. van Tiggelen, and D. S. Wiersma, “Fifty years of Anderson localization”, *Physics Today* **62**, 24–29 (2009) 10.1063/1.3206091 (cit. on p. 43).
- [92] J. Pendry, “Symmetry and transport of waves in one-dimensional disordered systems”, *Advances in Physics* **43**, 461–542 (1994) 10.1080/00018739400101515 (cit. on p. 43).
- [93] S. N. Mott, “Metal–insulator transitions”, *Physics Today* **31**, 42–47 (1978) 10.1063/1.2994815 (cit. on p. 43).
- [94] J. T. Edwards and D. J. Thouless, “Numerical studies of localization in disordered systems”, *J. Phys. C: Solid State Phys.* **5**, 807–820 (1972) 10.1088/0022-3719/5/8/007 (cit. on p. 43).
- [95] F. M. Izrailev and A. A. Krokhin, “Localization and the Mobility Edge in One-Dimensional Potentials with Correlated Disorder”, *Phys. Rev. Lett.* **82**, 4062–4065 (1999) 10.1103/PhysRevLett.82.4062 (cit. on p. 43).
- [96] A. Croy, P. Cain, and M. Schreiber, “Anderson localization in 1D systems with correlated disorder”, *Eur. Phys. J. B* **82**, 107 (2011) 10.1140/epjb/e2011-20212-1 (cit. on p. 43).

- [97] F. M. Izrailev, A. A. Krokhin, and N. M. Makarov, “Anomalous Localization in Low-Dimensional Systems with Correlated Disorder”, *Physics Reports* **512**, 125–254 (2012) 10.1016/j.physrep.2011.11.002, arXiv:1110.1762 (cit. on p. 43).
- [98] J. Z. Imbrie, “On Many-Body Localization for Quantum Spin Chains”, *J Stat Phys* **163**, 998–1048 (2016) 10.1007/s10955-016-1508-x (cit. on p. 43).
- [99] C. Gogolin and J. Eisert, “Equilibration, thermalisation, and the emergence of statistical mechanics in closed quantum systems”, *Rep. Prog. Phys.* **79**, 056001 (2016) 10.1088/0034-4885/79/5/056001 (cit. on p. 43).
- [100] Y. Kagan and L. Maksimov, “Localization in a system of interacting particles diffusing in a regular crystal”, *Zhurnal Ekspерimental’noi i Teoreticheskoi Fiziki* **87**, 348–365 (1984) (cit. on p. 44).
- [101] N. Y. Yao et al., “Quasi-Many-Body Localization in Translation-Invariant Systems”, *Phys. Rev. Lett.* **117**, 240601 (2016) 10.1103/PhysRevLett.117.240601 (cit. on p. 44).
- [102] M. Schiulaz, A. Silva, and M. Müller, “Dynamics in many-body localized quantum systems without disorder”, *Phys. Rev. B* **91**, 184202 (2015) 10.1103/PhysRevB.91.184202 (cit. on p. 44).
- [103] F. Yonezawa and T. Ninomiya, eds., *Topological disorder in condensed matter*, Vol. 46, Springer-Series in Solid State Sciences (Springer-Verlag, Berlin Heidelberg, 1983) (cit. on p. 44).
- [104] R. Zallen, *The physics of amorphous solids* (John Wiley & Sons, 2008) (cit. on p. 44).
- [105] D. Weaire and M. F. Thorpe, “Electronic properties of an amorphous solid. I. A simple tight-binding theory”, *Phys. Rev. B* **4**, 2508–2520 (1971) 10.1103/PhysRevB.4.2508 (cit. on p. 44).
- [106] G. Betteridge, “A possible model of amorphous silicon and germanium”, *Journal of Physics C: Solid State Physics* **6**, L427 (1973) (cit. on p. 44).
- [107] N. P. Mitchell et al., “Amorphous topological insulators constructed from random point sets”, *Nature Phys* **14**, 380–385 (2018) 10.1038/s41567-017-0024-5 (cit. on p. 44).
- [108] Q. Marsal, D. Varjas, and A. G. Grushin, “Topological Weaire-Thorpe models of amorphous matter”, *Proc. Natl. Acad. Sci. U.S.A.* **117**, 30260–30265 (2020) 10.1073/pnas.2007384117 (cit. on p. 44).
- [109] A. B. Harris, “Effect of random defects on the critical behaviour of Ising models”, *J. Phys. C: Solid State Phys.* **7**, 1671–1692 (1974) 10.1088/0022-3719/7/9/009 (cit. on p. 44).
- [110] Y. Imry and S.-k. Ma, “Random-Field Instability of the Ordered State of Continuous Symmetry”, *Phys. Rev. Lett.* **35**, 1399–1401 (1975) 10.1103/PhysRevLett.35.1399 (cit. on p. 44).
- [111] H. Barghathi and T. Vojta, “Phase Transitions on Random Lattices: How Random is Topological Disorder?”, *Phys. Rev. Lett.* **113**, 120602 (2014) 10.1103/PhysRevLett.113.120602 (cit. on p. 44).
- [112] M. Schrauth, J. Portela, and F. Goth, “Violation of the Harris-Barghathi-Vojta Criterion”, *Physical Review Letters* **121**, 10.1103/PhysRevLett.121.100601 (2018) 10.1103/PhysRevLett.121.100601 (cit. on p. 44).

- [113] J. Nasu, M. Udagawa, and Y. Motome, “Thermal fractionalization of quantum spins in a Kitaev model: Temperature-linear specific heat and coherent transport of Majorana fermions”, *Phys. Rev. B* **92**, 115122 (2015) 10.1103/PhysRevB.92.115122 (cit. on p. 45).
- [114] J. Knolle, “Dynamics of a quantum spin liquid” (Max Planck Institute for the Physics of Complex Systems, Dresden, 2016) (cit. on p. 45).
- [115] J.-J. Wen et al., “Disordered Route to the Coulomb Quantum Spin Liquid: Random Transverse Fields on Spin Ice in $\mathrm{Pr}_2\mathrm{Zr}_2\mathrm{O}_7$ ”, *Phys. Rev. Lett.* **118**, 107206 (2017) 10.1103/PhysRevLett.118.107206 (cit. on p. 45).
- [116] G.-Y. Zhu and M. Heyl, “Subdiffusive dynamics and critical quantum correlations in a disorder-free localized Kitaev honeycomb model out of equilibrium”, *Phys. Rev. Research* **3**, L032069 (2021) 10.1103/PhysRevResearch.3.L032069, arXiv:2012.05753 [cond-mat, physics:quant-ph] (cit. on p. 45).
- [117] F. Evers and A. D. Mirlin, “Anderson Transitions”, *Rev. Mod. Phys.* **80**, 1355–1417 (2008) 10.1103/RevModPhys.80.1355, arXiv:0707.4378 (cit. on p. 46).
- [118] B. L. Altshuler, D. Khmel’nitzkii, A. I. Larkin, and P. A. Lee, “Magnetoconductance and Hall effect in a disordered two-dimensional electron gas”, *Phys. Rev. B* **22**, 5142–5153 (1980) 10.1103/PhysRevB.22.5142 (cit. on p. 46).
- [119] S. Datta, *Electronic Transport in Mesoscopic Systems*, Cambridge Studies in Semiconductor Physics and Microelectronic Engineering (Cambridge University Press, Cambridge, 1995), 10.1017/CBO9780511805776 (cit. on p. 46).

Chapter 3

The Long-Range Falicov-Kimball Model

Contributions

This chapter expands on work presented in

[1] [One-dimensional long-range Falikov-Kimball model: Thermal phase transition and disorder-free localization](#), Hodson, T. and Willsher, J. and Knolle, J., Phys. Rev. B, **104**, 4, 2021,

The code is available online [2].

Johannes had the initial idea to use a long range Ising term to stabilise order in a one dimension Falicov-Kimball model. Josef developed a proof of concept during a summer project at Imperial along with Alexander Belcik. I wrote the simulation code and performed all the analysis presented here.

Chapter Summary

The paper is organised as follows. First, I will introduce the long range Falicov-Kimball (LRFK) model and motivate its definition. Second, I will present the [methods](#) used to solve it numerically, including Markov chain Monte Carlo and finite size scaling. I will then present and interpret the [results](#) obtained.

3.1 The Model

Dimensionality is crucial for the physics of both localisation and phase transitions. We have already seen that the one dimensional standard FK model cannot support an ordered phase at finite temperatures and therefore has no finite temperature phase transition (FTPT).

On bipartite lattices in dimensions 2 and above the FK model exhibits a finite temperature phase transition to an ordered charge density wave (CDW) phase [3]. In this phase, the spins order anti-ferromagnetically, breaking the \mathbb{Z}_2 symmetry. In 1D, however, Peierls's argument [4, 5] states that domain walls only introduce a constant energy penalty into the free energy while bringing a entropic contribution logarithmic in system size. Hence the 1D model does not have a finite temperature phase transition. However 1D systems are much easier to study numerically and admit simpler realisations experimentally. We therefore introduce a long-range coupling between the ions in order to stabilise a CDW phase in 1D.

We interpret the FK model as a model of spinless fermions, c_i^\dagger , hopping on a 1D lattice against a classical Ising spin background, $S_i \in \pm \frac{1}{2}$. The fermions couple to the spins via an onsite interaction with strength U which we supplement by a long-range interaction,

$$J_{ij} = 4\kappa J (-1)^{|i-j|} |i - j|^{-\alpha}, \quad (3.1)$$

between the spins. The additional coupling is very similar to that of the long range Ising model, it stabilises the Antiferromagnetic (AFM) order of the Ising spins which promotes the finite temperature CDW phase of the fermionic sector.

The hopping strength of the electrons, $t = 1$, sets the overall energy scale and we concentrate throughout on the particle-hole symmetric point at zero chemical potential and half filling [6].

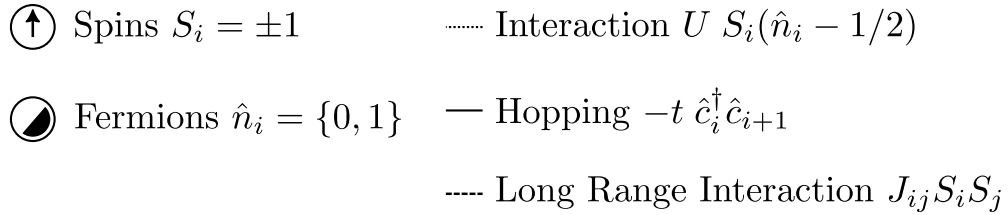


Figure 3.1: The Long Range Falicov-Kimball (LRFK) Model is a model of classical spins S_i coupled to spinless fermions \hat{c}_i where the fermions are mobile with hopping t and the fermions are coupled to the spins by an Ising type interaction with strength U . The difference from the standard FK model is the presence of a long range interaction between the spins $J_{ij} S_i S_j$.

$$H_{\text{FK}} = U \sum_i S_i (c_i^\dagger c_i - \frac{1}{2}) - t \sum_i (c_i^\dagger c_{i+1} + h.c.) + \sum_{i,j}^N J_{ij} S_i S_j \quad (3.2)$$

Without proper normalisation, the long range coupling would render the critical temperature strongly system size dependent for small system sizes. Within a mean field approximation the critical temperature scales with the effective coupling to all the neighbours of each site, which for a system with N sites is $\sum_{i=1}^N i^{-\alpha}$. Hence, the normalisation $\kappa^{-1} = \sum_{i=1}^N i^{-\alpha}$, renders the critical temperature independent of system size in the mean field approximation. This greatly improves the finite size behaviour of the model.

Taking the limit $U = 0$ decouples the spins from the fermions, which gives a spin sector governed by a classical LRI model. Note, the transformation of the spins $S_i \rightarrow (-1)^i S_i$ maps the AFM model to the FM one. As discussed in the background section, Peierls' classic argument can be extended to long range couplings to show that, for the 1D LRI model, a power law decay of $\alpha < 2$ is required for a FTPT as the energy of defect domain then scales with the system size and can overcome the entropic contribution. A renormalisation group analysis supports this finding and shows that the critical exponents are only universal for $\alpha \leq 3/2$ [7–9]. In the following, we choose $\alpha = 5/4$ to avoid the additional complexity of non-universal critical points.

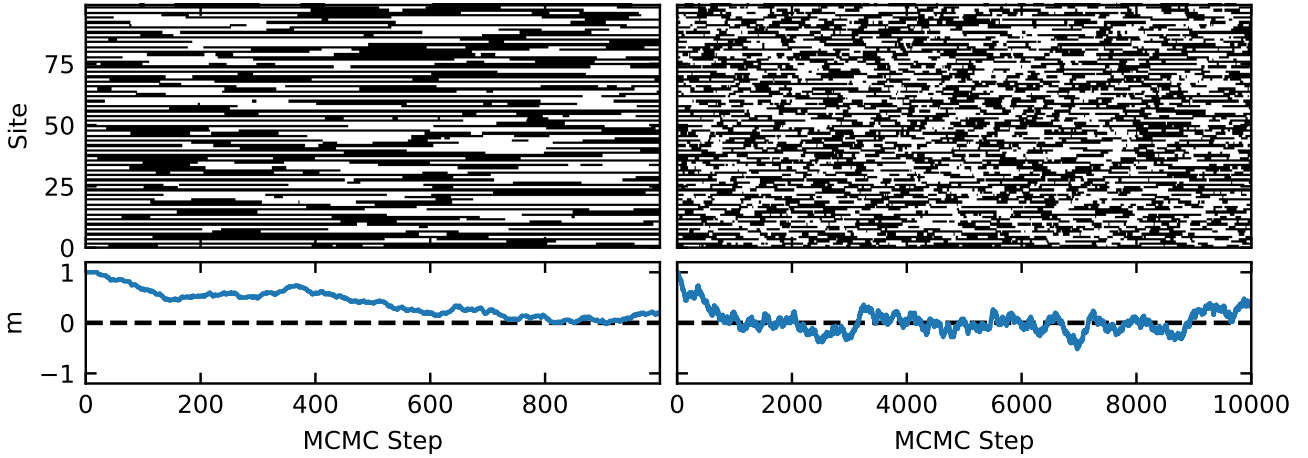


Figure 3.2: Two MCMC walks starting from the CDW state for a system with $N = 100$ sites and 10,000 MCMC steps but at a temperature close to but above the ordered state (left column) and much higher than it (right column). In this simulation only a single spin can be flipped per step according to the Metropolis-Hastings Algorithm. The staggered magnetisation $m = N^{-1} \sum_i (-1)^i S_i$ order parameter is plotted below. At both temperatures the thermal average of m is zero, while the initial state has $m = 1$. The higher temperature allows the MCMC to converge more quickly and to fluctuate about the mean with a shorter autocorrelation time. $t = 1, \alpha = 1.25, T = 2.5, 5, J = U = 5$

3.2 Methods

To evaluate thermodynamic averages I perform classical Markov Chain Monte Carlo random walks over the space of spin configurations of the LRFK model, at each step diagonalising the effective electronic Hamiltonian [3]. Using a Binder-cumulant method [10, 11], I demonstrate the model has a finite temperature phase transition when the interaction is sufficiently long ranged. In this section I will discuss the thermodynamics of the model and how they are amenable to an exact Markov Chain Monte Carlo method.

3.2.1 Thermodynamics of the LRFK Model

The classical Markov Chain Monte Carlo (MCMC) method which we discuss in the following allows us to solve our long-range FK model efficiently, yielding unbiased estimates of thermal expectation values.

Since the spin configurations are classical, the LRFK Hamiltonian can be split into a classical spin part H_s and an operator valued part H_c .

$$\begin{aligned} H_s &= -\frac{U}{2}S_i + \sum_{i,j}^N J_{ij}S_iS_j \\ H_c &= \sum_i US_i c_i^\dagger c_i - t(c_i^\dagger c_{i+1} + c_{i+1}^\dagger c_i) \end{aligned} \tag{3.3}$$

The partition function can then be written as a sum over spin configurations, $\vec{S} = (S_0, S_1 \dots S_{N-1})$:

$$\mathcal{Z} = \text{Tr} e^{-\beta H} = \sum_{\vec{S}} e^{-\beta H_s} \text{Tr}_c e^{-\beta H_c}. \quad (3.4)$$

The contribution of H_c to the grand canonical partition function can be obtained by performing the sum over eigenstate occupation numbers giving $-\beta F_c[\vec{S}] = \sum_k \ln(1 + e^{-\beta \epsilon_k})$ where $\epsilon_k[\vec{S}]$ are the eigenvalues of the matrix representation of H_c determined through exact diagonalisation. This gives a partition function containing a classical energy which corresponds to the long-range interaction of the spins, and a free energy which corresponds to the quantum subsystem.

$$\mathcal{Z} = \sum_{\vec{S}} e^{-\beta H_S[\vec{S}] - \beta F_c[\vec{S}]} = \sum_{\vec{S}} e^{-\beta E[\vec{S}]} \quad (3.5)$$

3.2.2 Markov Chain Monte Carlo and Emergent Disorder

Classical MCMC defines a weighted random walk over the spin states $(\vec{S}_0, \vec{S}_1, \vec{S}_2, \dots)$, such that the likelihood of visiting a particular state converges to its Boltzmann probability $p(\vec{S}) = \mathcal{Z}^{-1} e^{-\beta E}$. Hence, any observable can be estimated as a mean over the states visited by the walk [12–14],

$$\begin{aligned} \langle O \rangle &= \sum_{\vec{S}} p(\vec{S}) \langle O \rangle \\ &= \sum_{i=0}^M \langle O \rangle \pm \mathcal{O}(M^{-\frac{1}{2}}) \end{aligned} \quad (3.6)$$

where the former sum runs over the entire state space while the later runs over all the states visited by a particular MCMC run.

$$\langle O \rangle_{\vec{S}} = \sum_{\nu} n_F(\epsilon_{\nu}) \langle O \rangle_{\nu} \quad (3.7)$$

Where ν runs over the eigenstates of H_c for a particular spin configuration and $n_F(\epsilon) = (e^{-\beta \epsilon} + 1)^{-1}$ is the Fermi function.

The choice of the transition function for MCMC is under-determined as one only needs to satisfy a set of balance conditions for which there are many solutions [15]. Here, we incorporate a modification to the standard Metropolis-Hastings algorithm [16] gleaned from Krauth [17].

The standard algorithm decomposes the transition probability into $\mathcal{T}(a \rightarrow b) = p(a \rightarrow b) \mathcal{A}(a \rightarrow b)$. Here, p is the proposal distribution that we can directly sample from while \mathcal{A} is the acceptance probability. The standard Metropolis-Hastings choice is

$$\mathcal{A}(a \rightarrow b) = \min \left(1, \frac{p(b \rightarrow a)}{p(a \rightarrow b)} e^{-\beta \Delta E} \right), \quad (3.8)$$

with $\Delta E = E_b - E_a$. The walk then proceeds by sampling a state b from p and moving to b with probability $\mathcal{A}(a \rightarrow b)$. The latter operation is typically implemented by performing a transition if a uniform random sample from the unit interval is less than $\mathcal{A}(a \rightarrow b)$ and otherwise repeating the current state as the next step in the random walk. The proposal distribution is often symmetric so does not appear in \mathcal{A} . Here, we flip a small number of sites in b at random to generate proposals, which is a symmetric proposal.

In our computations [2] the modification to this algorithm that we employ is based on the observation that the free energy of the FK system is composed of a classical part which is much quicker to compute than the quantum part. Hence, we can obtain a computational speed up by first considering the value of the classical energy difference ΔH_s and rejecting the transition if the former is too high. We only compute the quantum energy difference ΔF_c if the transition is accepted. We then perform a second rejection sampling step based upon it. This corresponds to two nested comparisons with the majority of the work only occurring if the first test passes. This modified scheme has the acceptance function

$$\mathcal{A}(a \rightarrow b) = \min(1, e^{-\beta \Delta H_s}) \min(1, e^{-\beta \Delta F_c}) . \quad (3.9)$$

For the model parameters used, we find that with our new scheme the matrix diagonalisation is skipped around 30% of the time at $T = 2.5$ and up to 80% at $T = 1.5$. We observe that for $N = 50$, the matrix diagonalisation, if it occurs, occupies around 60% of the total computation time for a single step. This rises to 90% at $N = 300$ and further increases for larger N . We therefore get the greatest speedup for large system sizes at low temperature where many prospective transitions are rejected at the classical stage and the matrix computation takes up the greatest fraction of the total computation time. The upshot is that we find a speedup of up to a factor of 10 at the cost of very little extra algorithmic complexity.

Our two-step method should be distinguished from the more common method for speeding up MCMC which is to add asymmetry to the proposal distribution to make it as similar as possible to $\min(1, e^{-\beta \Delta E})$. This reduces the number of rejected states, which brings the algorithm closer in efficiency to a direct sampling method. However it comes at the expense of requiring a way to directly sample from this complex distribution, a problem which MCMC was employed to solve in the first place. For example, recent work trains restricted Boltzmann machines (RBMs) to generate samples for the proposal distribution of the FK model [18]. The RBMs are chosen as a parametrisation of the proposal distribution that can be efficiently sampled from while offering sufficient flexibility that they can be adjusted to match the target distribution. Our proposed method is considerably simpler and does not require training while still reaping some of the benefits of reduced computation.

3.2.3 Scaling

To improve the scaling of finite size effects, we make the replacement $|i - j|^{-\alpha} \rightarrow |f(i - j)|^{-\alpha}$, in both J_{ij} and κ , where $f(x) = \frac{N}{\pi} \sin \frac{\pi x}{N}$. f is smooth across the circular boundary and its effect diminished for larger systems [19]. We only consider even system sizes given that odd system sizes are not commensurate with a CDW state.

To identify critical points we use the the Binder cumulant U_B defined by

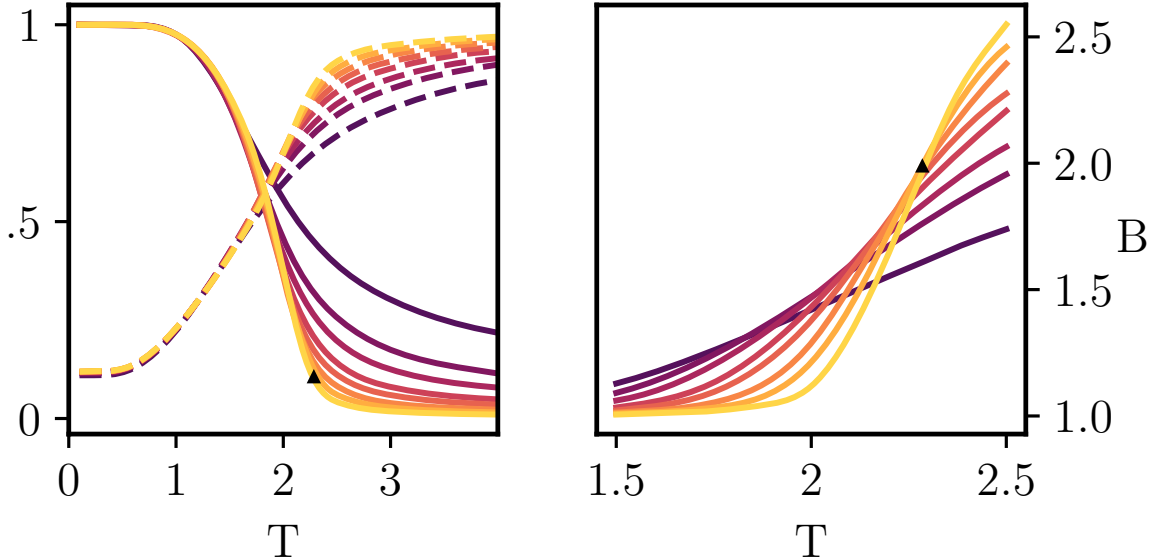


Figure 3.3: (Left) The order parameters, $\langle m^2 \rangle$ (solid) and $1 - f$ (dashed) describing the onset of the charge density wave phase of the long-range 1D Falicov model at low temperature with staggered magnetisation $m = N^{-1} \sum_i (-1)^i S_i$ and fermionic order parameter $f = 2N^{-1} |\sum_i (-1)^i \langle c_i^\dagger c_i \rangle|$. (Right) The crossing of the Binder cumulant, $B = \langle m^4 \rangle / \langle m^2 \rangle^2$, with system size provides a diagnostic that the phase transition is not a finite size effect, it is used to estimate the critical lines shown in the phase diagram later. All plots use system sizes $N = [10, 20, 30, 50, 70, 110, 160, 250]$ and lines are coloured from $N = 10$ in dark blue to $N = 250$ in yellow. The parameter values $U = 5$, $J = 5$, $\alpha = 1.25$ except where explicitly mentioned.

$$U_B = 1 - \frac{\langle \mu_4 \rangle}{3\langle \mu_2 \rangle^2} \quad (3.10)$$

where $\mu_n = \langle (m - \langle m \rangle)^n \rangle$ are the central moments of the order parameter $m = \sum_i (-1)^i (2n_i - 1)/N$. The Binder cumulant evaluated against temperature is a diagnostic for the existence of a phase transition. If multiple such curves are plotted for different system sizes, a crossing indicates the location of a critical point while the lines do not cross for systems that don't have a phase transition in the thermodynamic limit [10, 11].

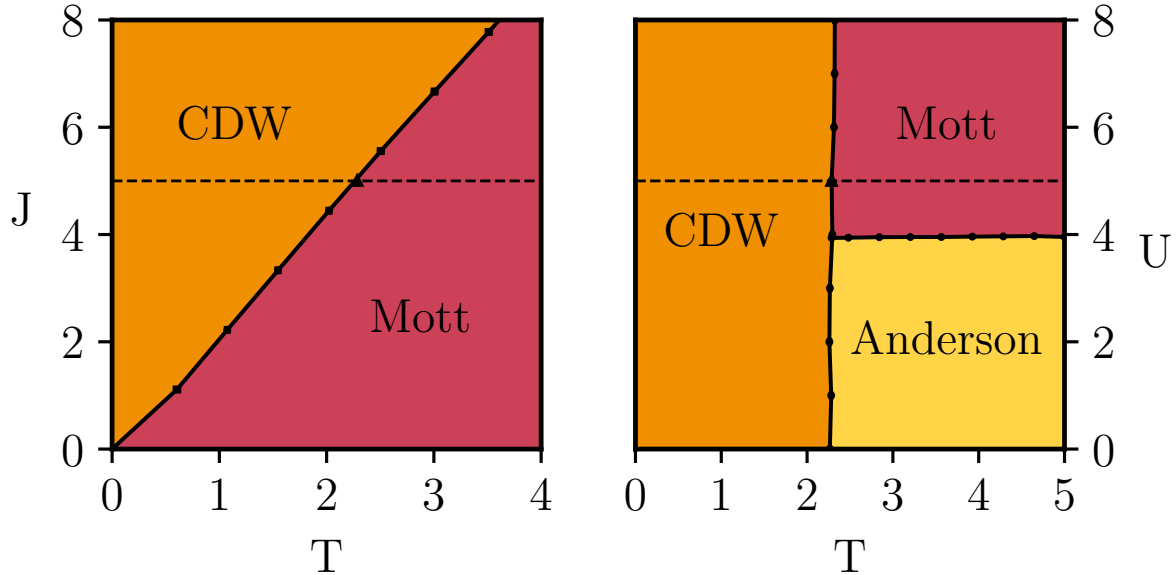


Figure 3.4: Phase diagrams of the long-range 1D FK model. (Left) The TJ plane at $U = 5$: the CDW ordered phase is separated from a disordered Mott insulating phase by a critical temperature T_c , linear in J . (Right) The TU plane at $J = 5$: the disordered phase is split into two: at large/small U there's a MI/Anderson phase characterised by the presence/absence of a gap at $E = 0$ in the single particle energy spectrum. U_c is independent of temperature. At $U = 0$ the fermions are decoupled from the spins forming a simple Fermi gas.

3.3 Results

Looking at the results of our MCMC simulations, we find a rich phase diagram with a CDW FTPT and interaction-tuned Anderson versus Mott localized phases similar to the 2D FK model [20]. We explore the localization properties of the fermionic sector and find that the localisation lengths vary dramatically across the phases and for different energies. Although moderate system sizes indicate the coexistence of localized and delocalized states within the CDW phase, we find quantitatively similar behaviour in a model of uncorrelated binary disorder on a CDW background. For large system sizes, i.e. for our 1D disorder model we can treat linear sizes of several thousand sites, we find that all states are eventually localized with a localization length which diverges towards zero temperature.

3.3.1 Phase Diagram

Using the MCMC methods described in the previous section I will now discuss the results of extensive MCMC simulations of the model, starting with the phase diagram in the fermion spin coupling U , the strength of the long range spin-spin coupling J and the temperature T .

Figure 3.4 shows the phase diagram for constant $U = 5$ and constant $J = 5$, respectively. The transition temperatures were determined from the crossings of the Binder cumulants $B_4 = \langle m^4 \rangle / \langle m^2 \rangle^2$ [10].

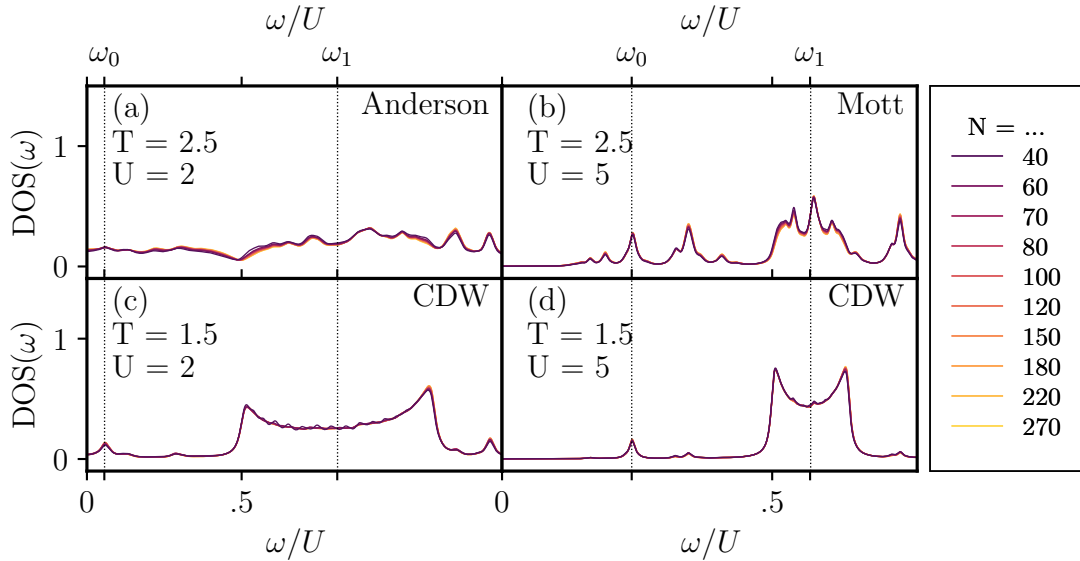


Figure 3.5: Energy resolved $\text{DOS}(\omega)$ against system size N in all three phases. The charge density wave phase is shown in both the high and low U regime for completeness. The top left panel shows the Anderson phase at $U = 2$ and high $T = 2.5$, this phase is gapless but does not conduct due to Anderson localisation. In the lower left pane at $U = 2$ and low $T = 1.5$, charge density wave order sets in, allowing the single particle eigenstates to become extended but opening a gap in their band structure. In the upper right panel at $U = 5$ and high $T = 2.5$ the states are localised by disorder and an interaction driven gap opens, a Mott insulator. Finally the charge density wave phase at $U = 5$ and $T = 1.5$ is qualitatively similar to the lower left panel except that the gap scales with U . For all the plots $J = 5$, $\alpha = 1.25$.

The CDW transition temperature is largely independent from the strength of the interaction U . This demonstrates that the phase transition is driven by the long-range term J with little effect from the coupling to the fermions U . The physics of the spin sector in the long-range FK model mimics that of the long range Ising (LRI) model and is not significantly altered by the presence of the fermions. In two dimensions the transition to the CDW phase is mediated by an RKKY-like interaction [21] but this is insufficient to stabilise long range order in one dimension. That the critical temperature T_c does not depend on U in our model further confirms this.

The main order parameters for this model is the staggered magnetisation $m = N^{-1} \sum_i (-1)^i S_i$ that signals the onset of a charge density wave (CDW) phase at low temperature. However, my main interest concerns the additional structure of the fermionic sector in the high temperature phase. Following Ref. [20], we can distinguish between the Mott and Anderson insulating phases. The Mott insulator is characterised by a gapped DOS in the absence of a CDW, instead the gap is driven entirely by interaction effect. Thus, the opening of a gap for large U is distinct from the gap-opening induced by the translational symmetry breaking in the CDW state below T_c . The Anderson phase is gapless but, as we explain below, shows localised fermionic eigenstates hence it also has insulating character.

3.3.2 Localisation Properties

The MCMC formulation suggests viewing the spin configurations as a form of annealed binary disorder whose probability distribution is given by the Boltzmann weight $e^{-\beta H_S[\vec{S}]-\beta F_c[\vec{S}]}$. This makes apparent the link to the study of disordered systems and Anderson localisation. While these systems are typically studied by defining the probability distribution for the quenched disorder potential externally, here we have a translation invariant system with disorder as a natural consequence of the Ising background field conserved under the dynamics.

In the limits of zero and infinite temperature, our model becomes a simple tight-binding model for the fermions. At zero temperature, the spin background is in one of the two translation invariant AFM ground states with two gapped fermionic CDW bands at energies

$$E_{\pm} = \pm \sqrt{\frac{1}{4}U^2 + 2t^2(1 + \cos ka)^2} . \quad (3.11)$$

At infinite temperature, all the spin configurations become equally likely and the fermionic model reduces to one of binary uncorrelated disorder in which all eigenstates are Anderson localised [22]. An Anderson localised state centered around r_0 has magnitude that drops exponentially over some localisation length ξ i.e $|\psi(r)|^2 \sim \exp\{-|r - r_0|/\xi\}$. Calculating ξ directly is numerically demanding. Therefore, we determine if a given state is localised via the energy-resolved IPR and the DOS defined as

$$\begin{aligned} \text{DOS}(\vec{S}, \omega) &= N^{-1} \sum_i \delta(\epsilon_i - \omega) \\ \text{IPR}(\vec{S}, \omega) &= N^{-1} \text{DOS}(\vec{S}, \omega)^{-1} \sum_{i,j} \delta(\epsilon_i - \omega) \psi_{i,j}^4 \end{aligned} \quad (3.12)$$

where ϵ_i and $\psi_{i,j}$ are the i th energy level and j th element of the corresponding eigenfunction, both dependent on the background spin configuration \vec{S} .

The scaling of the IPR with system size $\text{IPR} \propto N^{-\tau}$ depends on the localisation properties of states at that energy. For delocalised states, e.g. Bloch waves, τ is the physical dimension. For fully localised states τ goes to zero in the thermodynamic limit. However, for special types of disorder such as binary disorder, the localisation lengths can be large comparable to the system size at hand, which can make it difficult to extract the correct scaling. An additional complication arises from the fact that the scaling exponent may display intermediate behaviours for correlated disorder and in the vicinity of a localisation-delocalisation transition [23, 24]. The thermal defects of the CDW phase lead to a binary disorder potential with a finite correlation length, which in principle could result in delocalized eigenstates.

The key question for our system is then: How is the $T = 0$ CDW phase with fully delocalized fermionic states connected to the fully localized phase at high temperatures?

For a representative set of parameters covering all three phases fig. 3.5 shows the density of states as function of energy while fig. 3.6 shows τ , the scaling exponent of the IPR with system size. The DOS is symmetric about 0 because of the particle hole symmetry of the model. At high temperatures, all of the eigenstates are localised in both the Mott and Anderson phases

3.3. RESULTS

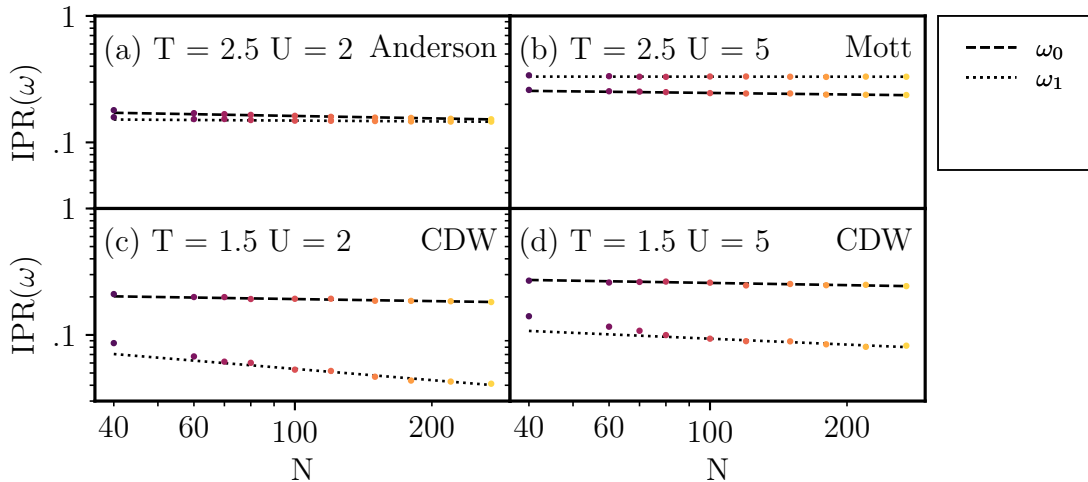


Figure 3.6: The $\text{IPR}(\omega)$ scaling with N at fixed energy for each phase and for points both in the gap (ω_0) and in a band (ω_1). The slope of the line yields the scaling exponent τ defined by $\text{IPR} \propto N^{-\tau}$. τ close to zero implies that the states at that energy are localised while $\tau = -d$ corresponds to extended states where d is the system dimension. All but the bands of the charge density wave phase are approximately localised with τ is very close to zero. The bands in the charge density wave phase are localised with long localisation lengths at finite temperatures that extend to infinity as the temperature approaches zero. For all the plots $J = 5$, $\alpha = 1.25$. The measured τ_0, τ_1 for each figure are: (a) $(0.06 \pm 0.01, 0.02 \pm 0.01)$ (b) $(0.04 \pm 0.02, 0.00 \pm 0.01)$ (c) $(0.05 \pm 0.03, 0.30 \pm 0.03)$ (d) $(0.06 \pm 0.04, 0.15 \pm 0.05)$ We show later that the apparent slight scaling of the IPR with system size in the localised cases can be explained by finite size effects due to the changing defect density with system size rather than due to delocalisation of the states.

(with $\tau \leq 0.07$ for our system sizes). We also checked that the states are localised by direct inspection. Note that there are in-gap states for instance at ω_0 , below the upper band which are localized and smoothly connected across the phase transition.

In the CDW phases at $U = 2$ and $U = 5$, we find for the states within the gapped CDW bands, e.g. at ω_1 , scaling exponents $\tau = 0.30 \pm 0.03$ and $\tau = 0.15 \pm 0.05$, respectively. This surprising finding suggests that the CDW bands are partially delocalised with multi-fractal behaviour of the wavefunctions [24]. This phenomenon would be unexpected in a 1D model as they generally do not support delocalisation in the presence of disorder except as the result of correlations in the emergent disorder potential [25, 26]. However, we later show by comparison to an uncorrelated Anderson model that these nonzero exponents are a finite size effect and the states are localised with a finite ξ similar to the system size, an example of weak localisation. As a result, the IPR does not scale correctly until the system size has grown much larger than ξ . fig. 3.10 shows that the scaling of the IPR in the CDW phase does flatten out eventually.

Next, we use the DOS and the scaling exponent τ to explore the localisation properties over the energy-temperature plane in fig. 3.8 and fig. 3.7. Gapped areas are shown in white, which highlights the distinction between the gapped Mott phase and the ungapped Anderson phase.

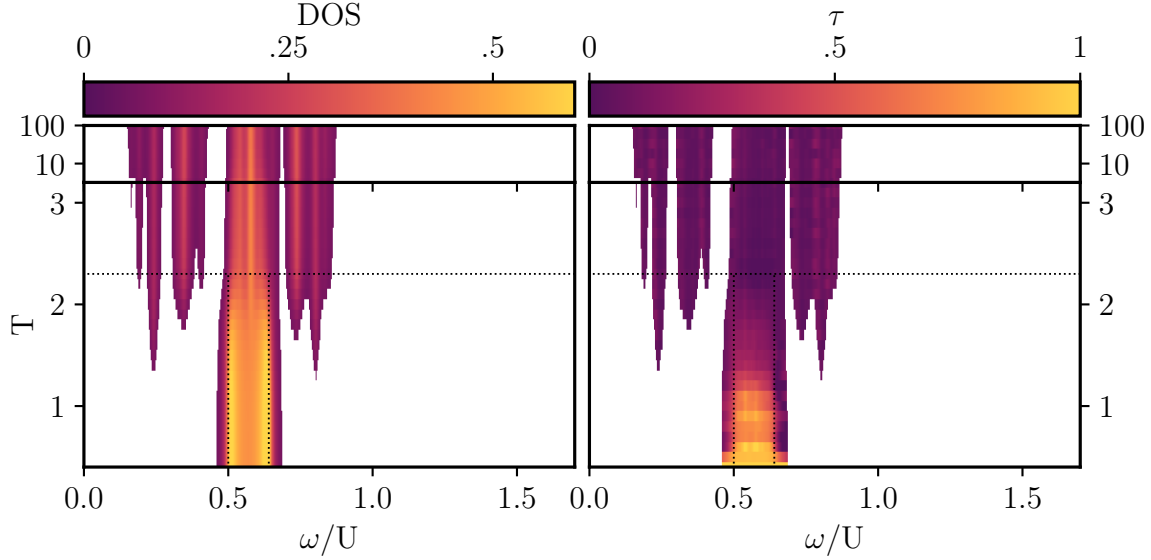


Figure 3.7: The DOS (a) and scaling exponent τ (b) as a function of energy for the CDW to gapped Mott phase transition at $U = 5$. Regions where the DOS is close to zero are shown in white. The scaling exponent τ is obtained from fits to $IPR(N) = AN^{-\lambda}$ for a range of system sizes. $J = 5$, $\alpha = 1.25$

In-gap states appear just below the critical point, smoothly filling the bandgap in the Anderson phase and forming islands in the Mott phase. As in the finite [27] and infinite dimensional [28] cases, the in-gap states merge and are pushed to lower energy for decreasing U as the $T = 0$ CDW gap closes. Intuitively, the presence of in-gap states can be understood as a result of domain wall fluctuations away from the AFM ordered background. These domain walls act as local potentials for impurity-like bound states [27].

In order to understand the localization properties we can compare the behaviour of our model with that of a simpler Anderson disorder model (DM) in which the spins are replaced by a CDW background with uncorrelated binary defect potentials. This is defined by replacing the spin degree of freedom in the FK model $S_i = \pm \frac{1}{2}$ with a disorder potential $d_i = \pm \frac{1}{2}$ controlled by a defect density ρ such that $d_i = -\frac{1}{2}$ with probability $\rho/2$ and $d_i = \frac{1}{2}$ otherwise. $\rho/2$ is used rather than ρ so that the disorder potential takes on the zero temperature CDW ground state at $\rho = 0$ and becomes a random choice over spin states at $\rho = 1$ i.e the infinite temperature limit.

$$H_{\text{DM}} = U \sum_i (-1)^i d_i (c_i^\dagger c_i - \frac{1}{2}) - t \sum_i c_i^\dagger c_{i+1} + c_{i+1}^\dagger c_i \quad (3.13)$$

fig. 3.9 and fig. 3.10 compare the FK model to the disorder model at different system sizes, matching the defect densities of the disorder model to the FK model at $N = 270$ above and below the CDW transition. We find very good, even quantitative, agreement between the FK and disorder models, which suggests that correlations in the spin sector do not play a significant

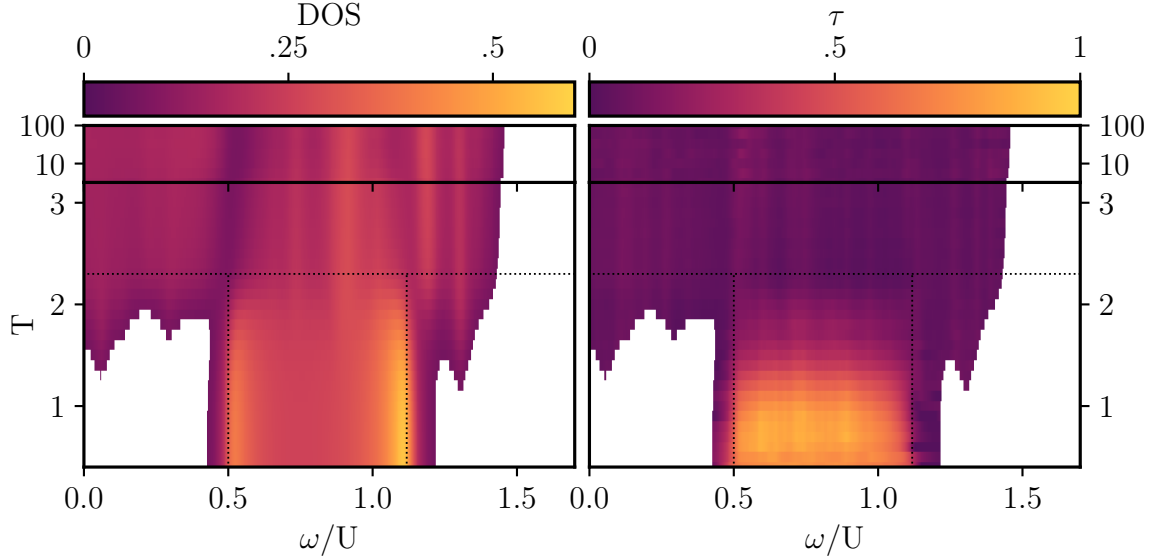


Figure 3.8: The DOS (a) and scaling exponent τ (b) as a function of energy for the CDW phase to the gapless Anderson insulating phase at $U = 2$. Regions where the DOS is close to zero are shown in white. The scaling exponent τ is obtained from fits to $IPR(N) = AN^{-\lambda}$ for a range of system sizes. $J = 5$, $\alpha = 1.25$

role.

As we can sample directly from the disorder model, rather than through MCMC, the samples are uncorrelated. Hence we can evaluate much larger system sizes with the disorder model which enables us to pin down the correct localisation effects. In particular, what appear to be delocalized states for small system sizes eventually turn out to be states with large localization length. The localization length diverges towards the ordered zero temperature CDW state. The interplay of interactions, which here produce a peculiar binary potential, and localization can be very intricate and the added advantage of a 1D model is that we can explore very large system sizes.

3.4 Discussion and Conclusion

The FK model is one of the simplest non-trivial models of interacting fermions. We studied its thermodynamic and localisation properties brought down in dimensionality to one dimension by adding a novel long-ranged coupling designed to stabilise the CDW phase present in dimension two and above.

Our MCMC approach emphasises the presence of a disorder-free localisation mechanism within our translationally invariant system. Further, it gives a significant speed up over the naive method. We show that our LRFK model retains much of the rich phase diagram of its higher dimensional cousins. Careful scaling analysis indicates that all the single particle eigenstates eventually localise at non-zero temperature albeit only for very large system sizes of several thousand.

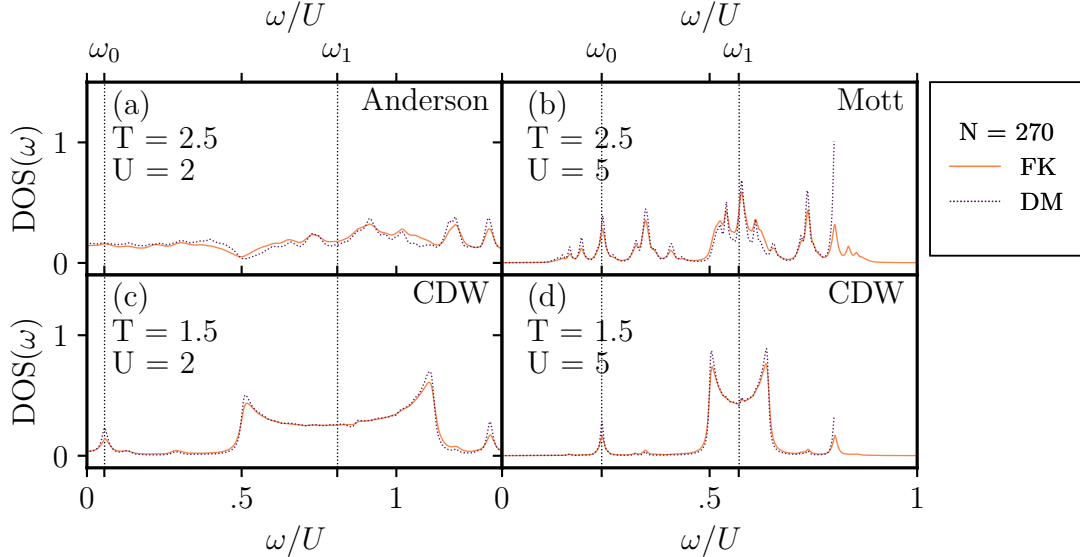


Figure 3.9: A comparison of the full FK model to a simple binary disorder model (DM) with a CDW wave background perturbed by uncorrelated defects at density $0 < \rho < 1$ matched to the ρ for the largest corresponding FK model. As in fig. 3.5, the Energy resolved DOS(ω) is shown. The DOSs match well implying that correlations in the CDW wave fluctuations are not relevant at these system parameters.

Our work raises a number of interesting questions for future research. A straightforward but numerically challenging problem is to pin down the model's behaviour closer to the critical point where correlations in the spin sector would become significant. Would this modify the localisation behaviour? Similar to other soluble models of disorder-free localisation, we expect intriguing out-of equilibrium physics, for example slow entanglement dynamics akin to more generic interacting systems [29]. One could also investigate whether the rich ground state phenomenology of the FK model as a function of filling [30] such as the devil's staircase [31] as well as superconductor like states [32] could be stabilised at finite temperature.

In a broader context, we envisage that long-range interactions can also be used to gain a deeper understanding of the temperature evolution of topological phases. One example would be a long-ranged FK version of the celebrated Su-Schrieffer-Heeger model where one could explore the interplay of topological bound states and thermal domain wall defects. Finally, the rich physics of our model should be realizable in systems with long-range interactions, such as trapped ion quantum simulators, where one can also explore the fully interacting regime with a dynamical background field.

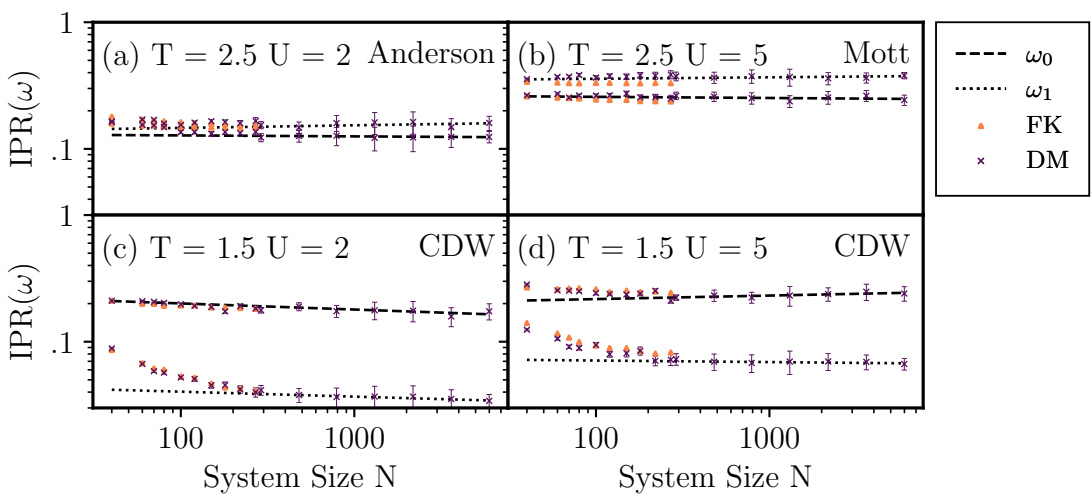


Figure 3.10: A comparison of the full FK model to a simple binary disorder model (DM) with a CDW wave background perturbed by uncorrelated defects at density $0 < \rho < 1$ matched to the ρ for the largest corresponding FK model. As in fig. 3.6 $\tau(\omega)$ the scaling of $\text{IPR}(\omega)$ with system size, , is shown both in gap (ω_0) and in the band (ω_1). This data makes clear that the apparent scaling of IPR with system size at small sysis a finite size effect due to weak localisation [20], hence all the states are indeed localised as one would expect in 1D. The disorder model τ_0, τ_1 for each figure are: (a) $0.01 \pm 0.05, -0.02 \pm 0.06$ (b) $0.01 \pm 0.04, -0.01 \pm 0.04$ (c) $0.05 \pm 0.06, 0.04 \pm 0.06$ (d) $-0.03 \pm 0.06, 0.01 \pm 0.06$. The lines are fit on system sizes $N > 400$

References

- [1] T. Hodson, J. Willsher, and J. Knolle, “One-dimensional long-range Falikov-Kimball model: Thermal phase transition and disorder-free localization”, *Phys. Rev. B* **104**, 045116 (2021) 10.1103/PhysRevB.104.045116 (cit. on p. 57).
- [2] T. Hodson, *Markov Chain Monte Carlo for the Kitaev Model*, version v1.0, Mar. 19, 2021, 10.5281/zenodo.4593904 (cit. on pp. 57, 61).
- [3] M. M. Maśka and K. Czajka, “Thermodynamics of the two-dimensional Falicov-Kimball model: A classical Monte Carlo study”, *Phys. Rev. B* **74**, 035109 (2006) 10.1103/PhysRevB.74.035109, arXiv:cond-mat/0504533 (cit. on pp. 57, 59).
- [4] R. Peierls, “On Ising’s model of ferromagnetism”, *Mathematical Proceedings of the Cambridge Philosophical Society* **32**, 477–481 (1936) 10.1017/S0305004100019174 (cit. on p. 57).
- [5] T. Kennedy and E. H. Lieb, “An itinerant electron model with crystalline or magnetic long range order”, *Physica A: Statistical Mechanics and its Applications* **138**, 320–358 (1986) 10.1016/0378-4371(86)90188-3 (cit. on p. 57).
- [6] C. Gruber and N. Macris, “The Falicov-Kimball model: A review of exact results and extensions”, *Helvetica Physica Acta* **69** (1996) (cit. on p. 57).
- [7] D. Ruelle, “Statistical mechanics of a one-dimensional lattice gas”, *Comm. Math. Phys.* **9**, 267–278 (1968), <https://mathscinet.ams.org/mathscinet-getitem?mr=0234697> (visited on 01/28/2019) (cit. on p. 58).
- [8] D. J. Thouless, “Long-Range Order in One-Dimensional Ising Systems”, *Phys. Rev.* **187**, 732–733 (1969) 10.1103/PhysRev.187.732 (cit. on p. 58).
- [9] M. C. Angelini, G. Parisi, and F. Ricci-Tersenghi, “Relations between short-range and long-range Ising models”, *Phys. Rev. E* **89**, 062120 (2014) 10.1103/PhysRevE.89.062120 (cit. on p. 58).
- [10] K. Binder, “Finite size scaling analysis of ising model block distribution functions”, *Z. Physik B - Condensed Matter* **43**, 119–140 (1981) 10.1007/BF01293604 (cit. on pp. 59, 62–63).
- [11] G. Musiał, L. Dbski, and G. Kamieniarz, “Monte Carlo simulations of Ising-like phase transitions in the three-dimensional Ashkin-Teller model”, *Phys. Rev. B* **66**, 012407 (2002) 10.1103/PhysRevB.66.012407 (cit. on pp. 59, 62).
- [12] K. Binder and D. W. Heermann, “Guide to Practical Work with the Monte Carlo Method”, in *Monte Carlo Simulation in Statistical Physics: An Introduction*, edited by K. Binder and D. W. Heermann, Springer Series in Solid-State Sciences (Springer Berlin Heidelberg, Berlin, Heidelberg, 1988), pp. 68–112, 10.1007/978-3-662-08854-8_3 (cit. on p. 60).
- [13] J. Kertesz and I. Kondor, eds., *Advances in Computer Simulation: Lectures Held at the Eötvös Summer School in Budapest, Hungary, 16–20 July 1996*, Lecture Notes in Physics (Springer-Verlag, Berlin Heidelberg, 1998), 10.1007/BFb0105456 (cit. on p. 60).
- [14] U. Wolff, “Monte Carlo errors with less errors”, *Computer Physics Communications* **156**, 143–153 (2004) 10.1016/S0010-4655(03)00467-3 (cit. on p. 60).

- [15] F. Kelly, “Reversibility and stochastic networks / F.P. Kelly”, SERBIULA (sistema Librum 2.0) **76**, 10.2307/2287860 (1981) 10.2307/2287860 (cit. on p. 60).
- [16] W. K. Hastings, “Monte Carlo sampling methods using Markov chains and their applications”, *Biometrika* **57**, 97–109 (1970) 10.1093/biomet/57.1.97 (cit. on p. 60).
- [17] W. Krauth, “Introduction To Monte Carlo Algorithms”, in *Advances in Computer Simulation: Lectures Held at the Eötvös Summer School in Budapest, Hungary, 16–20 July 1996*, Lecture Notes in Physics (Springer-Verlag, Berlin Heidelberg, 1998), 10.1007/BFb0105456 (cit. on p. 60).
- [18] L. Huang and L. Wang, “Accelerated Monte Carlo simulations with restricted Boltzmann machines”, *Phys. Rev. B* **95**, 035105 (2017) 10.1103/PhysRevB.95.035105 (cit. on p. 61).
- [19] K. Fukui and S. Todo, “Order-N cluster Monte Carlo method for spin systems with long-range interactions”, *Journal of Computational Physics* **228**, 2629–2642 (2009) 10.1016/j.jcp.2008.12.022 (cit. on p. 61).
- [20] A. E. Antipov, Y. Javanmard, P. Ribeiro, and S. Kirchner, “Interaction-Tuned Anderson versus Mott Localization”, *Phys. Rev. Lett.* **117**, 146601 (2016) 10.1103/PhysRevLett.117.146601 (cit. on pp. 63–64, 70).
- [21] T. M. Rusin and W. Zawadzki, “On calculation of RKKY range function in one dimension”, *Journal of Magnetism and Magnetic Materials* **441**, 387–391 (2017) 10.1016/j.jmmm.2017.06.007, arXiv:1701.06198 (cit. on p. 64).
- [22] E. Abrahams, P. W. Anderson, D. C. Licciardello, and T. V. Ramakrishnan, “Scaling Theory of Localization: Absence of Quantum Diffusion in Two Dimensions”, *Phys. Rev. Lett.* **42**, 673–676 (1979) 10.1103/PhysRevLett.42.673 (cit. on p. 65).
- [23] B. Kramer and A. MacKinnon, “Localization: theory and experiment”, *Rep. Prog. Phys.* **56**, 1469–1564 (1993) 10.1088/0034-4885/56/12/001 (cit. on p. 65).
- [24] F. Evers and A. D. Mirlin, “Anderson Transitions”, *Rev. Mod. Phys.* **80**, 1355–1417 (2008) 10.1103/RevModPhys.80.1355, arXiv:0707.4378 (cit. on pp. 65–66).
- [25] A. Croy, P. Cain, and M. Schreiber, “Anderson localization in 1D systems with correlated disorder”, *Eur. Phys. J. B* **82**, 107 (2011) 10.1140/epjb/e2011-20212-1 (cit. on p. 66).
- [26] I. Y. Gol’dshtain, S. A. Molchanov, and L. A. Pastur, “A pure point spectrum of the stochastic one-dimensional schrödinger operator”, *Funct Anal Its Appl* **11**, 1–8 (1977) 10.1007/BF01135526 (cit. on p. 66).
- [27] M. Žonda, J. Okamoto, and M. Thoss, “Gapless regime in the charge density wave phase of the finite dimensional Falicov-Kimball model”, *Phys. Rev. B* **100**, 075124 (2019) 10.1103/PhysRevB.100.075124, arXiv:1907.04697 (cit. on p. 67).
- [28] S. R. Hassan and H. R. Krishnamurthy, “Spectral properties in the charge-density-wave phase of the half-filled Falicov-Kimball model”, *Phys. Rev. B* **76**, 205109 (2007) 10.1103/PhysRevB.76.205109 (cit. on p. 67).
- [29] O. Hart, S. Gopalakrishnan, and C. Castelnovo, “Logarithmic entanglement growth from disorder-free localisation in the two-leg compass ladder”, Sept. 1, 2020, arXiv:2009.00618 [cond-mat], <http://arxiv.org/abs/2009.00618> (visited on 11/26/2020) (cit. on p. 69).
- [30] C. Gruber, J. Iwanski, J. Jedrzejewski, and P. Lemberger, “Ground states of the spinless Falicov-Kimball model”, *Phys. Rev. B* **41**, 2198–2209 (1990) 10.1103/PhysRevB.41.2198 (cit. on p. 69).

- [31] C. Micheletti, A. B. Harris, and J. M. Yeomans, “A complete devil\textquotesingles staircase in the Falicov - Kimball model”, *J. Phys. A: Math. Gen.* **30**, L711–L717 (1997) 10.1088/0305-4470/30/21/002 (cit. on p. 69).
- [32] P. Cai et al., “Visualizing the evolution from the Mott insulator to a charge-ordered insulator in lightly doped cuprates”, *Nature Phys* **12**, 1047–1051 (2016) 10.1038/nphys3840 (cit. on p. 69).

Chapter 4

The Amorphous Kitaev Honeycomb Model

Contributions

The material in this chapter expands on work presented in

- [1] Cassella, G., D'Ornellas, P., Hodson, T., Natori, W. M., & Knolle, J. (2022). An exact chiral amorphous spin liquid. *arXiv preprint arXiv:2208.08246*.

All the code is available online [2].

This was a joint project of Gino, Peru and myself with advice and guidance from Willian and Johannes (all authors of the above). The project grew out of an interest the three of us had in studying amorphous systems, coupled with Johannes' expertise on the Kitaev model. The idea to use Voronoi partitions came from [3] and Gino did the implementation of this. The idea and implementation of the edge colouring using SAT solvers and the mapping from flux sector to bond sector using A* search were both entirely my work. Peru produced the numerical evidence for the ground state and implemented the local markers. Gino and I did much of the rest of the programming for Koala collaboratively, often pair programming, this included the phase diagram, edge mode and finite temperature analyses as well as the derivation of the projector in the amorphous case.

4.1 The Model

Already at its introduction it was known that Kitaev honeycomb model would remain solvable on any tri-coordinated graph. This has been used to generalise the model to many lattices [4–7] but so far none have fully broken the translation symmetry of the model by putting it onto a amorphous lattice.

Amorphous lattices are characterised by local constraints but no long range order. These arise, for instance, in amorphous semiconductors like Silicon and Germanium [8, 9]. Recent work has shown that topological insulating (TI) phases, characterized by protected edge states and topological bulk invariants, can exist in amorphous systems [10–16]. TI phases, however, arise in non-interacting systems. In this context, we might ask whether QSL systems and the KH model in particular could be realised on amorphous lattices. The phases of the KH model have many similarities with TIs but differ in that the KH model is an interacting system. In general, research on amorphous electronic systems has been focused mainly on non-interacting systems with the exception of amorphous superconductivity [17–21] or very recent work looking to understand the effect of strong electron repulsion in TIs [22].

Looking more towards the KH model, magnetism in amorphous systems has been investigated since the 1960s, mostly through the adaptation of theoretical tools developed for disordered systems [23–26]. We have already seen that the topological disorder of amorphous lattices can be qualitatively different from standard bond or site disorder, especially in two dimensions [27, 28]. Research focused on classical Heisenberg and Ising models has accounted for the observed behaviour of ferromagnetism, disordered antiferromagnetism and widely observed spin glass behaviour [29]. However, the role of the spin-anisotropic interactions and quantum effects that we see in the KH model has not been addressed in amorphous magnets. It is an open question whether frustrated magnetic interactions on amorphous lattices can give rise genuine quantum

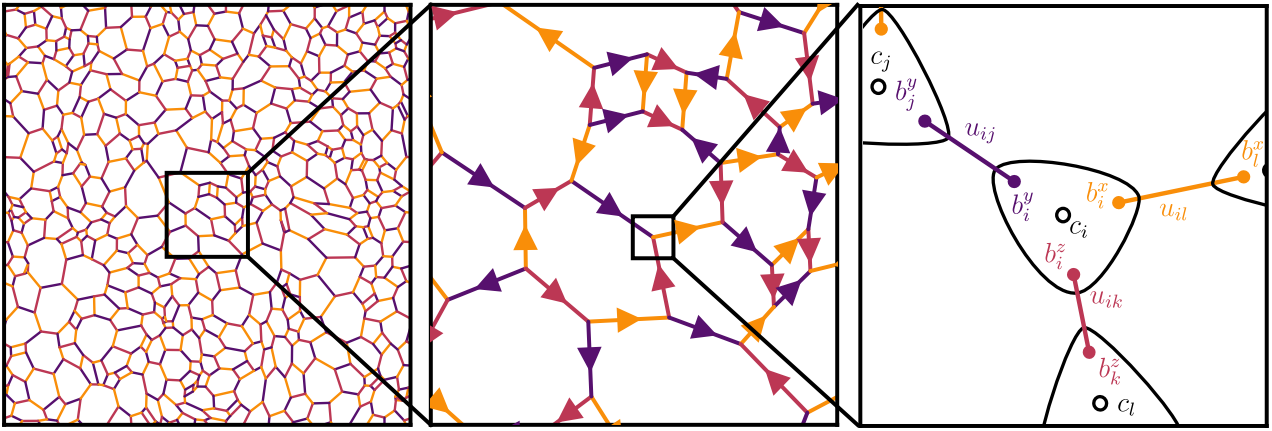


Figure 4.1: (a) The standard Kitaev model is defined on a honeycomb lattice. The special feature of the honeycomb lattice that makes the model solvable is that each vertex is joined by exactly three bonds, i.e. the lattice is trivalent. One of three labels is assigned to each (b). We represent the antisymmetric gauge degree of freedom $u_{jk} = \pm 1$ with arrows that point in the direction $u_{jk} = +1$ (c). The Majorana transformation can be visualised as breaking each spin into four Majoranas which then pair along the bonds. The pairs of x,y and z Majoranas become part of the classical \mathbb{Z}_2 gauge field u_{ij} . This leaves a single Majorana c_i per site.

phases such as QSLs [30–33]. This chapter will answer that question by demonstrating that the Kitaev model on amorphous lattices leads to a kind of QSL called a chiral spin liquid (CSL).

In this section I will discuss how to generalise the Kitaev model to an amorphous lattice. The methods section discusses how to generate such lattices using Voronoi partitions of the plane [10, 12], colour them using a SAT solver and how to map back and forth between gauge field configurations and flux configurations. In the results section, I will show extensive numerical evidence that the model follows the simple generalisation to Lieb’s theorem [34] found by other works [4–7]. I then map out the phase diagram of the model and show that the chiral phase around the symmetric point ($J_x = J_y = J_z$) is gapped and non-Abelian as characterized by a quantized local Chern number ν [10, 35] as well as protected chiral Majorana edge modes. Finally, I look at the role of finite temperature fluctuations and show that the proliferation of flux excitations leads to an Anderson transition (similar to that of the FK model) to a thermal metal phase [36–38]. Finally I consider possible physical realisations of the model and other generalisations.

The KH model must remain solvable on any lattice which satisfies two properties. First the lattice must first be trivalent, every vertex must have three edges attached to it [39, 40]. A well studied class of amorphous trivalent lattices are the 2D Voronoi lattices [10, 12, 41]. These arise from Voronoi partitions of the plane. Given a set of seed points, the Voronoi partition divides the plane into regions based on which seed point is closest by some metric, usually the euclidean metric. The ‘spheres of influence’ of each seed point form the plaquettes of the resulting lattices, while the boundaries become the edges. The Voronoi partition exists in arbitrary dimensions and produces lattices with coordination number $d+1$ except for degenerate cases with measure zero [42, 43]. Hence Voronoi lattices in two dimensions lends themselves naturally to the Kitaev model.

Other methods of lattice generation are possible, one can connect randomly placed sites based on proximity [11] or create simplices from random sites [44]. However these methods do not

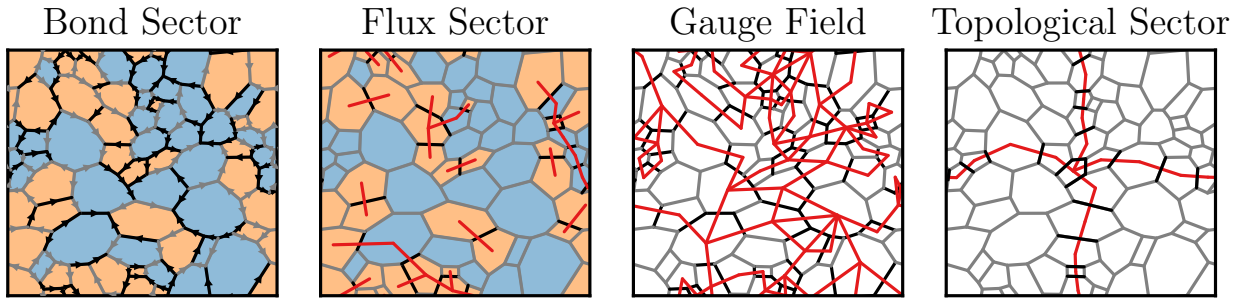


Figure 4.2: (Bond Sector) A state in the bond sector is specified by assigning ± 1 to each edge of the lattice. However, this description has a substantial gauge degeneracy. We can simplify things by decomposing each state into the product of three kinds of objects: (Vortex Sector) Only a small number of bonds need to be flipped (compared to some arbitrary reference) to reconstruct the vortex sector. Here, the edges are chosen from a spanning tree of the dual lattice, so there are no loops. (Gauge Field) The ‘loopiness’ of the bond sector can be factored out. This gives a network of loops that can always be written as a product of the gauge operators D_j . (Topological Sector) Finally, there are two loops that have no effect on the vortex sector, nor can they be constructed from gauge symmetries. These can be thought of as two fluxes $\Phi_{x/y}$ that thread through the major and minor axes of the torus. Measuring $\Phi_{x/y}$ amounts to constructing Wilson loops around the axes of the torus. We can flip the value of Φ_x by transporting a vortex pair around the torus in the y direction, as shown here. In each of the three figures on the right, black bonds correspond to those that must be flipped. Composing the three together gives back the original bond sector on the left. [Animated version online](#).

present a natural way to restrict the vertex degree to a constant. Perhaps ideally, we would sample uniformly from the space of possible trivalent graphs, there has been some work on how to do this using a Markov Chain Monte Carlo approach [45]. However, it does not guarantee that the resulting graph is planar, which is necessary to be able to 3-edge-colour the lattice, our second constraint.

The second constraint required for the Kitaev model to remain solvable is that we must be able to assign labels to each bond $\{x, y, z\}$ such that each no two edges of the same label meet at a vertex. Such an assignment is known as a 3-edge-colouring. For translation invariant models we need only find a solution for the unit cell which is usually small enough that this can be done by hand. For amorphous lattices the difficulty is compounded by the fact that, to the best of my knowledge, the problem of edge-colouring is in NP. To find colourings in practice, we will employ a standard method from the computer science literature for finding solutions of NP problems called a SAT solver, this is discussed in more detail in the [methods section](#).

We find that for larger lattices there are many valid colourings. In the isotropic case $J^\alpha = 1$ the colouring has no physical significance. As the definition of the four Majoranas at a site is arbitrary, we can define a local operator that transforms the colouring of any particular site to another permutation and show that these operators commute with the Hamiltonian, see [appendix A.4](#). We cannot do this in the anisotropic case but we nevertheless expect the lattices to exhibit a self averaging behaviour in larger systems when the colouring is chosen arbitrarily.

On a lattice with the above properties, the solution laid out in [the kitaev model](#) remains

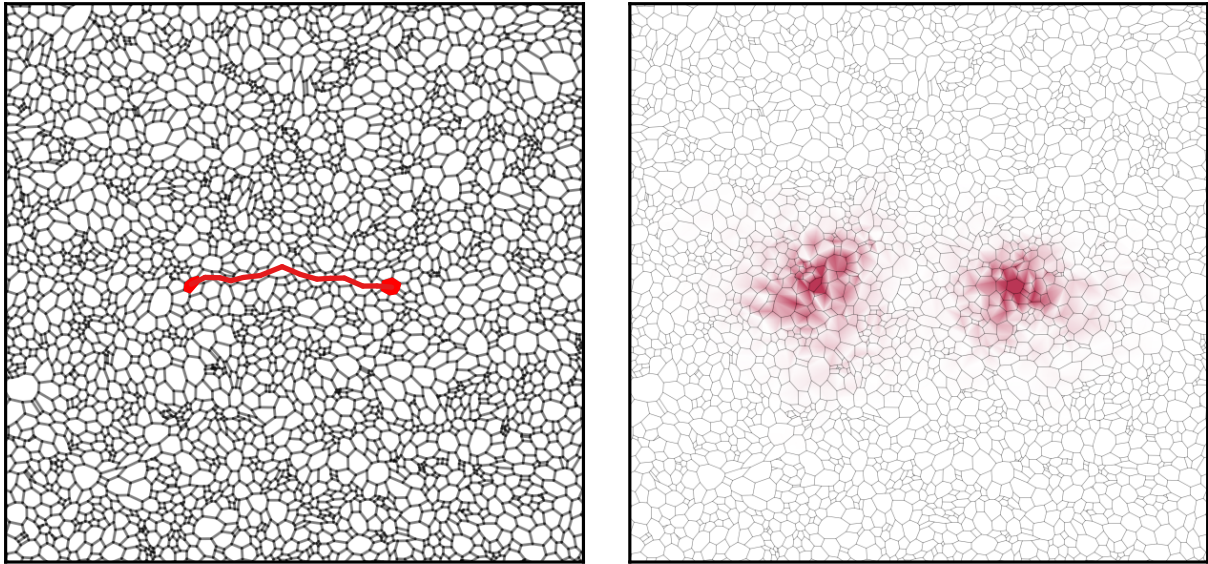


Figure 4.3: (Left) A large amorphous lattice in the ground state save for a single pair of vortices shown in red, separated by the string of bonds that we flipped to create them. (Right) The density of the lowest energy Majorana state in this vortex sector. These Majorana states are bound to the vortices. They ‘dress’ the vortices to create a composite object.

applicable to our Amorphous Kitaev (AK) model. See fig. 4.1 for an example lattice generated by our method. The main differences are twofold. Firstly, the lattices are no longer bipartite in general and therefore contain plaquettes with an odd number of sides which have flux $\pm i$. This leads the AK model to have a ground state with spontaneously broken chiral symmetry [7, 46–52]. This is also similar to the behaviour of the original Kitaev model in response to a magnetic field. One ground state is related to the other by globally inverting the imaginary ϕ_i fluxes [47].

Secondly, as the model is no longer translationally invariant, Lieb’s theorem for the ground state flux sector no longer applies. However as discussed in the background, a simple generalisation of Lieb’s theorem has been shown numerically to be applicable to many generalised Kitaev models [4–7]. This generalisation states that the ground state flux configuration depends on the number of sides of each plaquette $\phi = -(\pm i)^{n_{\text{sides}}}$ with a twofold global chiral degeneracy.

The obvious approach would be to verify that this generalises to the AK model numerically via exhaustive checking of flux configurations. However this is problematic because the number of states to check scales exponentially with system size. We side step this by gluing together two methods, we first work with lattices small enough that we can fully enumerate their flux sectors but tile them to reduce finite size effects. We then show that the effect of tiling scales away with system size.

In order to evaluate the Chern marker later, we need a way to evaluate the model on open boundary conditions. Simply removing bonds from the lattice leaves behind unpaired b^α operators that must be paired in some way to arrive at fermionic modes. To fix a pairing, we always start from a lattice defined on the torus and generate a lattice with open boundary conditions by defining the bond coupling $J_{ij}^\alpha = 0$ for sites joined by bonds (i, j) that we want

to remove. This creates fermionic zero modes u_{ij} associated with these cut bonds which we set to 1 when calculating the projector. Alternatively, since all the fermionic zero modes are degenerate anyway, an arbitrary pairing of the unpaired b^α operators could be performed.

4.1.1 The Euler Equation

Euler's equation provides a convenient way to understand how the states of the AK model factorise into flux sectors, gauge sectors and topological sectors. The Euler equation states if we embed a lattice with B bonds, P plaquettes and V vertices onto a closed surface of genus g , (0 for the sphere, 1 for the torus) then

$$B = P + V + 2 - 2g \quad (4.1)$$

For the case of the torus where $g = 1$, we can rearrange this and exponentiate it to read:

$$2^B = 2^{P-1} \cdot 2^{V-1} \cdot 2^2 \quad (4.2)$$

There are 2^B configurations of the bond variables $\{u_{ij}\}$. Each of these configurations can be uniquely decomposed into a flux sector, a gauge sector and a topological sector, see fig. 4.2. Each of the P plaquette operators ϕ_i takes two values but vortices are created in pairs so there are 2^{P-1} vortex sectors in total. There are 2^{V-1} gauge symmetries formed from the V symmetry operators D_i because $\prod_j D_j = \mathbb{I}$ is enforced by the projector. Finally, the two topological fluxes Φ_x and Φ_y account for the last factor of 2^2 .

In addition, the fact that we only work with trivalent lattices implies that each vertex shares three bonds with other vertices so effectively comes with $\frac{3}{2}$ bonds. This is consistent with the fact that, in the Majorana representation on the torus, each vertex brings three b^α operators which then pair along bonds to give $3/2$ bonds per vertex. Substituting $3V = 2B$ into Euler's equation tells us that any trivalent lattice on the torus with N plaquettes has $2N$ vertices and $3N$ bonds. Since each bond is part of two plaquettes this implies that the mean number of sides of a plaquette is exactly six and that odd sides plaquettes must come in pairs.

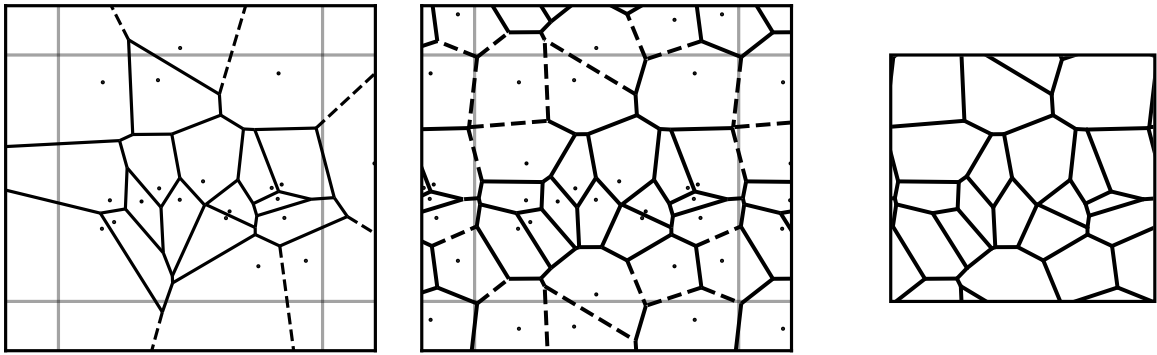


Figure 4.4: (Left) Lattice construction begins with the Voronoi partition of the plane with respect to a set of seed points (black points) sampled uniformly from \mathbb{R}^2 . (Center) However, we want the Voronoi partition of the torus, so we tile the seed points into a three by three grid. The boundaries of each tile are shown in light grey. (Right) Finally, we identify edges corresponding to each other across the boundaries to produce a graph on the torus. [Animated version online](#).

4.2 Methods

This section describes the novel methods we developed to simulate the AK model including lattice generation, bond colouring and the inverse mapping between flux sector and gauge sector. Implementations are available online as a Python package called Koala (Kitaev On Amorphous LAttices) [2]. All results and figures herein were generated with Koala.

4.2.1 Voronisation

The lattices we use are Voronoi partitions of the torus [10, 12, 41]. We start by sampling *seed points* uniformly (or otherwise) on the torus. As most off the shelf routines for computing Voronoi partitions are defined on the plane rather than the torus, we tile our seed points into a 3×3 pr 5×5 grid before calling a standard Voronoi routine [53] from the python package Scipy [54]. Finally, we undo the tiling to the grid by identifying edges in the tiled lattice which are identical, yielding a trivalent lattice on the torus. We encode our lattices with edge lists $[(i, j), (j, k) \dots]$ and an additional vector $(\{-1, 0, +1\}, \{-1, 0, +1\})$ for each edge that encodes the sense in which it crosses the periodic boundary conditions, equivalent to how the edge leaves the unit cell were the system to tile the plane, see [appendix A.3](#) for more detail.

The graph generated by a Voronoi partition of a two dimensional surface is always planar. This means that no edges cross each other when the graph is embedded into the plane. It is also trivalent in that every vertex is connected to exactly three edges [42, 43].

4.2.2 Colouring the Bonds

To be solvable the AK model requires that each edge in the lattice be assigned a label x , y or z , such that each vertex has exactly one edge of each type connected to it. This problem must

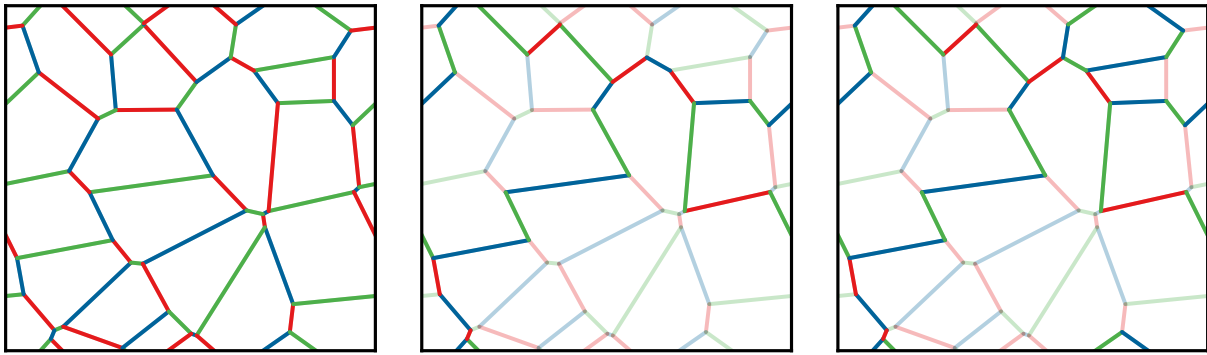


Figure 4.5: Different valid three-edge-colourings of an amorphous lattice. Colors that differ from the leftmost panel are highlighted in the other panels.

be distinguished from that considered by the famous four-colour theorem [55]. The four-colour theorem is concerned with assigning colours to the **vertices** of planar graphs, such that no vertices that share an edge have the same colour. Here we are instead concerned with finding an edge colouring.

For a graph of maximum degree Δ , $\Delta + 1$ colours are always enough to edge-colour it. An $\mathcal{O}(mn)$ algorithm exists to do this for a graph with m edges and n vertices [56]. Restricting ourselves to graphs with $\Delta = 3$, these graphs are known as cubic graphs. Cubic graphs can be four-edge-coloured in linear time [57]. However we need a three-edge-colouring of our cubic graphs, which turns out to be more difficult. Cubic, planar, *bridgeless* graphs can be three-edge-coloured if and only if they can be four-face-coloured [58]. Bridges are edges that connect otherwise disconnected components. An $\mathcal{O}(n^2)$ algorithm exists for these [59]. However, it is not clear whether this extends to cubic, **toroidal** bridgeless graphs.

A four-face-colouring is equivalent to a four-vertex-colouring of the dual graph, see [appendix A.3](#). So if we could find a four-vertex-colouring of the dual graph we would be done. However vertex-colouring a toroidal graph may require up to seven colours [60]! The complete graph of seven vertices K_7 is a good example of a toroidal graph that requires seven colours.

Luckily, some problems are harder in theory than in practice. Three-edge-colouring cubic toroidal graphs appears to be one of those things. To find colourings, we use a Boolean Satisfiability Solver or SAT solver. A SAT problem is a set of statements about a set of boolean variables, such as “ x_1 or not x_3 is true”. A solution to a SAT problem is a assignment $x_i \in 0, 1$ that satisfies all the statements [61]. General purpose, high performance programs for solving SAT problems have been an area of active research for decades [62]. Such programs are useful because, by the Cook-Levin theorem, any NP problem can be encoded (in polynomial time) as an instance of a SAT problem . This property is what makes SAT one of the subset of NP problems called NP-Complete [63, 64]. Thus, it is a relatively standard technique in the computer science community to solve NP problems by first transforming them to SAT instances and then using an off the shelf SAT solver. The output of this can then be mapped back to the original problem domain.

Whether graph colouring problems are in NP or P seems to depend delicately on the class of graphs considered, the maximum degree and the number of colours used. Since we I didn't

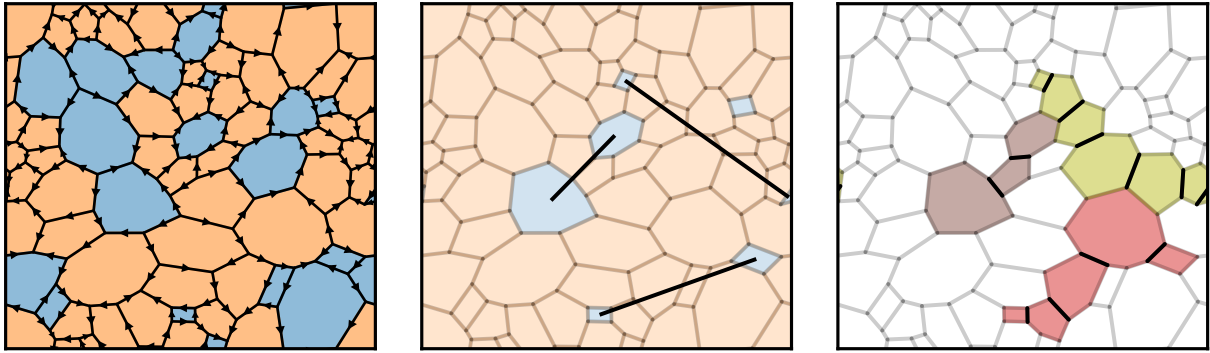


Figure 4.6: (Left) The ground state flux sector and bond sector for an amorphous lattice. Bond arrows indicate the direction in which $u_{jk} = +1$. Plaquettes are coloured blue when $\hat{\phi}_i = -1$ ($-i$) for even/odd plaquettes and orange when $\hat{\phi}_i = +1$ ($+i$) for even/odd plaquettes. (Centre) To transform this to the target flux sector (all $+1/+i$), we first flip any u_{jk} that are between two fluxes. This leaves a set of isolated fluxes that must be annihilated. Then, these are paired up as indicated by the black lines. (Right) A* search is used to find paths (coloured plaquettes) on the dual lattice between each pair of fluxes and the corresponding u_{jk} (shown in black) are flipped. One flux will remain because the starting and target flux sectors differed by an odd number of fluxes.

know of any better algorithm for the problem at hand using a SAT solver appeared to be a reasonable first method to try and it turns out to be fast enough in practice that it is by no means to rate limiting step for solving instances of our model. In [appendix A.3](#) I detail the specifics of how I mapped edge-colouring problems to SAT instances and show a breakdown of where the computational effort is spent, the majority being on diagonalisation.

4.2.3 Mapping between flux sectors and bond sectors

In the AK model, going from the bond sector to flux sector is done simply from the definition of the fluxes

$$\phi_i = \prod_{(j,k) \in \partial\phi_i} i u_{jk}. \quad (4.3)$$

The reverse, constructing the bond sector $\{u_{jk}\}$ that corresponds to a particular flux sector $\{\Phi_i\}$ is not so trivial. The algorithm, shown visually in fig. 4.6 is this:

1. Fix the gauge by choosing some arbitrary u_{jk} configuration. In practice, we use $u_{jk} = +1$. This chooses an arbitrary one of the four topological sectors.
2. Compute the current flux configuration and how it differs from the target one. Consider any plaquette that differs from the target as a defect.
3. Find any adjacent pairs of defects and flip the u_{jk} between them. This leaves a set of isolated defects.

4. Pair the defects up using a greedy algorithm and compute paths along the dual lattice between each pair of plaquettes using A*. Flipping the corresponding set of bonds transports one flux to the other and annihilates both.

4.3 Results

4.3.1 The Ground State Flux Sector

Here I will discuss the numerical evidence that our guess for the ground state flux sector is correct. We will do this by enumerating all the flux sectors of many separate system realisations. However we have two seemingly irreconcilable problems. Finite size effects have a large energetic contribution for small systems [39] so we would like to perform our analysis for very large lattices. However for an amorphous system with N plaquettes, $2N$ edges and $3N$ vertices we have 2^{N-1} flux sectors to check and diagonalisation scales with $\mathcal{O}(N^3)$. That exponential scaling makes it infeasible to work with lattices much larger than 16 plaquettes.

To get around this we instead look at periodic systems with amorphous unit cells. For a similarly sized periodic system with A unit cells and B plaquettes in each unit cell where $N \sim AB$ things get much better. We can use Bloch's theorem to diagonalise this system in about $\mathcal{O}(AB^3)$ operations, and more importantly there are only 2^{B-1} flux sectors to check. We fully enumerated the flux sectors of $\sim 25,000$ periodic systems with disordered unit cells of up to $B = 16$ plaquettes and $A = 100$ unit cells. However, showing that our guess is correct for periodic systems with disordered unit cells is not quite convincing on its own as we have effectively removed longer-range disorder from our lattices.

The second part of the argument is to show that the energetic effect of introducing periodicity scales away as we go to larger system sizes and has already diminished to a small enough value at 16 plaquettes, which is indeed what we find. From this we argue that the results for small periodic systems generalise to large amorphous systems. In the isotropic case ($J^\alpha = 1$), our conjecture correctly predicted the ground state flux sector for all of the lattices we tested. For the toric code phase ($J^x = J^y = 0.25, J^z = 1$) all but around ($\sim 0.5\%$) lattices had ground states conforming to our conjecture. In these cases, the energy difference between the true ground state and our prediction was on the order of $10^{-6}J$. It is unclear whether this is a finite size effect or something else.

The spin Kitaev Hamiltonian is real and therefore has time reversal symmetry (TRS). However in the ground state the flux ϕ_p through any plaquette with an odd number of sides has imaginary eigenvalues $\pm i$. Thus, states with a fixed flux sector spontaneously break time reversal symmetry. This was first described by Yao and Kivelson for a translation invariant Kitaev model with odd sided plaquettes [65].

So we have flux sectors that come in degenerate pairs, where time reversal is equivalent to inverting the flux through every odd plaquette, a general feature for lattices with odd plaquettes [7, 47]. This spontaneously broken symmetry serves a role analogous to the external magnetic field in the original honeycomb model, leading the AK model to have a non-Abelian anyonic phase without an external magnetic field.

4.3.2 Ground State Phase Diagram

The triangular phase J_x, J_y, J_z phase diagram of this family of models arises from setting the energy scale with $J_x + J_y + J_z = 1$, the intersection of this plane and the unit cube is what

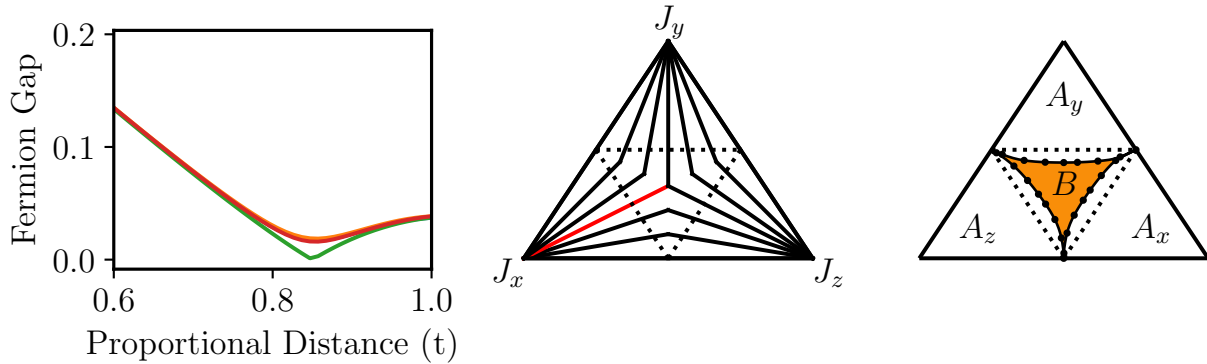


Figure 4.7: The phase diagram of the model can be characterised by an equilateral triangle whose corners indicate points where $J_\alpha = 1$, $J_\beta = J_\gamma = 0$ while the centre denotes $J_x = J_y = J_z$. (Center) To compute critical lines efficiently in this space we evaluate the order parameter of interest along rays shooting from the corners of the phase diagram. The ray highlighted in red defines the values of J used for the left figure. (Left) The fermion gap as a function of J for an amorphous system with 20 plaquettes, where the x axis is the position on the red line in the central figure from 0 to 1. For finite size systems the four topological sectors are not degenerate and only one of them (in green) has a true gap closing. (Right) The Abelian A_α phases of the model and the non-Abelian B phase separated by critical lines where the fermion gap closes. Later we will show that the Chern number ν changes from 0 to ± 1 from the A phases to the B phase. Indeed the gap *must* close in order for the Chern number to change [72].

yields the equilateral triangles seen in diagrams like fig. 4.7. The KH model has an Abelian, gapped phase in the anisotropic region (the A phase) and is gapless in the isotropic region. The introduction of a magnetic field breaks the chiral symmetry, leading to the isotropic region becoming a gapped, non-Abelian phase, the B phase.

Similar to the Kitaev Honeycomb model with a magnetic field, we find that the amorphous model is only gapless along critical lines, see fig. 4.7 (Left). Interestingly, in finite size systems the gap closing exists in only one of the four topological sectors though the sectors must become degenerate in the thermodynamic limit. Nevertheless this could be a useful way to define the $(0, 0)$ topological flux sector for the amorphous model which otherwise has no natural way to choose it.

In the honeycomb model, the phase boundaries are located on the straight lines $|J^x| = |J^y| + |J^z|$ and permutations of x, y, z . These are shown as dotted lines on fig. 4.7 (Right). We find that on the amorphous lattice these boundaries exhibit an inward curvature, similar to honeycomb Kitaev models with flux or bond disorder [66–71].

Abelian or non-Abelian of the Gapped Phase

The two phases of the amorphous model are clearly gapped, though later I'll double check this with finite size scaling.

The next question is: do these phases support excitations with trivial, Abelian or non-Abelian statistics? To answer that we turn to Chern numbers [73–75]. As discussed earlier the Chern

number is a quantity intimately linked to both the topological properties and the anyonic statistics of a model. Here we will make use of the fact that the Abelian/non-Abelian character of a model is linked to its Chern number [39]. The Chern number is only defined for the translation invariant case because it relies on integrals defined in k-space. We instead use a family of real space generalisations of the Chern number that work for amorphous systems exist called local topological markers [10, 76, 77], indeed Kitaev defines one in his original paper on the KH model [39].

Here we use the crosshair marker of [35] because it works well on smaller systems. We calculate the projector $P = \sum_i |\psi_i\rangle\langle\psi_i|$ onto the occupied fermion eigenstates of the system in open boundary conditions. The projector encodes local information about the occupied eigenstates of the system and in gapped systems it is exponentially localised [78]. The name *crosshair* comes from the fact that the marker is defined with respect to a particular point (x_0, y_0) by step functions in x and y

$$\nu(x, y) = 4\pi \operatorname{Im} \operatorname{Tr}_B \left(\hat{P} \hat{\theta}(x - x_0) \hat{P} \hat{\theta}(y - y_0) \hat{P} \right), \quad (4.4)$$

when the trace is taken over a region B around (x_0, y_0) that is large enough to include local information about the system but does not come too close to the edges. If these conditions are met then this quantity will be very close to quantised to the Chern number, see fig. 4.8. We'll use the crosshair marker to assess the Abelian/non-Abelian character of the phases.

In the A phase of the amorphous model we find that $\nu = 0$ and hence the excitations have Abelian character, similar to the honeycomb model. This phase is thus the amorphous analogue of the Abelian toric-code quantum spin liquid [79]. The B phase has $\nu = \pm 1$ so is a non-Abelian *chiral spin liquid* (CSL) similar to that of the Yao-Kivelson model [47]. The CSL state is the magnetic analogue of the fractional quantum Hall state [80]. Hereafter we focus our attention on this phase.

Edge Modes

Chiral Spin Liquids support topological protected edge modes on open boundary conditions [81]. Figure 4.9 shows the probability density of one such edge mode. It is near zero energy and exponentially localised to the boundary of the system. While the model is gapped in periodic boundary conditions (i.e on the torus) these edge modes appear in the gap when the boundary is cut.

The localization of the edge modes can be quantified by their inverse participation ratio (IPR),

$$\text{IPR} = \int d^2r |\psi(\mathbf{r})|^4 \propto L^{-\tau}, \quad (4.5)$$

where $L \sim \sqrt{N}$ is the linear dimension of the amorphous lattices and τ the dimensional scaling exponent of IPR. This is relevant because localised in-gap states do not participate in transport and hence do not turn band insulators into metals. It is only when the gap fills with extended states that we get a metallic state.

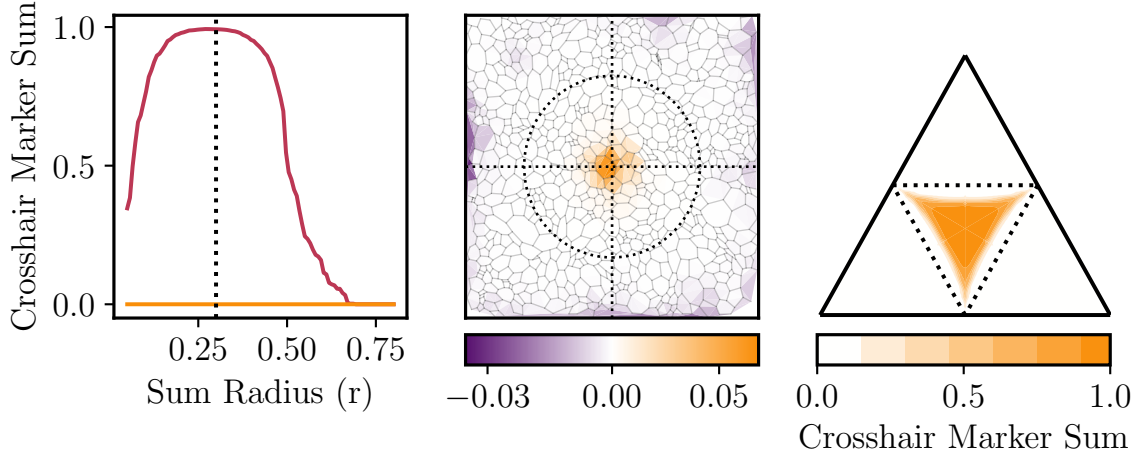


Figure 4.8: (Center) The crosshair marker [35], a local topological marker, evaluated on the Amorphous Kitaev Model. The marker is defined around a point, denoted by the dotted crosshair. Information about the local topological properties of the system are encoded within a region around that point. (Left) Summing these contributions up to some finite radius (dotted line here, dotted circle in the centre) gives a generalised version of the Chern number for the system which becomes quantised in the thermodynamic limit. The radius must be chosen large enough to capture information about the local properties of the lattice while not so large as to include contributions from the edge states. The isotropic regime $J_\alpha = 1$ in red has $\nu = \pm 1$ implying it supports excitations with non-Abelian statistics, while the anisotropic regime in orange has $\nu = 0$ implying it has Abelian statistics. (Right) Extending this analysis to the whole J_α phase diagram with fixed $r = 0.3$ nicely confirms that the isotropic phase is non-Abelian.

4.3.3 Anderson Transition to a Thermal Metal

Previous work on the honeycomb model at finite temperature has shown that the B phase undergoes a thermal transition from a quantum spin liquid phase a to a **thermal metal** phase [38].

This happens because at finite temperature, thermal fluctuations lead to spontaneous vortex-pair formation. As discussed previously these fluxes are dressed by Majorana bounds states and the composite object is an Ising-type non-Abelian anyon [82]. The interactions between these anyons are oscillatory similar to the RKKY exchange and decay exponentially with separation [36, 37, 83]. At sufficient density, the anyons hybridise to a macroscopically degenerate state known as *thermal metal* [36]. At close range the oscillatory behaviour of the interactions can be modelled by a random sign which forms the basis for a random matrix theory description of the thermal metal state.

The amorphous chiral spin liquid undergoes the same form of Anderson transition to a thermal metal state. Markov Chain Monte Carlo would be necessary to simulate this in full detail [38] but in order to avoid that complexity in the current work we instead opted to use vortex density ρ as a proxy for temperature. We give each plaquette probability ρ of being a vortex, possibly with one additional adjustment to preserve overall vortex parity. This approximation is exact in the limits $T = 0$ (corresponding to $\rho = 0$) and $T \rightarrow \infty$ (corresponding to $\rho = 0.5$) while at

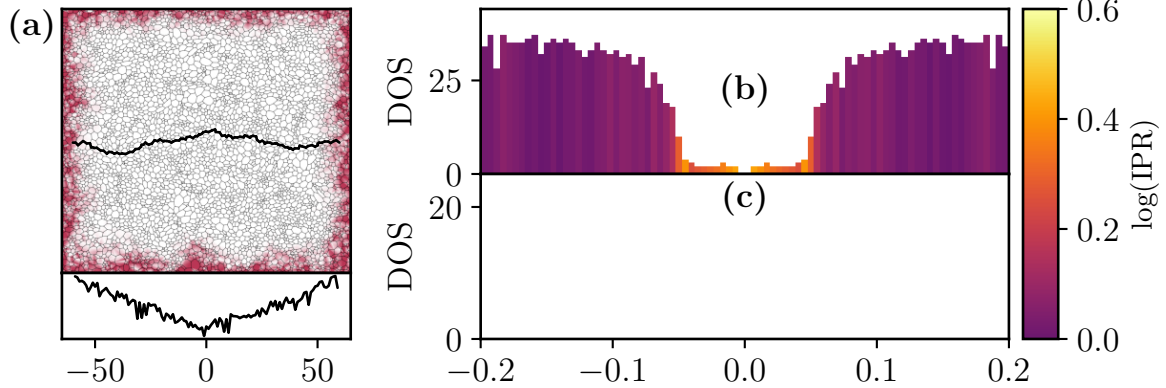


Figure 4.9: (a) The density of one of the topologically protected edge states in the B phase. (Below) the log density plotted along the black path showing that the state is exponentially localised. (a)/(b) The density of states of the corresponding lattice in (a) periodic boundary conditions, (b) open boundary conditions. The colour of the bars shows the mean log IPR for each energy window. Cutting the boundary fills the gap with localised states.

intermediate temperatures there may be vortex-vortex correlations that are not captured by positioning vortices using uncorrelated random variables.

First we performed a finite size scaling to that the presence of a gap in the CSL ground state and absence of a gap in the thermal phase are both robust as we go to larger systems, see fig. 4.10.

Next we evaluated the fermionic density of states (DOS), Inverse Participation Ratio (IPR) and IPR scaling exponent τ as functions of the vortex density ρ , see fig. 4.11. This leads to a nice picture of what happens as we raise the temperature of the system away from the gapped, insulating CSL phase. At small ρ , states begin to populate the gap but they have $\tau \approx 0$, indicating that they are localised states pinned to the vortices, and the system remains insulating. At large ρ , the in-gap states merge with the bulk band and become extensive, closing the gap, and the system transitions to the thermal metal phase.

The thermal metal phase has a signature logarithmic divergence at zero energy and oscillations in the DOS. These signatures can be shown to occur by a recursive argument that involves mapping the original model onto a Majorana model with interactions that take random signs which can itself be mapped onto a coarser lattice with lower energy excitations and so on. This can be repeating indefinitely, showing the model must have excitations at arbitrarily low energies in the thermodynamic limit [38, 84].

These signatures for our model and for the honeycomb model are shown in fig. 4.12. They do not occur in the honeycomb model unless the chiral symmetry is broken by a magnetic field.

We found a small number of lattices for which the ground state conjecture did not correctly predict the true ground state flux sector. I see two possibilities for what could cause this. Firstly it could be a finite size effect that is amplified by certain rare lattice configurations. It would be interesting to try to elucidate what lattice features are present when the ground state conjecture fails. Alternatively, it might be telling that the ground state conjecture failed in the toric code A phase where the couplings are anisotropic. We showed that the colouring does not matter in the B phase. However an avenue that I did not explore was whether the particular

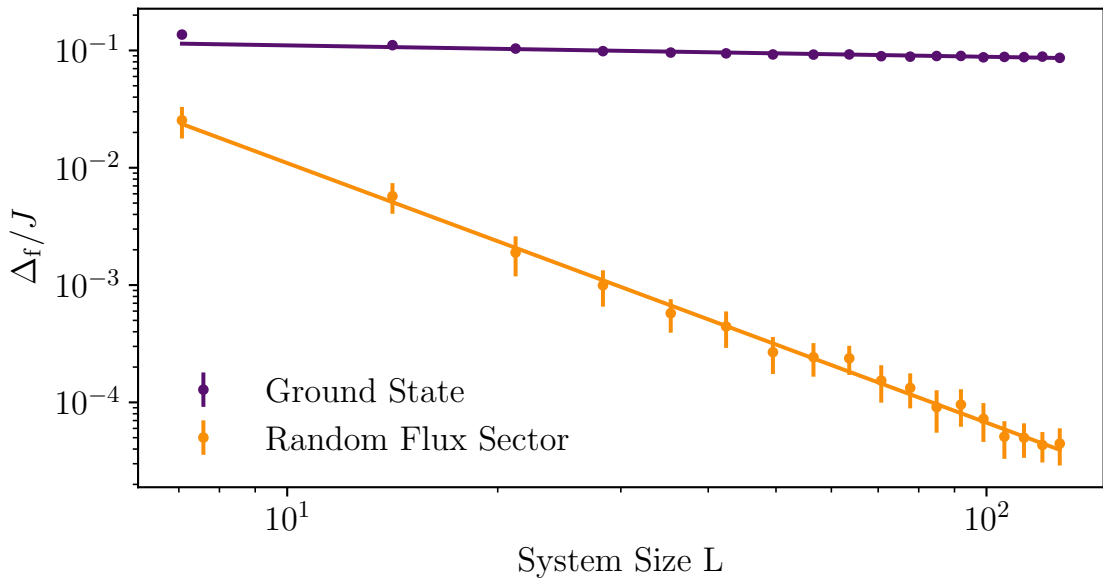


Figure 4.10: Within a flux sector, the fermion gap Δ_f measures the energy between the fermionic ground state and the first excited state. This graph shows the fermion gap as a function of system size for the ground state flux sector and for a configuration of random fluxes. We see that the disorder induced by putting the Kitaev model on an amorphous lattice does not close the gap in the ground state. The gap closes in the flux disordered limit is good evidence that the system transitions to a gapless thermal metal state at high temperature. Each point shows an average over 100 lattice realisations. System size L is defined \sqrt{N} where N is the number of plaquettes in the system. Error bars shown are 3 times the standard error of the mean. The lines shown are fits of $\frac{\Delta_f}{J} = aL^b$ with fit parameters: Ground State: $a = 0.138 \pm 0.002, b = -0.0972 \pm 0.004$ Random Flux Sector: $a = 1.8 \pm 0.2, b = -2.21 \pm 0.03$

choice of colouring for a lattice affects the physical properties in the toric code A phase. It is possible that some property of the particular colouring chosen is what leads to failure of the ground state conjecture here.

4.4 Conclusion

In this chapter we have looked at an extension of the Kitaev honeycomb model to amorphous lattices with coordination number three. We discussed a method to construct arbitrary trivalent lattices using Voronoi partitions, how to embed them onto the torus and how to edge-colour them using a SAT solver. We showed numerically that the ground state flux sector of the model is given by a simple extension of Lieb's theorem. The model has two gapped quantum spin liquid phases. The two phases support excitations with different anyonic statistics, Abelian and non-Abelian, distinguished using a real-space generalisation of the Chern number [35]. The presence of odd-sided plaquettes in the model results in spontaneous breaking of time reversal symmetry, leading to the emergence of a chiral spin liquid phase. Finally we showed evidence that the amorphous system undergoes an Anderson transition to a thermal metal phase, driven by the proliferation of vortices with increasing temperature.

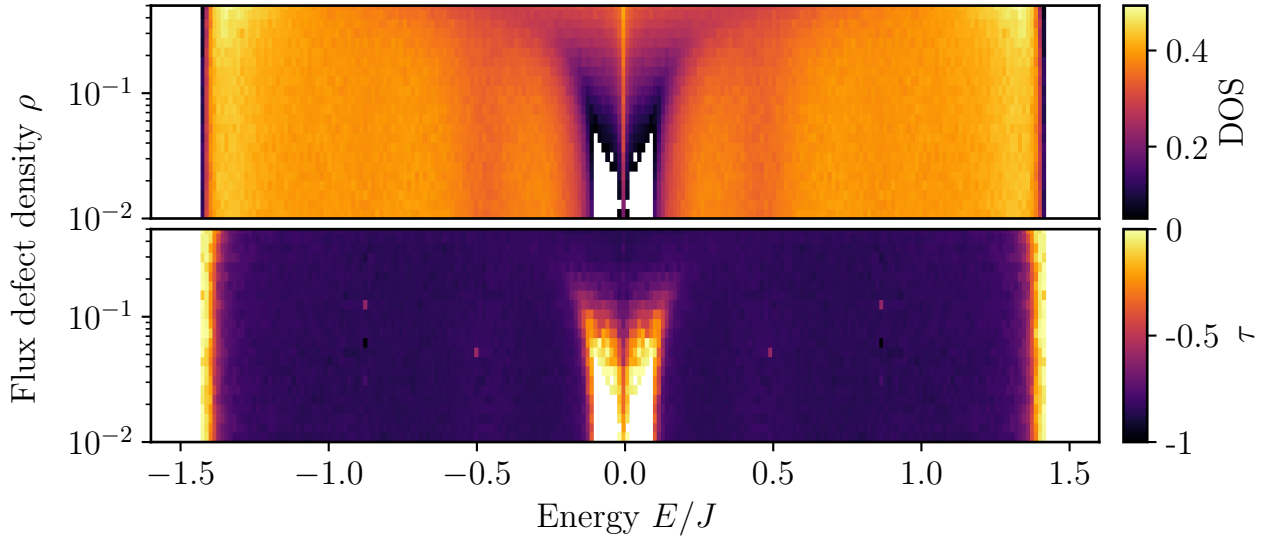


Figure 4.11: (Top) Density of states and (Bottom) scaling exponent τ of the amorphous Kitaev model as a vortex density ρ is increased. The scaling exponent τ is the exponent with which the inverse participation ratio scales with system size. It gives a measure of the degree of localisation of the states in each $(E/J, \rho)$ bin. At zero ρ we have the gapped ground state. At small ρ , states begin to populate the gap. These states have $\tau \approx 0$, indicating that they are localised states pinned to fluxes, and the system remains insulating. As ρ increases further, the in-gap states merge with the bulk band and become extensive, fully closing the gap, and the system transitions to a thermal metal phase.

The AK model is an exactly solvable model of the chiral QSL state, one of the first models to exhibit a topologically non-trivial quantum many-body phase on an amorphous lattice. As such this study provides a number of future lines of research.

Experimental Realisations and Signatures

We should also consider whether a physical amorphous system that supports a QSL ground state could exist. The search for translation invariant Kitaev systems is already motivated by the prospect of a physically realised QSL state, Majorana fermions and direct access to a system with emergent \mathbb{Z}_2 gauge physics [85]. An amorphous Kitaev model would provide all this but in addition the possibility of exploring the CSL state as well as potentially very different routes to a physical realisation. One route would be to ask if any crystalline Kitaev material candidates can be heated and rapidly quenched [24, 26, 86] to produce amorphous analogues that might preserve enough of their local structure to support a QSL state.

Instead looking to more designer materials, metal organic frameworks (MOFs) could present a platform for a synthetic Kitaev material. These materials are composed of repeating units of large organic molecular frameworks coordinated with metal ions. Amorphous MOFs can be generated with mechanical processes that introduce disorder into crystalline MOFs [87]. There have been recent proposals for realizing strong Kitaev interactions [88] in them as potential signatures of a resonating valence bond QSL state in MOFs with Kagome geometry [89]. Finally MOFs are composed of large synthetic molecules so may provide more opportunity for fine

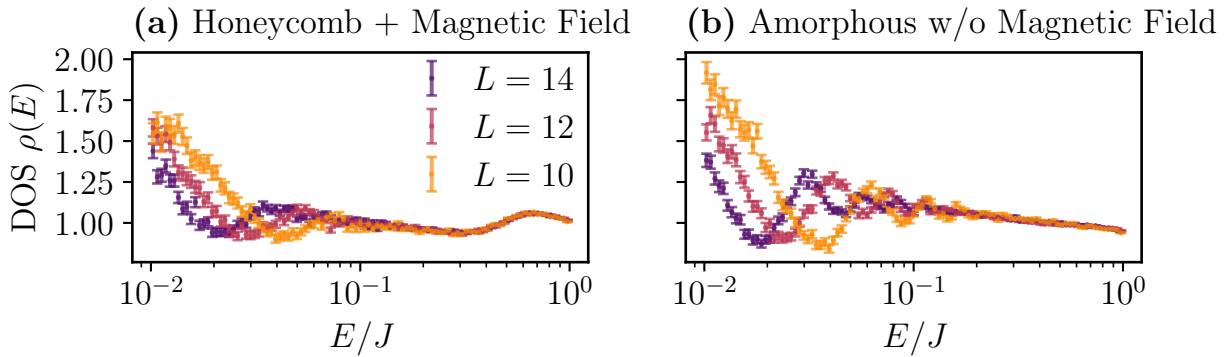


Figure 4.12: Density of states at high temperature showing the logarithmic divergence at zero energy and oscillations characteristic of the thermal metal state [38, 84]. (a) shows the honeycomb lattice model in the B phase with magnetic field, while (b) shows that our model transitions to a thermal metal phase without an external magnetic field but rather due to the spontaneous chiral symmetry breaking. In both plots the density of vortices is $\rho = 0.5$ corresponding to the $T = \infty$ limit.

tuning to target particular physics than elemental compounds. There have also been proposals to realise Kitaev physics in optical lattice experiments [90, 91] which can also support amorphous lattices [92].

A physical realisation in either an amorphous compound or a MOF would likely entail a high degree of defects. Amorphous silicon for instance tends to contain a high degree of dangling bonds which must be passivated by hydrogenation to improve its physical properties [93]. In both cases, if we assume that Kitaev physics can be realised by crystalline systems, it is not clear if the necessary superexchange couplings would survive the addition of disorder to the MOF lattice. It would therefore make sense to examine how robust the CSL ground state of the AK model is to additional disorder in the Hamiltonian, for example mis-colourings of the bonds, vertex degree disorder and disorder in coupling strengths. Relatedly, one could look at perturbations to the Hamiltonian that break integrability [94–98].

Considering experimental signatures, we expect that the chiral amorphous QSL will display a half-quantized thermal Hall effect similar to the magnetic field induced behaviour of KH materials [99–102]. Alternatively, the CSL state could be characterized by local probes such as spin-polarized scanning tunnelling microscopy [103–105] and the thermal metal phase displays characteristic longitudinal heat transport signatures [82].

Local perturbations such as those that might come from an atomic force microscope could potentially be used to create and control vortices [106]. To this end it may make sense to look at how the move to amorphous lattices affects vortex time dynamics in perturbed KH models [107].

Given the lack of unambiguous signatures of the QSL state it can be hard to distinguish the effects of the QSL state from the effect of disorder. So introducing topological disorder from amorphous lattices may pose considerable experimental challenges. Three dimensional realisations could get around this as they would be expected to have a true FTPT to the thermal metal state that could be a useful experimental signature [4, 108]. Three dimensional Kitaev systems can also support CSL ground states [109].

Thermodynamics

The KH model can be extended to three dimensional tri-coordinate lattices [4, 108] or it can be generalised to an exactly solvable spin- $\frac{3}{2}$ model on four-coordinate lattices [40, 46, 51, 52, 65, 110–117]. In [110] the two dimensional square lattice with 4 bond types (J_w, J_x, J_y, J_z) is considered. Since Voronoi partitions in three dimensions produce lattices of degree four, one interesting generalisation of this work would be to look at the spin- $\frac{3}{2}$ Kitaev model on amorphous lattices.

We did not perform a full MCMC simulation of the AK model at finite temperature but the possible extension of the model to three dimensions with an FTPT would motive this full analysis in different dimensions. This would be a numerically challenging task but poses no conceptual barriers [36–38]. Doing this would, firstly, allow one to look for possible violations of the Harris criterion [118] for the Ising transition of the flux sector. Recall that topological disorder in two dimensions has radically different properties to that of other kinds of disorder due to the constraints imposed by the Euler equation and maintaining coordination number which allows it to violate otherwise quite general rules like the Harris criterion [27, 28]. Second, incorporating the projector in addition to MCMC would allow for a full investigation of whether the effect of topological degeneracy is apparent at finite temperatures as is done in [38].

Next, one could investigate whether a QSL phase may exist for other models defined on amorphous lattices with a view to more realistic prospects of observation. For instance, it would be interesting to see if the properties of the Kitaev-Heisenberg model generalise from the honeycomb to the amorphous case [Chaloupka, Jackeli, and Khaliullin [95]; Chaloupka and Khaliullin [97]; Jackeli and Khaliullin [119]; Kalmeyer and Laughlin [120]; Manousakis [121]];]. Alternatively we might look at other lattice construction techniques. For instance we could construct lattices by linking close points [11] or create simplices from random sites [44]. Lattices constructed these ways would like have a large number of lattice defects $z \neq 3$ in the bulk, leading to persistent zero modes.

Overall, there has been surprisingly little research on amorphous quantum many body phases despite there being plenty of material candidates. I expect the exact chiral amorphous spin liquid to find many generalisation to realistic amorphous quantum magnets.

References

- [1] G. Cassella et al., *An exact chiral amorphous spin liquid*, Aug. 17, 2022, 10.48550/arXiv.2208.08246, arXiv:2208.08246 [cond-mat] (cit. on p. 75).
- [2] T. Hodson, P. D’Ornellas, and G. Cassella, *Koala: Kitaev on Amorphous Lattices*, Feb. 28, 2022, 10.5281/zenodo.6303275 (cit. on pp. 75, 80).
- [3] Q. Marsal, D. Varjas, and A. G. Grushin, “Topological Weaire–Thorpe models of amorphous matter”, *Proceedings of the National Academy of Sciences* **117**, 30260–30265 (2020) 10.1073/pnas.2007384117 (cit. on p. 75).
- [4] T. Eschmann et al., “Thermodynamic classification of three-dimensional Kitaev spin liquids”, *Phys. Rev. B* **102**, 075125 (2020) 10.1103/PhysRevB.102.075125 (cit. on pp. 75–76, 78, 91–92).
- [5] H. Yao, S.-C. Zhang, and S. A. Kivelson, “Algebraic spin liquid in an exactly solvable spin model”, *Phys. Rev. Lett.* **102**, 217202 (2009) 10.1103/PhysRevLett.102.217202 (cit. on pp. 75–76, 78).
- [6] T. Eschmann et al., “Thermodynamics of a gauge-frustrated Kitaev spin liquid”, *Physical Review Research* **1**, 032011(R) (2019) (cit. on pp. 75–76, 78).
- [7] V. Peri et al., “Non-Abelian chiral spin liquid on a simple non-Archimedean lattice”, *Phys. Rev. B* **101**, 041114 (2020) 10.1103/PhysRevB.101.041114 (cit. on pp. 75–76, 78, 84).
- [8] F. Yonezawa and T. Ninomiya, eds., *Topological disorder in condensed matter*, Vol. 46, Springer-Series in Solid State Sciences (Springer-Verlag, Berlin Heidelberg, 1983) (cit. on p. 75).
- [9] R. Zallen, *The physics of amorphous solids* (John Wiley & Sons, 2008) (cit. on p. 75).
- [10] N. P. Mitchell et al., “Amorphous topological insulators constructed from random point sets”, *Nature Phys* **14**, 380–385 (2018) 10.1038/s41567-017-0024-5 (cit. on pp. 75–76, 80, 86).
- [11] A. Agarwala, “Topological insulators in amorphous systems”, in *Excursions in ill-condensed quantum matter* (Springer, 2019), pp. 61–79 (cit. on pp. 75–76, 92).
- [12] Q. Marsal, D. Varjas, and A. G. Grushin, “Topological Weaire–Thorpe models of amorphous matter”, *Proc. Natl. Acad. Sci. U.S.A.* **117**, 30260–30265 (2020) 10.1073/pnas.2007384117 (cit. on pp. 75–76, 80).
- [13] M. Costa et al., “Toward realistic amorphous topological insulators”, *Nano letters* **19**, 8941–8946 (2019) (cit. on p. 75).
- [14] A. Agarwala, V. Juričić, and B. Roy, “Higher-order topological insulators in amorphous solids”, *Physical Review Research* **2**, 012067 (2020) (cit. on p. 75).
- [15] H. Spring, A. Akhmerov, and D. Varjas, “Amorphous topological phases protected by continuous rotation symmetry”, *SciPost Physics* **11**, 022 (2021) (cit. on p. 75).
- [16] P. Corbae et al., “Evidence for topological surface states in amorphous Bi – {2} Se – {3}”, 2019, arXiv:1910.13412 (cit. on p. 75).
- [17] W. Buckel and R. Hilsch, “Einfluß der kondensation bei tiefen temperaturen auf den elektrischen widerstand und die supraleitung für verschiedene metalle”, *Zeitschrift für Physik* **138**, 109–120 (1954) (cit. on p. 75).

- [18] W. McMillan and J. Mochel, “Electron tunneling experiments on amorphous ge 1- x au x”, Physical Review Letters **46**, 556 (1981) (cit. on p. 75).
- [19] L. V. Meisel and P. J. Cote, “Eliashberg function in amorphous metals”, Phys. Rev. B **23**, 5834–5838 (1981) 10.1103/PhysRevB.23.5834 (cit. on p. 75).
- [20] G. Bergmann, “Amorphous metals and their superconductivity”, Physics Reports **27**, 159–185 (1976) (cit. on p. 75).
- [21] S. Manna, S. K. Das, and B. Roy, *Noncrystalline topological superconductors*, July 5, 2022, arXiv:2207.02203 [cond-mat], <http://arxiv.org/abs/2207.02203> (visited on 08/22/2022) (cit. on p. 75).
- [22] S. Kim, A. Agarwala, and D. Chowdhury, “Fractionalization and topology in amorphous electronic solids”, 2022, arXiv:2205.11523 (cit. on p. 75).
- [23] A. Aharony, “Critical behavior of amorphous magnets”, Physical Review B **12**, 1038 (1975) (cit. on p. 75).
- [24] G. A. Petrakovskii, “Amorphous magnetic materials”, Soviet Physics Uspekhi **24**, 511–525 (1981) 10.1070/pu1981v024n06abeh004850 (cit. on pp. 75, 90).
- [25] T. Kaneyoshi, *Introduction to amorphous magnets* (World Scientific Publishing Company, 1992) (cit. on p. 75).
- [26] T. Kaneyoshi, ed., *Amorphous magnetism*, CRC Revivals (CRC Press, Boca Raton, 2018) (cit. on pp. 75, 90).
- [27] H. Barghathi and T. Vojta, “Phase Transitions on Random Lattices: How Random is Topological Disorder?”, Phys. Rev. Lett. **113**, 120602 (2014) 10.1103/PhysRevLett.113.120602 (cit. on pp. 75, 92).
- [28] M. Schrauth, J. Portela, and F. Goth, “Violation of the Harris-Barghathi-Vojta Criterion”, Physical Review Letters **121**, 10.1103/PhysRevLett.121.100601 (2018) 10.1103/PhysRevLett.121.100601 (cit. on pp. 75, 92).
- [29] J. Coey, “Amorphous magnetic order”, Journal of Applied Physics **49**, 1646–1652 (1978) (cit. on p. 75).
- [30] P. W. Anderson, “Resonating valence bonds: a new kind of insulator?”, Mater. Res. Bull. **8**, 153–160 (1973) (cit. on p. 76).
- [31] J. Knolle and R. Moessner, “A field guide to spin liquids”, Annual Review of Condensed Matter Physics **10**, 451–472 (2019) 10.1146/annurev-conmatphys-031218-013401 (cit. on p. 76).
- [32] L. Savary and L. Balents, “Quantum spin liquids: a review”, Reports on Progress in Physics **80**, 016502 (2017) (cit. on p. 76).
- [33] C. Lacroix, P. Mendels, and F. Mila, eds., *Introduction to frustrated magnetism*, Vol. 164, Springer-Series in Solid State Sciences (Springer-Verlag, Berlin Heidelberg, 2011) (cit. on p. 76).
- [34] E. H. Lieb, “Flux Phase of the Half-Filled Band”, Physical Review Letters **73**, 2158–2161 (1994) 10.1103/PhysRevLett.73.2158 (cit. on p. 76).
- [35] P. d’Ornellas, R. Barnett, and D. K. K. Lee, “Quantised bulk conductivity as a local chern marker”, arXiv preprint, 10.48550/ARXIV.2207.01389 (2022) 10.48550/ARXIV.2207.01389 (cit. on pp. 76, 86–87, 89).

- [36] C. R. Laumann, A. W. W. Ludwig, D. A. Huse, and S. Trebst, “Disorder-induced Majorana metal in interacting non-Abelian anyon systems”, *Phys. Rev. B* **85**, 161301 (2012) 10.1103/PhysRevB.85.161301 (cit. on pp. 76, 87, 92).
- [37] V. Lahtinen, A. W. W. Ludwig, J. K. Pachos, and S. Trebst, “Topological liquid nucleation induced by vortex-vortex interactions in Kitaev’s honeycomb model”, *Phys. Rev. B* **86**, 075115 (2012) 10.1103/PhysRevB.86.075115 (cit. on pp. 76, 87, 92).
- [38] C. N. Self, J. Knolle, S. Iblisdir, and J. K. Pachos, “Thermally induced metallic phase in a gapped quantum spin liquid - a Monte Carlo study of the Kitaev model with parity projection”, *Phys. Rev. B* **99**, 045142 (2019) 10.1103/PhysRevB.99.045142, arXiv:1807.07926 [cond-mat, physics:quant-ph] (cit. on pp. 76, 87–88, 91–92).
- [39] A. Kitaev, “Anyons in an exactly solved model and beyond”, *Annals of Physics*, January Special Issue **321**, 2–111 (2006) 10.1016/j.aop.2005.10.005 (cit. on pp. 76, 84, 86).
- [40] Z. Nussinov and G. Ortiz, “Bond algebras and exact solvability of Hamiltonians: spin $S=\frac{1}{2}$ multilayer systems”, *Physical Review B* **79**, 214440 (2009) 10.1103/PhysRevB.79.214440 (cit. on pp. 76, 92).
- [41] M. Florescu, S. Torquato, and P. J. Steinhardt, “Designer disordered materials with large, complete photonic band gaps”, *Proceedings of the National Academy of Sciences* **106**, 20658–20663 (2009) 10.1073/pnas.0907744106 (cit. on pp. 76, 80).
- [42] G. Voronoi, “Nouvelles applications des paramètres continus à la théorie des formes quadratiques. Premier mémoire. Sur quelques propriétés des formes quadratiques positives parfaites.”, *Journal für die reine und angewandte Mathematik (Crelles Journal)* **1908**, 97–102 (1908) 10.1515/crll.1908.133.97 (cit. on pp. 76, 80).
- [43] D. F. Watson, “Computing the n-dimensional Delaunay tessellation with application to Voronoi polytopes*”, *The Computer Journal* **24**, 167–172 (1981) 10.1093/comjnl/24.2.167 (cit. on pp. 76, 80).
- [44] N. H. Christ, R. Friedberg, and T. D. Lee, “Random lattice field theory: General formulation”, *Nuclear Physics B* **202**, 89–125 (1982) 10.1016/0550-3213(82)90222-X (cit. on pp. 76, 92).
- [45] S. A. Alyami, A. K. M. Azad, and J. M. Keith, “Uniform Sampling of Directed and Undirected Graphs Conditional on Vertex Connectivity”, *Electronic Notes in Discrete Mathematics, International Conference on Graph Theory and Its Applications* **53**, 43–55 (2016) 10.1016/j.endm.2016.05.005 (cit. on p. 77).
- [46] V. Chua, H. Yao, and G. A. Fiete, “Exact chiral spin liquid with stable spin Fermi surface on the kagome lattice”, *Phys. Rev. B* **83**, 180412 (2011) 10.1103/PhysRevB.83.180412 (cit. on pp. 78, 92).
- [47] H. Yao and S. A. Kivelson, “An exact chiral spin liquid with non-Abelian anyons”, *Phys. Rev. Lett.* **99**, 247203 (2007) 10.1103/PhysRevLett.99.247203, arXiv:0708.0040 (cit. on pp. 78, 84, 86).
- [48] V. Chua and G. A. Fiete, “Exactly solvable topological chiral spin liquid with random exchange”, *Phys. Rev. B* **84**, 195129 (2011) 10.1103/PhysRevB.84.195129 (cit. on p. 78).
- [49] G. A. Fiete et al., “Topological insulators and quantum spin liquids”, *Physica E: Low-dimensional Systems and Nanostructures* **44**, 845–859 (2012) 10.1016/j.physe.2011.11.011 (cit. on p. 78).

- [50] W. M. H. Natori, E. C. Andrade, E. Miranda, and R. G. Pereira, “Chiral spin-orbital liquids with nodal lines”, *Phys. Rev. Lett.* **117**, 017204 (2016), <https://link.aps.org/doi/10.1103/PhysRevLett.117.017204> (cit. on p. 78).
- [51] C. Wu, D. Arovas, and H.-H. Hung, “T-matrix generalization of the Kitaev model”, *Physical Review B* **79**, 134427 (2009) (cit. on pp. 78, 92).
- [52] H. Wang and A. Principi, “Majorana edge and corner states in square and kagome quantum spin-3/2 liquids”, *Phys. Rev. B* **104**, 214422 (2021) [10.1103/PhysRevB.104.214422](https://doi.org/10.1103/PhysRevB.104.214422) (cit. on pp. 78, 92).
- [53] C. B. Barber, D. P. Dobkin, and H. Huhdanpaa, “The quickhull algorithm for convex hulls”, *ACM Trans. Math. Softw.* **22**, 469–483 (1996) [10.1145/235815.235821](https://doi.org/10.1145/235815.235821) (cit. on p. 80).
- [54] P. Virtanen et al., “SciPy 1.0: fundamental algorithms for scientific computing in Python”, *Nature Methods* **17**, 261–272 (2020) [10.1038/s41592-019-0686-2](https://doi.org/10.1038/s41592-019-0686-2) (cit. on p. 80).
- [55] K. Appel and W. Haken, “Every Planar Map Is Four Colorable”, in (1989), [10.1090/conm/098](https://doi.org/10.1090/conm/098) (cit. on p. 81).
- [56] V. V. G, “On an estimate of the chromatic class of a p-graph”, *Discret Analiz* **3**, 25–30 (1964), <https://cir.nii.ac.jp/crid/1571980075458819456> (visited on 07/26/2022) (cit. on p. 81).
- [57] S. Skulrattanakulchai, “4-edge-coloring graphs of maximum degree 3 in linear time”, *Inf. Process. Lett.* **81**, 191–195 (2002) [10.1016/S0020-0190\(01\)00221-6](https://doi.org/10.1016/S0020-0190(01)00221-6) (cit. on p. 81).
- [58] P. G. Tait, “Remarks on the colouring of maps”, in *Proc. Roy. Soc. Edinburgh*, Vol. 10, 729 (1880), pp. 501–503 (cit. on p. 81).
- [59] N. Robertson, D. P. Sanders, P. Seymour, and R. Thomas, “Efficiently four-coloring planar graphs”, in *Proceedings of the twenty-eighth annual ACM symposium on Theory of computing* (1996), pp. 571–575 (cit. on p. 81).
- [60] P. J. Heawood, “Map colouring theorems”, *Quarterly Journal of Mathematics, First Series*, 322–339 (cit. on p. 81).
- [61] R. M. Karp, “Reducibility among combinatorial problems”, in *Complexity of computer computations*, edited by R. E. Miller, J. W. Thatcher, and J. D. Bohlinger (Springer US, Boston, MA, 1972), pp. 85–103, [10.1007/978-1-4684-2001-2_9](https://doi.org/10.1007/978-1-4684-2001-2_9) (cit. on p. 81).
- [62] S. Alouneh, S. Abed, M. H. Al Shayeji, and R. Mesleh, “A comprehensive study and analysis on SAT-solvers: advances, usages and achievements”, *Artif Intell Rev* **52**, 2575–2601 (2019) [10.1007/s10462-018-9628-0](https://doi.org/10.1007/s10462-018-9628-0) (cit. on p. 81).
- [63] S. A. Cook, “The complexity of theorem-proving procedures”, in *Proceedings of the third annual ACM symposium on Theory of computing*, STOC ’71 (May 3, 1971), pp. 151–158, [10.1145/800157.805047](https://doi.org/10.1145/800157.805047) (cit. on p. 81).
- [64] L. A. Levin, “Universal sequential search problems”, *Problemy peredachi informatsii* **9**, 115–116 (1973) (cit. on p. 81).
- [65] H. Yao and D.-H. Lee, “Fermionic magnons, non-abelian spinons, and the spin quantum hall effect from an exactly solvable spin-1/2 kitaev model with SU(2) symmetry”, *Phys. Rev. Lett.* **107**, 087205 (2011) [10.1103/PhysRevLett.107.087205](https://doi.org/10.1103/PhysRevLett.107.087205) (cit. on pp. 84, 92).
- [66] J. Knolle, “Dynamics of a quantum spin liquid” (Max Planck Institute for the Physics of Complex Systems, Dresden, 2016) (cit. on p. 85).

- [67] J. Nasu, M. Udagawa, and Y. Motome, “Thermal fractionalization of quantum spins in a Kitaev model: Temperature-linear specific heat and coherent transport of Majorana fermions”, *Phys. Rev. B* **92**, 115122 (2015) 10.1103/PhysRevB.92.115122 (cit. on p. 85).
- [68] V. Lahtinen, A. W. W. Ludwig, and S. Trebst, “Perturbed vortex lattices and the stability of nucleated topological phases”, *Phys. Rev. B* **89**, 085121 (2014) 10.1103/PhysRevB.89.085121 (cit. on p. 85).
- [69] A. J. Willans, J. T. Chalker, and R. Moessner, “Disorder in a Quantum Spin Liquid: Flux Binding and Local Moment Formation”, *Phys. Rev. Lett.* **104**, 237203 (2010) 10.1103/PhysRevLett.104.237203 (cit. on p. 85).
- [70] F. Zschocke and M. Vojta, “Physical states and finite-size effects in Kitaev’s honeycomb model: Bond disorder, spin excitations, and NMR line shape”, *Phys. Rev. B* **92**, 014403 (2015) 10.1103/PhysRevB.92.014403 (cit. on p. 85).
- [71] W.-H. Kao and N. B. Perkins, “Disorder upon disorder: Localization effects in the Kitaev spin liquid”, *Annals of Physics, Special Issue on Philip W. Anderson* **435**, 168506 (2021) 10.1016/j.aop.2021.168506 (cit. on p. 85).
- [72] M. Ezawa, Y. Tanaka, and N. Nagaosa, “Topological Phase Transition without Gap Closing”, *Sci Rep* **3**, 2790 (2013) 10.1038/srep02790 (cit. on p. 85).
- [73] M. V. Berry, “Quantal phase factors accompanying adiabatic changes”, *Proceedings of the Royal Society of London. A. Mathematical and Physical Sciences* **392**, 45–57 (1984) 10.1098/rspa.1984.0023 (cit. on p. 85).
- [74] B. Simon, “Holonomy, the Quantum Adiabatic Theorem, and Berry’s Phase”, *Phys. Rev. Lett.* **51**, 2167–2170 (1983) 10.1103/PhysRevLett.51.2167 (cit. on p. 85).
- [75] D. J. Thouless, M. Kohmoto, M. P. Nightingale, and M. den Nijs, “Quantized Hall Conductance in a Two-Dimensional Periodic Potential”, *Phys. Rev. Lett.* **49**, 405–408 (1982) 10.1103/PhysRevLett.49.405 (cit. on p. 85).
- [76] R. Bianco and R. Resta, “Mapping topological order in coordinate space”, *Physical Review B* **84**, 241106 (2011) 10.1103/PhysRevB.84.241106 (cit. on p. 86).
- [77] M. B. Hastings and T. A. Loring, “Almost commuting matrices, localized Wannier functions, and the quantum Hall effect”, *Journal of Mathematical Physics* **51**, 015214 (2010) 10.1063/1.3274817, eprint: <https://doi.org/10.1063/1.3274817> (cit. on p. 86).
- [78] M. B. Hastings, “Lieb-Schultz-Mattis in higher dimensions”, *Phys. Rev. B* **69**, 104431 (2004) 10.1103/PhysRevB.69.104431 (cit. on p. 86).
- [79] A. Y. Kitaev, “Fault-tolerant quantum computation by anyons”, *Annals of Physics* **303**, 2–30 (2003) 10.1016/S0003-4916(02)00018-0 (cit. on p. 86).
- [80] R. B. Laughlin and Z. Zou, “Properties of the chiral-spin-liquid state”, *Phys. Rev. B* **41**, 664–687 (1990) 10.1103/PhysRevB.41.664 (cit. on p. 86).
- [81] X.-L. Qi, Y.-S. Wu, and S.-C. Zhang, “General theorem relating the bulk topological number to edge states in two-dimensional insulators”, *Physical Review B* **74**, 045125 (2006) 10.1103/PhysRevB.74.045125 (cit. on p. 86).
- [82] C. Beenakker, “Search for majorana fermions in superconductors”, *Annual Review of Condensed Matter Physics* **4**, 113–136 (2013) 10.1146/annurev-conmatphys-030212-184337, eprint: <https://doi.org/10.1146/annurev-conmatphys-030212-184337> (cit. on pp. 87, 91).

- [83] V. Lahtinen, “Interacting non-Abelian anyons as Majorana fermions in the honeycomb lattice model”, *New Journal of Physics* **13**, 075009 (2011) 10.1088/1367-2630/13/7/075009 (cit. on p. 87).
- [84] M. Bocquet, D. Serban, and M. R. Zirnbauer, “Disordered 2d quasiparticles in class D: Dirac fermions with random mass, and dirty superconductors”, *Nuclear Physics B* **578**, 628–680 (2000) 10.1016/S0550-3213(00)00208-X (cit. on pp. 88, 91).
- [85] S. Trebst and C. Hickey, “Kitaev materials”, *Physics Reports, Kitaev Materials* **950**, 1–37 (2022) 10.1016/j.physrep.2021.11.003 (cit. on p. 90).
- [86] D. Weaire and M. F. Thorpe, “The structure of amorphous solids”, *Contemporary Physics* **17**, 173–191 (1976) 10.1080/00107517608210851 (cit. on p. 90).
- [87] T. D. Bennett and A. K. Cheetham, “Amorphous Metal–Organic Frameworks”, *Acc. Chem. Res.* **47**, 1555–1562 (2014) 10.1021/ar5000314 (cit. on p. 90).
- [88] M. G. Yamada, H. Fujita, and M. Oshikawa, “Designing Kitaev Spin Liquids in Metal–Organic Frameworks”, *Phys. Rev. Lett.* **119**, 057202 (2017) 10.1103/PhysRevLett.119.057202 (cit. on p. 90).
- [89] Y. Misumi et al., “Quantum Spin Liquid State in a Two-Dimensional Semiconductive Metal–Organic Framework”, *J. Am. Chem. Soc.* **142**, 16513–16517 (2020) 10.1021/jacs.0c05472 (cit. on p. 90).
- [90] L.-M. Duan, E. Demler, and M. D. Lukin, “Controlling Spin Exchange Interactions of Ultracold Atoms in Optical Lattices”, *Phys. Rev. Lett.* **91**, 090402 (2003) 10.1103 / PhysRevLett.91.090402 (cit. on p. 91).
- [91] A. Micheli, G. K. Brennen, and P. Zoller, “A toolbox for lattice-spin models with polar molecules”, *Nature Phys* **2**, 341–347 (2006) 10.1038/nphys287 (cit. on p. 91).
- [92] S. M. Sadeghi, “Amorphous two-dimensional optical lattices with coherently controlled morphologies in quantum well structures”, *Phys. Rev. B* **72**, 125336 (2005) 10.1103 / PhysRevB.72.125336 (cit. on p. 91).
- [93] R. A. Street, *Hydrogenated Amorphous Silicon* (Cambridge University Press, Aug. 30, 1991), 433 pp., Google Books: zQMwsMt4VmOC (cit. on p. 91).
- [94] J. G. Rau, E. K.-H. Lee, and H.-Y. Kee, “Generic spin model for the honeycomb iridates beyond the kitaev limit”, *Phys. Rev. Lett.* **112**, 077204 (2014) 10.1103/PhysRevLett.112.077204 (cit. on p. 91).
- [95] J. Chaloupka, G. Jackeli, and G. Khaliullin, “Kitaev-Heisenberg Model on a Honeycomb Lattice: Possible Exotic Phases in Iridium Oxides $\{A\}_2\{\mathrm{IrO}\}_3$ ”, *Phys. Rev. Lett.* **105**, 027204 (2010) 10.1103/PhysRevLett.105.027204 (cit. on pp. 91–92).
- [96] J. Chaloupka, G. Jackeli, and G. Khaliullin, “Zigzag magnetic order in the iridium oxide $\mathrm{Na}_2\mathrm{IrO}_3$ ”, *Phys. Rev. Lett.* **110**, 097204 (2013) 10.1103/PhysRevLett.110.097204 (cit. on p. 91).
- [97] J. Chaloupka and G. Khaliullin, “Hidden symmetries of the extended Kitaev-Heisenberg model: Implications for honeycomb lattice iridates $A_2\mathrm{IrO}_3$ ”, *Phys. Rev. B* **92**, 024413 (2015) (cit. on pp. 91–92).
- [98] S. M. Winter, Y. Li, H. O. Jeschke, and R. Valentí, “Challenges in design of Kitaev materials: Magnetic interactions from competing energy scales”, *Phys. Rev. B* **93**, 214431 (2016) 10.1103/PhysRevB.93.214431 (cit. on p. 91).

- [99] Y. Kasahara, T. Ohnishi, Y. Mizukami, et al., “Majorana quantization and half-integer thermal quantum Hall effect in a Kitaev spin liquid”, *Nature* **559**, 227–231 (2018) 10.1038/s41586-018-0274-0 (cit. on p. 91).
- [100] T. Yokoi, S. Ma, Y. Kasahara, et al., “Majorana quantization and half-integer thermal quantum Hall effect in a Kitaev spin liquid”, *Science* **373**, 568–572 (2021) 10.1126/science.aay5551 (cit. on p. 91).
- [101] M. Yamashita et al., “Sample dependence of half-integer quantized thermal Hall effect in the Kitaev spin-liquid candidate $\alpha\text{-RuCl}_3$ ”, *Phys. Rev. B* **102**, 220404 (2020) 10.1103/PhysRevB.102.220404 (cit. on p. 91).
- [102] J. Bruin et al., “Majorana quantization and half-integer thermal quantum Hall effect in a Kitaev spin liquid”, *Nature Physics* **18**, 401–405 (2022) 10.1038/s41567-021-01501-y (cit. on p. 91).
- [103] J. Feldmeier, W. Natori, M. Knap, and J. Knolle, “Local probes for charge-neutral edge states in two-dimensional quantum magnets”, *Phys. Rev. B* **102**, 134423 (2020) 10.1103/PhysRevB.102.134423 (cit. on p. 91).
- [104] E. J. König, M. T. Randeria, and B. Jäck, “Tunneling spectroscopy of quantum spin liquids”, *Phys. Rev. Lett.* **125**, 267206 (2020) 10.1103/PhysRevLett.125.267206 (cit. on p. 91).
- [105] M. Udagawa, S. Takayoshi, and T. Oka, “Scanning tunneling microscopy as a single majorana detector of kitaev’s chiral spin liquid”, *Phys. Rev. Lett.* **126**, 127201 (2021) 10.1103/PhysRevLett.126.127201 (cit. on p. 91).
- [106] S.-H. Jang, Y. Kato, and Y. Motome, *Vortex creation and control in the Kitaev spin liquid by local bond modulations*, May 30, 2021, 10.1103/PhysRevB.104.085142, arXiv:2105.14562 [cond-mat] (cit. on p. 91).
- [107] A. P. Joy and A. Rosch, *Dynamics of vasons and thermal Hall effect in perturbed Kitaev models*, July 22, 2022, arXiv:2109.00250 [cond-mat], <http://arxiv.org/abs/2109.00250> (visited on 08/02/2022) (cit. on p. 91).
- [108] K. O’Brien, M. Hermanns, and S. Trebst, “Classification of gapless Z_2 spin liquids in three-dimensional Kitaev models”, *Phys. Rev. B* **93**, 085101 (2016) 10.1103/PhysRevB.93.085101 (cit. on pp. 91–92).
- [109] P. A. Mishchenko et al., “Chiral spin liquids with crystalline $\{\mathbb{Z}\}^2$ gauge order in a three-dimensional Kitaev model”, *Phys. Rev. B* **101**, 045118 (2020) 10.1103/PhysRevB.101.045118 (cit. on p. 91).
- [110] H. Yao, S.-C. Zhang, and S. A. Kivelson, “Algebraic Spin Liquid in an Exactly Solvable Spin Model”, *Phys. Rev. Lett.* **102**, 217202 (2009) 10.1103/PhysRevLett.102.217202 (cit. on p. 92).
- [111] S. Chulliparambil et al., “Flux crystals, Majorana metals, and flat bands in exactly solvable spin-orbital liquids”, *Phys. Rev. B* **103**, 075144 (2021) 10.1103/PhysRevB.103.075144 (cit. on p. 92).
- [112] U. F. P. Seifert et al., “Fractionalized fermionic quantum criticality in spin-orbital mott insulators”, *Phys. Rev. Lett.* **125**, 257202 (2020) 10.1103/PhysRevLett.125.257202 (cit. on p. 92).

4.4. CONCLUSION

- [113] X.-G. Wen, “Quantum order from string-net condensations and the origin of light and massless fermions”, *Phys. Rev. D* **68**, 065003 (2003) 10.1103/PhysRevD.68.065003 (cit. on p. 92).
- [114] S. Ryu, “Three-dimensional topological phase on the diamond lattice”, *Phys. Rev. B* **79**, 075124 (2009) 10.1103/PhysRevB.79.075124 (cit. on p. 92).
- [115] G. Baskaran, D. Sen, and R. Shankar, “Spin- S Kitaev model: Classical ground states, order from disorder, and exact correlation functions”, *Phys. Rev. B* **78**, 115116 (2008) 10.1103/PhysRevB.78.115116 (cit. on p. 92).
- [116] W. M. H. Natori and J. Knolle, “Dynamics of a two-dimensional quantum spin-orbital liquid: Spectroscopic signatures of fermionic magnons”, *Phys. Rev. Lett.* **125**, 067201 (2020) 10.1103/PhysRevLett.125.067201 (cit. on p. 92).
- [117] S. Chulliparambil et al., “Microscopic models for Kitaev’s sixteenfold way of anyon theories”, *Phys. Rev. B* **102**, 201111 (2020) 10.1103/PhysRevB.102.201111 (cit. on p. 92).
- [118] A. B. Harris, “Effect of random defects on the critical behaviour of Ising models”, *J. Phys. C: Solid State Phys.* **7**, 1671–1692 (1974) 10.1088/0022-3719/7/9/009 (cit. on p. 92).
- [119] G. Jackeli and G. Khaliullin, “Mott insulators in the strong spin-orbit coupling limit: from Heisenberg to a quantum compass and Kitaev models”, *Physical Review Letters* **102**, 017205 (2009) 10.1103/PhysRevLett.102.017205 (cit. on p. 92).
- [120] V. Kalmeyer and R. B. Laughlin, “Theory of the spin liquid state of the Heisenberg antiferromagnet”, *Phys. Rev. B* **39**, 11879–11899 (1989) 10.1103/PhysRevB.39.11879 (cit. on p. 92).
- [121] E. Manousakis, “The spin-\textonehalf{} Heisenberg antiferromagnet on a square lattice and its application to the cuprous oxides”, *Rev. Mod. Phys.* **63**, 1–62 (1991) 10.1103/RevModPhys.63.1 (cit. on p. 92).

Chapter 5

Conclusion

The FK model

FK model as a way to probe the Mott insulator state. Also the Mott insulator gives rise to the QSL and the doped Mott Insulator may be the source of the sought after High- T_c superconductor. The concept of quantum orders is relevant because for instance, if we can classify the kinds of order in the MI state, we can classify the kinds of high- T_c theories that can emerge from them.

As we discussed in the introduction, Quantum spin liquids can arise out of Mott insulators and both are highly interaction dependent. However interactions are hard to study. Using exactly solvable systems like the FK and KH model as a way to look at the physics of many-body interacting systems. Exactly solveable models are a useful part of the theoretical toolbox for investigating these systems.

Role of dimensionality

Role of Correlations Another theme from the two models is that longer range correlations from criticality in the LRFK model and anti-correlations in the topological disorder in the AK model, lead to a wider range of effects than short range correlations.

Role of disorder

paragraph about topological order as new addition to the pantheon of spontaneously broken symmetries

Xiao-Gang Wen [1] when talks about quantum orders as those that arise within quantum states at zero temperature, included QSLs, FQH states and superconductors¹. He also argues that the High- T_c superconductors is in terms of them being doped Mott insulators so that we should try to understand the QSL which emerges from the undoped Mott insulator (at half filling).

The existence of distinct, spatially limited quasiparticle excitations is not obvious.

emergent gauge physics, could condensed matter systems be useful in understanding the standard model too?

Electron-electron interactions play a dominant role in determining electronic and thermodynamic properties in these strongly correlated materials.

Specific examples where strongly correlated materials may figure prominently are high temperature superconductors and hard magnets without rare earth elements.

¹Wen argues that superconductors cannot be characterised by a local order parameter in the way that superfluids can.

5.1 Material Realisations

5.1.1 Amorphous Materials

5.1.2 Metal Organic Frameworks

5.2 Discussion

References

- [1] X.-G. Wen, “Quantum orders and symmetric spin liquids”, *Phys. Rev. B* **65**, 165113 (2002) [10.1103/PhysRevB.65.165113](https://doi.org/10.1103/PhysRevB.65.165113) (cit. on p. 102).

Appendices

A.1 Particle-Hole Symmetry

The Hubbard and FK models on a bipartite lattice have particle-hole (PH) symmetry $\mathcal{P}^\dagger H \mathcal{P} = -H$, accordingly they have symmetric energy spectra. The associated symmetry operator \mathcal{P} exchanges creation and annihilation operators along with a sign change between the two sublattices. In the language of the Hubbard model of electrons $c_{\alpha,i}$ with spin α at site i the particle hole operator corresponds to the substitution of new fermion operators $d_{\alpha,i}^\dagger$ and number operators $m_{\alpha,i}$ where

$$d_{\alpha,i}^\dagger = \epsilon_i c_{\alpha,i} \quad (\text{A.1})$$

$$m_{\alpha,i} = d_{\alpha,i}^\dagger d_{\alpha,i} \quad (\text{A.2})$$

the lattices must be bipartite because to make this work we set $\epsilon_i = +1$ for the A sublattice and -1 for the even sublattice [1].

The entirely filled state $|\Omega\rangle = \sum_{\alpha,i} c_{\alpha,i}^\dagger |0\rangle$ becomes the new vacuum state

$$d_{i\sigma} |\Omega\rangle = (-1)^i c_{i\sigma}^\dagger \sum_{j\rho} c_{j\rho}^\dagger |0\rangle = 0. \quad (\text{A.3})$$

The number operator $m_{\alpha,i} = 0, 1$ counts holes rather than electrons

$$m_{\alpha,i} = c_{\alpha,i} c_{\alpha,i}^\dagger = 1 - c_{\alpha,i}^\dagger c_{\alpha,i}. \quad (\text{A.4})$$

With the last equality following from the fermionic commutation relations. In the case of nearest neighbour hopping on a bipartite lattice this transformation also leaves the hopping term unchanged because $\epsilon_i \epsilon_j = -1$ when i and j are on different sublattices:

$$d_{\alpha,i}^\dagger d_{\alpha,j} = \epsilon_i \epsilon_j c_{\alpha,i} c_{\alpha,j}^\dagger = c_{\alpha,i}^\dagger c_{\alpha,j} \quad (\text{A.5})$$

Defining the particle density ρ as the number of fermions per site:

$$\rho = \frac{1}{N} \sum_i (n_{i\uparrow} + n_{i\downarrow}) \quad (\text{A.6})$$

The PH symmetry maps the Hamiltonian to itself with the sign of the chemical potential reversed and the density inverted about half filling:

$$\text{PH} : H(t, U, \mu) \rightarrow H(t, U, -\mu) \quad (\text{A.7})$$

$$\rho \rightarrow 2 - \rho \quad (\text{A.8})$$

The Hamiltonian is symmetric under PH at $\mu = 0$ and so must all the observables, hence half filling $\rho = 1$ occurs here. This symmetry and known observable acts as a useful test for the numerical calculations.

A.2 Evaluation of the Fermion Free Energy

There are 2^N possible ion configurations $\{n_i\}$, we define n_i^k to be the occupation of the i th site of the k th configuration. The quantum part of the free energy can then be defined through the quantum partition function \mathcal{Z}^k associated with each ionic state n_i^k :

$$F^k = -1/\beta \ln \mathcal{Z}^k \quad (\text{A.9})$$

% Such that the overall partition function is:

$$\begin{aligned} \mathcal{Z} &= \sum_k e^{-\beta H^k} Z^k \\ &= \sum_k e^{-\beta(H^k + F^k)} \end{aligned} \quad (\text{A.10})$$

Because fermions are limited to occupation numbers of 0 or 1 Z^k simplifies nicely. If $m_i^j = \{0, 1\}$ is defined as the occupation of the level with energy ϵ_i^k then the partition function is a sum over all the occupation states labelled by j :

$$\begin{aligned} Z^k &= \text{Tr} e^{-\beta F^k} = \sum_j e^{-\beta \sum_i m_i^j \epsilon_i^k} \\ &= \sum_j \prod_i e^{-\beta m_i^j \epsilon_i^k} = \prod_i \sum_j e^{-\beta m_i^j \epsilon_i^k} \\ &= \prod_i (1 + e^{-\beta \epsilon_i^k}) \\ F^k &= -1/\beta \sum_k \ln (1 + e^{-\beta \epsilon_i^k}) \end{aligned} \quad (\text{A.11})$$

% Observables can then be calculated from the partition function, for examples the occupation numbers:

$$\begin{aligned} \langle N \rangle &= \frac{1}{\beta} \frac{1}{Z} \frac{\partial Z}{\partial \mu} = -\frac{\partial F}{\partial \mu} \\ &= \frac{1}{\beta} \frac{1}{Z} \frac{\partial}{\partial \mu} \sum_k e^{-\beta(H^k + F^k)} \\ &= 1/Z \sum_k (N_{\text{ion}}^k + N_{\text{electron}}^k) e^{-\beta(H^k + F^k)} \end{aligned} \quad (\text{A.12})$$

% with the definitions:

$$\begin{aligned} N_{\text{ion}}^k &= -\frac{\partial H^k}{\partial \mu} = \sum_i n_i^k \\ N_{\text{electron}}^k &= -\frac{\partial F^k}{\partial \mu} = \sum_i (1 + e^{\beta \epsilon_i^k})^{-1} \end{aligned} \quad (\text{A.13})$$

A.3 Markov Chain Monte Carlo

Markov Chain Monte Carlo (MCMC) is a useful method whenever we have a probability distribution that we want to sample from but there is not direct sampling way to do so.

A.3.1 Direct Random Sampling

In almost any computer simulation the ultimate source of randomness is a stream of (close to) uniform, uncorrelated bits generated from a pseudo random number generator. A direct sampling method takes such a source and outputs uncorrelated samples from the target distribution. The fact they're uncorrelated is key as we'll see later. Examples of direct sampling methods range from the trivial: take n random bits to generate integers uniformly between 0 and 2^n to more complex methods such as inverse transform sampling and rejection sampling [2].

In physics the distribution we usually want to sample from is the Boltzmann probability over states of the system S :

$$p(S) = \frac{1}{Z} e^{-\beta H(S)} \quad (\text{A.14})$$

where $Z = \sum_S e^{-\beta H(S)}$ is the normalisation factor and ubiquitous partition function. In principle we could directly sample from this, for a discrete system there are finitely many choices. We could calculate the probability of each one and assign each a region of the unit interval which we could then sample uniformly from.

However if we actually try to do this we will run into two problems, we can't calculate Z for any reasonably sized systems because the state space grows exponentially with system size. Even if we could calculate Z , sampling from an exponentially large number of options quickly become tricky. This kind of problem happens in many other disciplines too, particularly when fitting statistical models using Bayesian inference [3].

A.3.2 MCMC Sampling

So what can we do? Well it turns out that if we're willing to give up in the requirement that the samples be uncorrelated then we can use MCMC instead.

MCMC defines a weighted random walk over the states (S_0, S_1, S_2, \dots) , such that in the long time limit, states are visited according to their probability $p(S)$. [4–6]. [7]

$$\lim_{i \rightarrow \infty} p(S_i) = P(S) \quad (\text{A.15})$$

In a physics context this lets us evaluate any observable with a mean over the states visited by the walk.

$$\langle O \rangle = \sum_S p(S) \langle O \rangle_S = \sum_{i=0}^M \langle O \rangle_{S_i} + \mathcal{O}\left(\frac{1}{\sqrt{M}}\right) \quad (\text{A.16})$$

The samples in the random walk are correlated so the samples effectively contain less information than N independent samples would. As a consequence the variance is larger than the $\langle O^2 \rangle - \langle O \rangle^2$ form it would have if the estimates were uncorrelated. Methods of estimating the true variance of $\langle O \rangle$ and decided how many steps are needed will be considered later.

A.3.3 Implementation of MCMC

In implementation MCMC can be boiled down to choosing a transition function $\mathcal{T}(S_t \rightarrow S_{t+1})$ where S are vectors representing classical spin configurations. We start in some initial state S_0 and then repeatedly jump to new states according to the probabilities given by \mathcal{T} . This defines a set of random walks $\{S_0 \dots S_i \dots S_N\}$.

In pseudo-code one could write the MCMC simulation for a single walker as:

```
# A skeleton implementation of MCMC
current_state = initial_state

for i in range(N_steps):
    new_state = sample_T(current_state)
    states[i] = current_state
```

Where the `sample\T` function samples directly from the transition function \mathcal{T} .

If we run many such walkers in parallel we can then approximate the distribution $p_t(S; S)$ which tells us where the walkers are likely to be after they've evolved for t steps from an initial state S_0 . We need to carefully choose \mathcal{T} such that the probability $p_t(S; S_0)$ approaches the distribution of interest. In this case the thermal distribution $P(S; \beta) = \mathcal{Z}^{-1} e^{-\beta F(S)}$.

A.3.4 Global and Detailed balance equations

We can quite easily write down the properties that \mathcal{T} must have in order to yield the correct target distribution. Since we must transition somewhere at each step, we first have the normalisation condition that

$$\sum_S \mathcal{T}(S' \rightarrow S) = 1. \quad (\text{A.17})$$

Second, let us move to an ensemble view, where rather than individual walkers and states, we think about the probability distribution of many walkers at each step. If we start all the walkers in the same place the initial distribution will be a delta function and as we step the walkers will wander around, giving us a sequence of probability distributions $\{p_0(S), p_1(S), p_2(S) \dots\}$. For discrete spaces we can write the action of the transition function on p_i as a matrix equation

$$p_{i+1}(S) = \sum_{S' \in \{S\}} p_i(S') \mathcal{T}(S' \rightarrow S) \quad (\text{A.18})$$

This equation is essentially just stating that total probability mass is conserved as our walkers flow around the state space.

In order that p_i converges to our target distribution p in the long time limit, we need the target distribution to be a fixed point of the transition function

$$P(S) = \sum_{S'} P(S')\mathcal{T}(S' \rightarrow S) \quad (\text{A.19})$$

Along with some more technical considerations such as ergodicity which won't be considered here, global balance suffices to ensure that a MCMC method is correct [8].

A sufficient but not necessary condition for global balance to hold is called detailed balance:

$$P(S)\mathcal{T}(S \rightarrow S') = P(S')\mathcal{T}(S' \rightarrow S) \quad (\text{A.20})$$

In practice most algorithms are constructed to satisfy detailed rather than global balance, though there are arguments that the relaxed requirements of global balance can lead to faster algorithms [9].

The goal of MCMC is then to choose \mathcal{T} so that it has the desired thermal distribution $P(S)$ as its fixed point and converges quickly onto it. This boils down to requiring that the matrix representation of $T_{ij} = \mathcal{T}(S_i \rightarrow S_j)$ has an eigenvector with entries $P_i = P(S_i)$ with eigenvalue 1 and all other eigenvalues with magnitude less than one. The convergence time depends on the magnitude of the second largest eigenvalue.

The choice of the transition function for MCMC is under-determined as one only needs to satisfy a set of balance conditions for which there are many solutions [8]. The standard choice that satisfies these requirements is called the Metropolis-Hastings algorithm.

A.3.5 The Metropolis-Hastings Algorithm

The Metropolis-Hastings algorithm breaks the transition function into a proposal distribution $q(S \rightarrow S')$ and an acceptance function $\mathcal{A}(S \rightarrow S')$. q must be a function we can directly sample from, and in many cases takes the form of flipping some number of spins in S , i.e if we're flipping a single random spin in the spin chain, $q(S \rightarrow S')$ is the uniform distribution on states reachable by one spin flip from S . This also gives the symmetry property that $q(S \rightarrow S') = q(S' \rightarrow S)$.

The proposal S' is then accepted or rejected with an acceptance probability $\mathcal{A}(S \rightarrow S')$, if the proposal is rejected then $S_{i+1} = S_i$. Hence:

$$\mathcal{T}(S \rightarrow S') = q(S \rightarrow S')\mathcal{A}(S \rightarrow S') \quad (\text{A.21})$$

The Metropolis-Hastings algorithm is a slight extension of the original Metropolis algorithm which allows for non-symmetric proposal distributions $q(S \rightarrow S') \neq q(S' \rightarrow S)$. It can be derived starting from

$$P(S)\mathcal{T}(S \rightarrow S') = P(S')\mathcal{T}(S' \rightarrow S) \quad (\text{A.22})$$

inserting the proposal and acceptance function

$$P(S)q(S \rightarrow S')\mathcal{A}(S \rightarrow S') = P(S')q(S' \rightarrow S)\mathcal{A}(S' \rightarrow S) \quad (\text{A.23})$$

rearranging gives us a condition on the acceptance function in terms of the target distribution and the proposal distribution which can be thought of as inputs to the algorithm

$$\frac{\mathcal{A}(S \rightarrow S')}{\mathcal{A}(S' \rightarrow S)} = \frac{P(S')q(S' \rightarrow S)}{P(S)q(S \rightarrow S')} = f(S, S') \quad (\text{A.24})$$

The Metropolis-Hastings algorithm is the choice

$$\mathcal{A}(S \rightarrow S') = \min(1, f(S, S')) \quad (\text{A.25})$$

for the acceptance function. The proposal distribution is left as a free choice.

Noting that $f(S, S') = 1/f(S', S)$, we can see that the MH algorithm satisfies detailed balance by considering the two cases $f(S, S') > 1$ and $f(S, S') < 1$.

By choosing the proposal distribution such that $f(S, S')$ is as close as possible to one, the rate of rejections can be reduced and the algorithm sped up. This can be challenging though, as getting $f(S, S')$ close to 1 would imply that we can directly sample from a distribution very close to the target distribution. As MCMC is usually applied to problems for which there is virtually no hope of sampling directly from the target distribution, it's rare that one can do so approximately.

When the proposal distribution is symmetric as ours is, it cancels out in the expression for the acceptance function and the Metropolis-Hastings algorithm is simply the choice

$$\mathcal{A}(S \rightarrow S') = \min(1, e^{-\beta \Delta F}) \quad (\text{A.26})$$

where F is the overall free energy of the system, including both the quantum and classical sector.

To implement the acceptance function in practice we pick a random number in the unit interval and accept if it is less than $e^{-\beta \Delta F}$:

```
# An implementation of the standard MH algorithm
current_state = initial_state

for i in range(N_steps):
    new_state = proposal(current_state)
    df = free_energy_change(current_state, new_state, parameters)

    if uniform(0,1) < exp(-beta * df):
        current_state = new_state

    states[i] = current_state
```

A.3.6 Two Step Trick

Our method already relies heavily on the split between the classical and quantum sector to derive a sign problem free MCMC algorithm but it turns out that there is a further trick we can play with it. The free energy term is the sum of an easy to compute classical energy and a more expensive quantum free energy, we can split the acceptance function into two in such as way as to avoid having to compute the full exact diagonalisation some of the time:

```
# Our two step MH implementation for models with classical and
# quantum energy terms
current_state = initial_state

for i in range(N_steps):
    new_state = proposal(current_state)

    df_classical = classical_free_energy_change(current_state,
        new_state, parameters)
    if exp(-beta * df_classical) < uniform(0,1):
        f_quantum = quantum_free_energy(current_state, new_state,
            parameters)

        if exp(- beta * df_quantum) < uniform(0,1):
            current_state = new_state

    states[i] = current_state
```

As discussed in the main text, for the model parameters used, we find that with our new scheme the matrix diagonalisation is skipped around 30% of the time at $T = 2.5$ and up to 80% at $T = 1.5$. We observe that for $N = 50$, the matrix diagonalisation, if it occurs, occupies around 60% of the total computation time for a single step. This rises to 90% at $N = 300$ and further increases for larger N . We therefore get the greatest speedup for large system sizes at low temperature where many prospective transitions are rejected at the classical stage and the matrix computation takes up the greatest fraction of the total computation time. The upshot is that we find a speedup of up to a factor of 10 at the cost of very little extra algorithmic complexity.

This modified scheme has the acceptance function

$$\mathcal{A}(a \rightarrow b) = \min\left(1, e^{-\beta \Delta H_s}\right) \min\left(1, e^{-\beta \Delta F_c}\right). \quad (\text{A.27})$$

We can show that this satisfies the detailed balance equations as follows. Defining $r_c = e^{-\beta H_c}$ and $r_q = e^{-\beta F_q}$ our target distribution is $\pi(a) = r_c r_q$. This method has $\mathcal{T}(a \rightarrow b) = q(a \rightarrow b) \mathcal{A}(a \rightarrow b)$ with symmetric $p(a \rightarrow b) = \pi(b \rightarrow a)$ and $\mathcal{A} = \min(1, r_c) \min(1, r_q)$

Substituting this into the detailed balance equation gives:

$$\mathcal{T}(a \rightarrow b) / \mathcal{T}(b \rightarrow a) = \pi(b) / \pi(a) = r_c r_q \quad (\text{A.28})$$

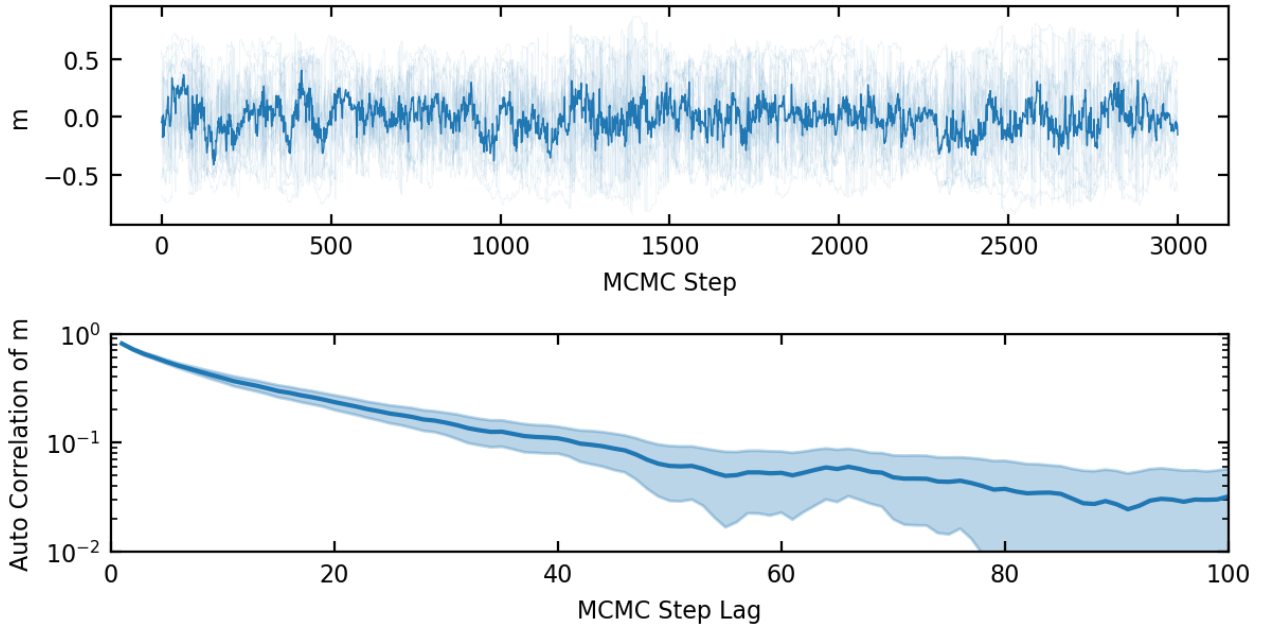


Figure A.1: (Upper) 10 MCMC chains starting from the same initial state for a system with $N = 150$ sites and 3000 MCMC steps. At each MCMC step, n spins are flipped where n is drawn from $\text{Uniform}(1, N)$ and this is repeated $N^2/100$ times. The simulations therefore have the potential to necessitate $10 * N^2$ matrix diagonalisations for each 100 MCMC steps. (Lower) The normalised auto-correlation $(\langle m_i m_{i-j} \rangle - \langle m_i \rangle \langle m_i \rangle) / \text{Var}(m_i)$ averaged over i . It can be seen that even with each MCMC step already being composed of many individual flip attempts, the auto-correlation is still non negligible and must be taken into account in the statistics. $t = 1, \alpha = 1.25, T = 2.2, J = U = 5$

Taking the LHS and substituting in our transition function:

$$\mathcal{T}(a \rightarrow b)/\mathcal{T}(b \rightarrow a) = \frac{\min(1, r_c) \min(1, r_q)}{\min(1, 1/r_c) \min(1, 1/r_q)} \quad (\text{A.29})$$

which simplifies to $r_c r_q$ as $\min(1, r)/\min(1, 1/r) = r$ for $r > 0$.

Auto-correlation Time

At this stage one might think we're done. We can indeed draw independent samples from our target Boltzmann distribution by starting from some arbitrary initial state and doing k steps to arrive at a sample. These are not, however, independent samples. In fig. A.1 it is already clear that the samples of the order parameter m have some auto-correlation because only a few spins are flipped each step. Even when the number of spins flipped per step is increased that it can be an important effect near the phase transition. Let's define the auto-correlation time $\tau(O)$ informally as the number of MCMC samples of some observable O that are statistically equal to one independent sample or equivalently as the number of MCMC steps after which the samples are correlated below some cut-off, see [10]. The auto-correlation time is generally shorter than the convergence time so it therefore makes sense from an efficiency standpoint to run a single walker for many MCMC steps rather than to run a huge ensemble for k steps each.

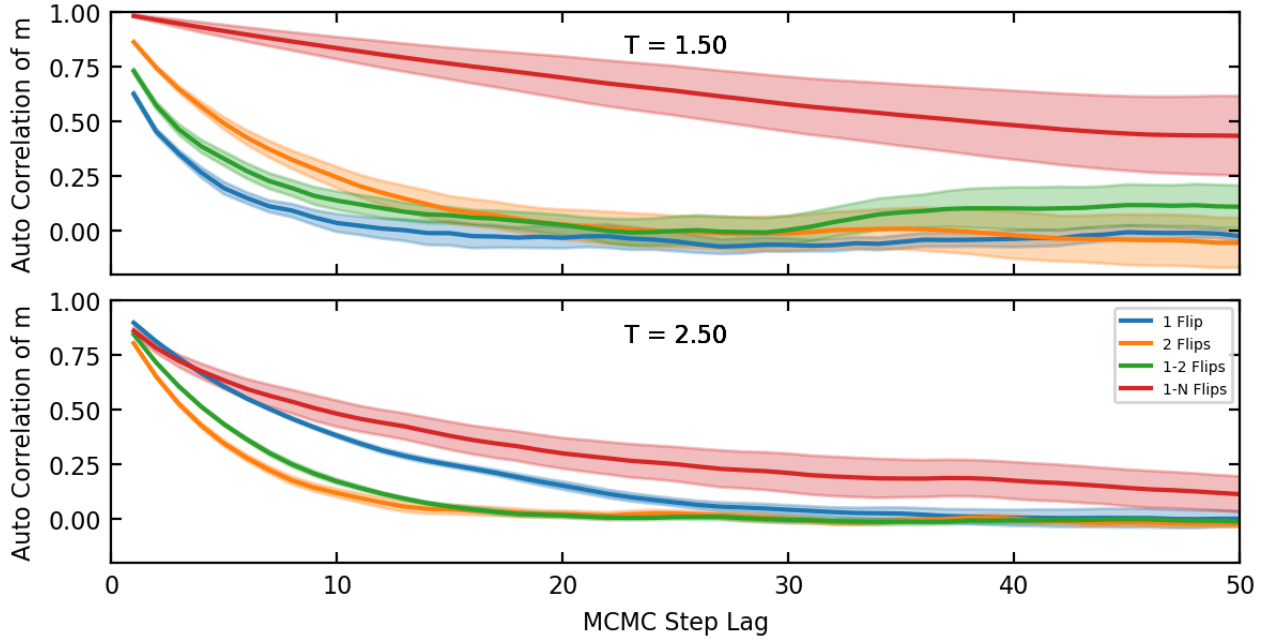


Figure A.2: Simulations showing how the autocorrelation of the order parameter depends on the proposal distribution used at different temperatures, we see that at $T = 1.5 < T_c$ a single spin flip is likely the best choice, while at the high temperature $T = 2.5 > T_c$ flipping two sites or a mixture of flipping two and 1 sites is likely a better choice. $\$t = 1, \alpha = 1.25, J = U = 5\$$

Once the random walk has been carried out for many steps, the expectation values of O can be estimated from the MCMC samples S_i :

$$\langle O \rangle = \sum_{i=0}^N O(S_i) + \mathcal{O}\left(\frac{1}{\sqrt{N}}\right) \quad (\text{A.30})$$

The samples are correlated so the N of them effectively contains less information than N independent samples would, in fact roughly N/τ effective samples. As a consequence the variance is larger than the $\langle O^2 \rangle - \langle O \rangle^2$ form it would have if the estimates were uncorrelated. There are many methods in the literature for estimating the true variance of $\langle O \rangle$ and deciding how many steps are needed but my approach has been to run a small number of parallel chains, which are independent, in order to estimate the statistical error produced. This is a slightly less computationally efficient because it requires throwing away those k steps generated before convergence multiple times but it is conceptually simple.

Tuning the proposal distribution

Now we can discuss how to minimise the auto-correlations. The general principle is that one must balance the proposal distribution between two extremes. Choose overlay small steps, like flipping only a single spin and the acceptance rate will be high because ΔF will usually be small, but each state will be very similar to the previous and the auto-correlations will be high too, making sampling inefficient. On the other hand, overlay large steps, like randomising a large portion of the spins each step, will result in very frequent rejections, especially at low temperatures.

I evaluated a few different proposal distributions for use with the FK model.

1. Flipping a single random site
2. Flipping N random sites for some N
3. Choosing n from $\text{Uniform}(1, N)$ and then flipping n sites for some fixed N .
4. Attempting to tune the proposal distribution for each parameter regime.

Fro fig. A.2 we see that even at moderately high temperatures $T > T_c$ flipping one or two sites is the best choice. However for some simulations at very high temperature flipping more spins is warranted.

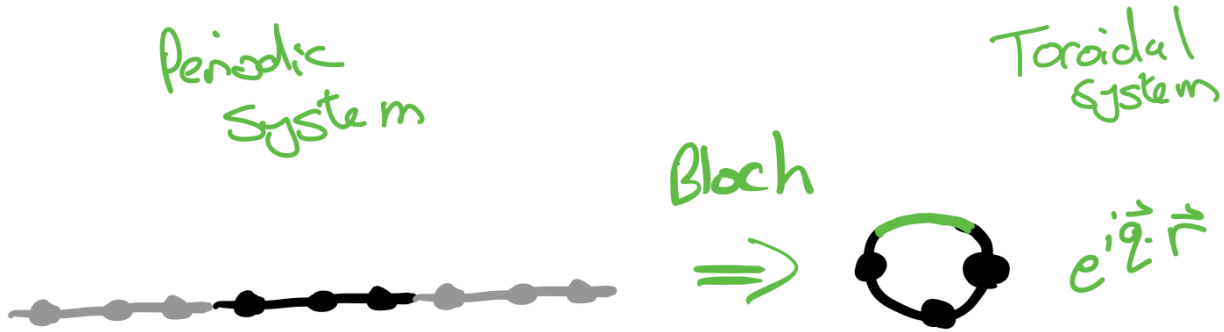


Figure A.3: Bloch's theorem can be thought of as transforming from a periodic Hamiltonian on the place to the unit cell defined an torus. In addition we get some phase factors $e^{i\vec{k} \cdot \vec{r}}$ associated with bonds that cross unit cells that depend on the sense in which they do so $\vec{r} = (\pm 1, \pm 1)$. Representing graphs on the torus turns out to require a similar idea, we unwrap the torus to one unit cell and keep track of which bonds cross the cell boundaries.

A.4 Lattice Generation

A.4.1 Graph Representation

Three keys pieces of information allow us to represent amorphous lattices.

Most of the graph connectivity is encoded by an ordered list of edges (i, j) . These are ordered to represent both directed and undirected graphs. This is useful for defining the sign of bond operators $u_{ij} = -u_{ji}$.

Information about the embedding of the lattice onto the torus is encoded into a point on the unit square associated with each vertex. The torus is unwrapped onto the square by defining an arbitrary pair of cuts along the major and minor axes. For simplicity, we take these axes to be the lines $x = 0$ and $y = 0$. We can wrap the unit square back up into a torus by identifying the lines $x = 0$ with $x = 1$ and $y = 0$ with $y = 1$.

Finally, we need to encode the topology of the graph. This is necessary because, if we are simply given an edge (i, j) we do not know how the edge gets from vertex i to vertex j . One method would be taking the shortest path, but it could also ‘go the long way around’ by crossing one of the cuts. To encode this information, we store an additional vector \vec{r} associated with each edge. $r_i^x = 0$ means that edge i does not cross the x . $r_i^x = +1$ (-1) means it crossed the cut in a positive (negative) sense.

This description of the lattice has a very nice relationship to Bloch's theorem. Applying Bloch's theorem to a periodic lattice essentially means wrapping the unit cell onto a torus. Variations that happen at longer length scales than the size of the unit cell are captured by the crystal momentum. The crystal momentum inserts a phase factor $e^{i\vec{q} \cdot \vec{r}}$ onto bonds that cross to adjacent unit cells. The vector \vec{r} is exactly what we use to encode the topology of our lattices.

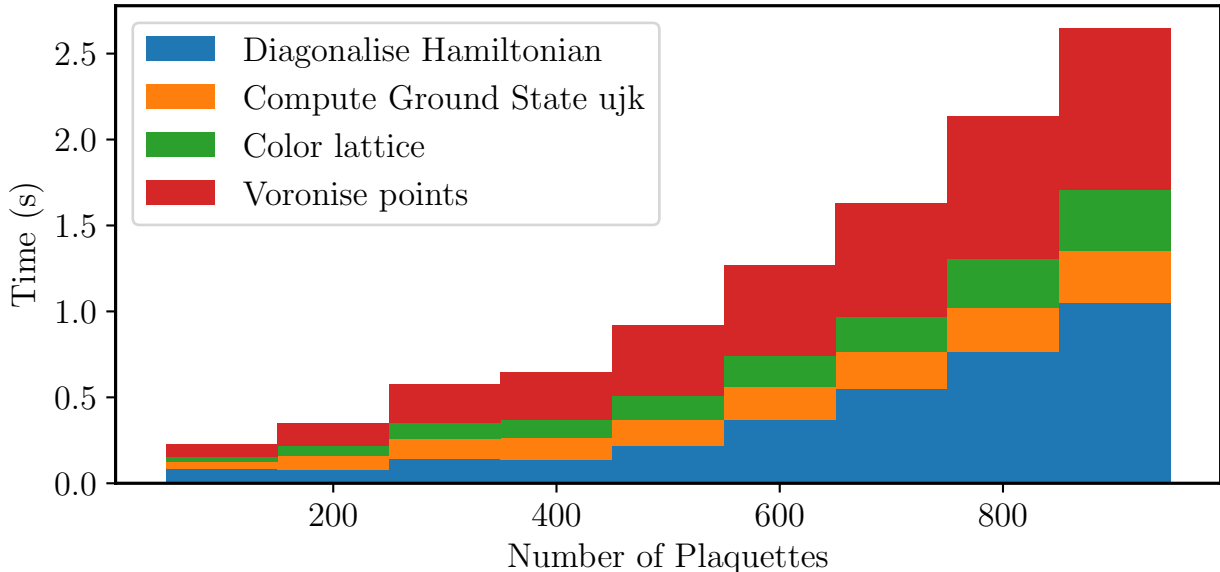


Figure A.4: The proportion of computation time taken up by the four longest running steps when generating a lattice. For larger systems, the time taken to perform the diagonalisation dominates.

A.4.2 Encoding edge-colouring problems as SAT instances

In the main text we discuss the problem of three-edge-colouring, assigning one of three labels to each edge of a graph such that no edges of the same label meet at a vertex.

To solve this in practice I use a solver called `MiniSAT` [11]. Like most modern SAT solvers, `MiniSAT` requires the input problem to be specified in Conjunctive Normal Form (CNF). CNF requires that the constraints be encoded as a set of *clauses* of the form

$$x_1 \text{ or } \neg x_3 \text{ or } x_5 \quad (\text{A.31})$$

that contain logical ORs of some subset of the variables where any of the variables may also be logically NOT'd, which we represent by negation here.

A solution of the problem is one that makes all the clauses simultaneously true.

I encode the edge colouring problem by assigning $3B$ boolean variables to each of the B edges of the graph, $x_{i\alpha}$ where $x_{i\alpha} = 1$ indicates that edge i has colour α .

For edge colouring graphs we need two types of constraints: 1. Each edge is exactly one colour. 2. No neighbouring edges are the same colour.

The first constraint is a product of doing this mapping to boolean variables. The solver does not know anything about the structure of the problem unless it is encoded into the variables.

Let's say we have three variables that correspond to particular edge being red r , green g or blue b .

To require that exactly one of the variables be true, we can enforce that no pair of variables be true: $-(r \text{ and } b) - (r \text{ and } g) - (b \text{ and } g)$

However, these clauses are not in CNF form. Therefore, we also have to use the fact that $-(a \text{ and } b) = (-a \text{ OR } -b)$. To enforce that at least one of these is true we simply OR them all together $(r \text{ or } b \text{ or } g)$

To encode the fact that no adjacent edges can have the same colour, we emit a clause that, for each pair of adjacent edges, they cannot be both red, both green or both blue.

We get a solution or set of solutions from the solver, which we can map back to a labelling of the edges. fig. 4.5 shows some examples.

The solution presented here works well enough for our purposes. It does not take up a substantial fraction of the overall computation time, see +fig:times but other approaches could likely work.

When translating problems to CNF form, there is often some flexibility. For instance, we used three boolean variables to encode the colour of each edge and, then, additional constraints to require that only one of these variables be true. An alternative method which we did not try would be to encode the label of each edge using two variables, yielding four states per edge, and then add a constraint that one of the states, say (true, true) is disallowed. This would, however, have added some complexity to the encoding of the constraint that no adjacent edges can have the same colour.

The popular *Networkx* Python library uses a greedy graph colouring algorithm. It simply iterates over the vertices/edges/faces of a graph and assigns them a colour that is not already disallowed. This does not work for our purposes because it is not designed to look for a particular n-colouring. However, it does include the option of using a heuristic function that determine the order in which vertices will be coloured [12, 13]. Perhaps

A.5 Lattice Colouring

Four-face-colourings and three-edge-colourings

A four-face-colouring can be converted into a three-edge-colouring quite easily: 1. Assume the faces of G can be four-coloured with labels $(0,1,2,3)$ 2. Label each edge of G according to $i + j \bmod 3$ where i and j are the labels of the face adjacent to that edge. For each edge label there are two face label pairs that do not share any face labels. i,e the edge label 0 can come about either from faces $0 + 3$ or $1 + 2$.

Explicitly, the mapping from face labels to edge labels is:

$$\begin{aligned} 0 + 3 \text{ or } 1 + 2 &= 0 \bmod 3 \\ 0 + 1 \text{ or } 2 + 3 &= 1 \bmod 3 \\ 0 + 2 \text{ or } 1 + 3 &= 2 \bmod 3 \end{aligned} \tag{A.32}$$

3. In a cubic planar G , a vertex v in G is always part of three faces and the colours of those faces determine the colours of the edges that connect to v . The three faces must take three distinct colours from the set $\{0, 1, 2, 3\}$.
4. From there, one can easily be convinced that those three distinct face colours can never produce repeated edge colours according to the $i + j \bmod 3$ rule.

This implies that all cubic planar graphs are three-edge-colourable. This does not apply to toroidal graphs. We have not yet generated a Voronoi lattices on the torus that is not three-edge-colourable. This suggests that Voronoi lattices may have additional structures that make them three-edge-colourable. Intuitively, it seems that the kinds of toroidal graphs that cannot be three-edge-coloured could never be generated by a Voronoi partition with more than a few seed points.

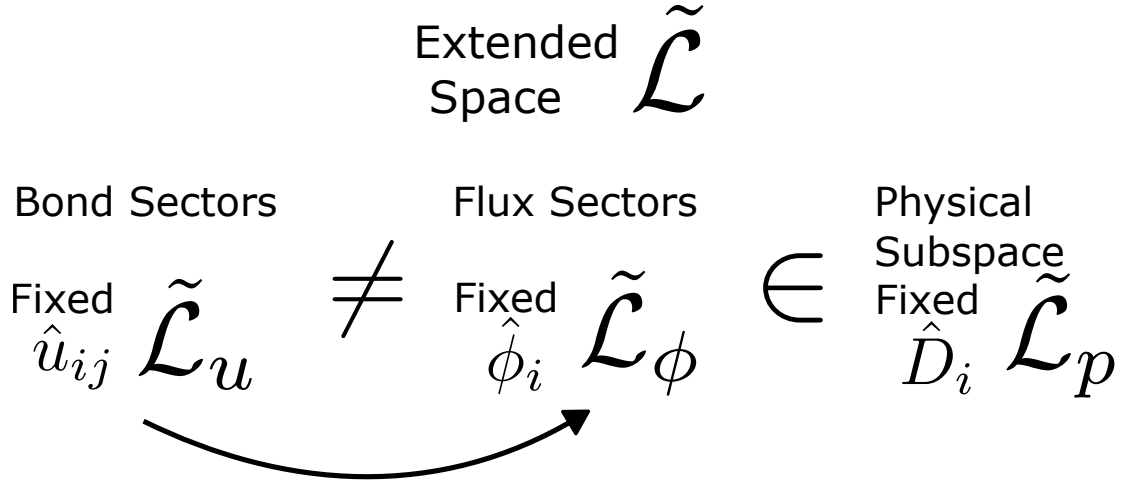


Figure A.5: The relationship between the different Hilbert spaces used in the solution. **needs updating**

A.6 The Projector

The projection from the extended space to the physical space will not be particularly important for the results presented here. However, the theory remains useful to explain why this is.

The physical states are defined as those for which $D_i|\phi\rangle = |\phi\rangle$ for all D_i . Since D_i has eigenvalues ± 1 , the quantity $\frac{(1+D_i)}{2}$ has eigenvalue 1 for physical states and 0 for extended states so is the local projector onto the physical subspace.

Therefore, the global projector is

$$\mathcal{P} = \prod_{i=1}^{2N} \left(\frac{1 + D_i}{2} \right) \quad (\text{A.33})$$

for a toroidal trivalent lattice with N plaquettes $2N$ vertices and $3N$ edges. As discussed earlier, the product over $(1 + D_j)$ can also be thought of as the sum of all possible subsets $\{i\}$ of the D_j operators, which is the set of all possible gauge symmetry operations.

$$\mathcal{P} = \frac{1}{2^{2N}} \sum_{\{i\}} \prod_{i \in \{i\}} D_i \quad (\text{A.34})$$

Since the gauge operators D_j commute and square to one, we can define the complement operator $C = \prod_{i=1}^{2N} D_i$ and see that it takes each set of $\prod_{i \in \{i\}} D_j$ operators and gives us the complement of that set. We will shortly see why C is the identity in the physical subspace, as noted earlier.

We use the complement operator to rewrite the projector as a sum over half the subsets of $\{i\}$ - referred to as Λ . The complement operator deals with the other half

$$\mathcal{P} = \left(\frac{1}{2^{2N-1}} \sum_{\Lambda} \prod_{i \in \{\Lambda\}} D_i \right) \left(\frac{1 + \prod_i^{2N} D_i}{2} \right) = \mathcal{S} \cdot \mathcal{P}_0 \quad (\text{A.35})$$

To compute \mathcal{P}_0 , the main quantity needed is the product of the local projectors D_i

$$\prod_i^{2N} D_i = \prod_i^{2N} b_i^x b_i^y b_i^z c_i \quad (\text{A.36})$$

for a toroidal trivalent lattice with N plaquettes $2N$ vertices and $3N$ edges.

First, we reorder the operators by bond type. This does not require any information about the underlying lattice.

$$\prod_i^{2N} D_i = \prod_i^{2N} b_i^x \prod_i^{2N} b_i^y \prod_i^{2N} b_i^z \prod_i^{2N} c_i \quad (\text{A.37})$$

The product over c_i operators reduces to a determinant of the Q matrix and the fermion parity, see [14]. The only difference from the honeycomb case is that we cannot explicitly compute the factors $p_x, p_y, p_z = \pm 1$ that arise from reordering the b operators such that pairs of vertices linked by the corresponding bonds are adjacent.

$$\prod_i^{2N} b_i^\alpha = p_\alpha \prod_{(i,j)} b_i^\alpha b_j^\alpha \quad (\text{A.38})$$

However, they are simply the parity of the permutation from one ordering to the other and can be computed in linear time with a cycle decomposition **cite**.

We find that

$$\mathcal{P}_0 = 1 + p_x p_y p_z \hat{\pi} \det(Q^u) \prod_{\{i,j\}} -iu_{ij} \quad (\text{A.39})$$

where $p_x p_y p_z = \pm 1$ are lattice structure factors and $\det(Q^u)$ is the determinant of the matrix mentioned earlier that maps c_i operators to normal mode operators b'_i, b''_i . These depend only on the lattice structure.

$\hat{\pi} = \prod i^N (1 - 2\hat{n}_i)$ is the parity of the particular many body state determined by fermionic occupation numbers n_i . As discussed in [14], $\hat{\pi}$ is gauge invariant in the sense that $[\hat{\pi}, D_i] = 0$.

This implies that $\det(Q^u) \prod -iu_{ij}$ is also a gauge invariant quantity. In translation invariant models this quantity which can be related to the parity of the number of vortex pairs in the system [15].

All these factors take values ± 1 so \mathcal{P}_0 is 0 or 1 for a particular state. Since \mathcal{S} corresponds to symmetrising over all the gauge configurations and cannot be 0, once we have determined the single particle eigenstates of a bond sector, the true many body ground state has the same energy as either the empty state with $n_i = 0$ or a state with a single fermion in the lowest level.

References

- [1] C. Gruber and D. Ueltschi, “The Falicov-Kimball model”, Feb. 16, 2005, arXiv:math-ph/0502041, <http://arxiv.org/abs/math-ph/0502041> (visited on 07/01/2019) (cit. on p. 106).
- [2] L. Devroye, “Random Sampling”, in *Non-Uniform Random Variate Generation*, edited by L. Devroye (Springer, New York, NY, 1986), pp. 611–641, 10.1007/978-1-4613-8643-8_12 (cit. on p. 108).
- [3] O. A. Martin, R. Kumar, and J. Lao, *Bayesian modeling and computation in python* (Boca Raton, Dec. 2021) (cit. on p. 108).
- [4] K. Binder and D. W. Heermann, “Guide to Practical Work with the Monte Carlo Method”, in *Monte Carlo Simulation in Statistical Physics: An Introduction*, edited by K. Binder and D. W. Heermann, Springer Series in Solid-State Sciences (Springer Berlin Heidelberg, Berlin, Heidelberg, 1988), pp. 68–112, 10.1007/978-3-662-08854-8_3 (cit. on p. 108).
- [5] J. Kertesz and I. Kondor, eds., *Advances in Computer Simulation: Lectures Held at the Eötvös Summer School in Budapest, Hungary, 16–20 July 1996*, Lecture Notes in Physics (Springer-Verlag, Berlin Heidelberg, 1998), 10.1007/BFb0105456 (cit. on p. 108).
- [6] U. Wolff, “Monte Carlo errors with less errors”, *Computer Physics Communications* **156**, 143–153 (2004) 10.1016/S0010-4655(03)00467-3 (cit. on p. 108).
- [7] W. Krauth, “Introduction To Monte Carlo Algorithms”, in *Advances in Computer Simulation: Lectures Held at the Eötvös Summer School in Budapest, Hungary, 16–20 July 1996*, Lecture Notes in Physics (Springer-Verlag, Berlin Heidelberg, 1998), 10.1007/BFb0105456 (cit. on pp. 108, 110).
- [8] F. Kelly, “Reversibility and stochastic networks / F.P. Kelly”, SERBIULA (sistema Librum 2.0) **76**, 10.2307/2287860 (1981) 10.2307/2287860 (cit. on p. 110).
- [9] S. C. Kapfer and W. Krauth, “Sampling from a polytope and hard-disk Monte Carlo”, *J. Phys.: Conf. Ser.* **454**, 012031 (2013) 10.1088/1742-6596/454/1/012031, arXiv:1301.4901 (cit. on p. 110).
- [10] W. Krauth, “Introduction To Monte Carlo Algorithms”, Dec. 19, 1996, arXiv:cond-mat/9612186, <http://arxiv.org/abs/cond-mat/9612186> (visited on 06/17/2019) (cit. on p. 113).
- [11] A. Ignatiev, A. Morgado, and J. Marques-Silva, “PySAT: A Python toolkit for prototyping with SAT oracles”, in *SAT* (2018), pp. 428–437, 10.1007/978-3-319-94144-8_26 (cit. on p. 117).
- [12] A. Kosowski and K. Manuszewski, “Classical coloring of graphs”, *Contemporary Mathematics* **352**, 1–20 (2004) (cit. on p. 118).
- [13] D. W. Matula and L. L. Beck, “Smallest-last ordering and clustering and graph coloring algorithms”, *J. ACM* **30**, 417–427 (1983) 10.1145/2402.322385 (cit. on p. 118).
- [14] F. L. Pedrocchi, S. Chesi, and D. Loss, “Physical solutions of the Kitaev honeycomb model”, *Phys. Rev. B* **84**, 165414 (2011) 10.1103/PhysRevB.84.165414 (cit. on p. 121).
- [15] H. Yao, S.-C. Zhang, and S. A. Kivelson, “Algebraic Spin Liquid in an Exactly Solvable Spin Model”, *Phys. Rev. Lett.* **102**, 217202 (2009) 10.1103/PhysRevLett.102.217202 (cit. on p. 121).